

ELECTROCHEMICAL SYNTHESIS OF CROWNED CONDUCTING
POLYMERS: NATURE OF RADICAL CATIONS IN POLYMERIZATION AND
MECHANISM OF CONDUCTIVITY

A THESIS SUBMITTED TO
THE GRADUATE SCHOOL OF NATURAL AND APPLIED SCIENCES
OF
MIDDLE EAST TECHNICAL UNIVERSITY

BY

ATILLA CIHANER

IN PARTIAL FULFILLMENT OF THE REQUIREMENTS FOR THE DEGREE OF
DOCTOR OF PHILOSOPHY
IN
CHEMISTRY

JUNE 2004

Approval of the Graduate School of Natural and Applied Sciences.

Prof. Dr. Canan Özgen
Director

I certify that this thesis satisfies all the requirements as a thesis for the degree of Doctor of Philosophy.

Prof. Dr. Hüseyin Isçi
Head of Department

This is to certify that we have read this thesis and that in our opinion it is fully adequate, in scope and quality, as a thesis for the degree of Doctor of Philosophy.

Prof. Dr. Ahmet M. Önal
Supervisor

Examining Committee Members

Prof. Dr. Zuhâl Küçükyavuz (METU, CHEM) _____

Prof. Dr. Ahmet M. Önal (METU, CHEM) _____

Prof. Dr. Levent Toppare (METU, CHEM) _____

Prof. Dr. Ali Usanmaz (METU, CHEM) _____

Prof. Dr. Attila Yıldız (HACETTEPE UNI., CHEM) _____

I hereby declare that all information in this document has been obtained and presented in accordance with academic rules and ethical conduct. I also declare that, as required by these rules and conduct, I have fully cited and referenced all materials and rules that are not original to this work.

Name, Last Name : Atilla Cihaner

Signature :

ABSTRACT

ELECTROCHEMICAL SYNTHESIS OF CROWNED CONDUCTING POLYMERS: NATURE OF RADICAL CATIONS IN POLYMERIZATION AND MECHANISM OF CONDUCTIVITY

Cihaner, Atilla

Ph. D., Department of Chemistry

Supervisor: Prof. Dr. Ahmet M. Önal

June 2004, 96 Pages

Poly(dibenzo-18-crown-6) (Poly(DB18C6)) was synthesized by electrochemical oxidation of dibenzo-18-crown-6 (DB18C6) using a mixture of acetonitrile and dichloromethane as solvent and tetrabutylammonium tetrafluoroborate (TBABF₄) or tetrabutylammonium hexafluorophosphate (TBAPF₆) as supporting electrolyte. The anodic polymerization of DB18C6 was investigated using *in-situ* ESR and *in-situ* UV-VIS spectroscopic techniques. Spectroelectrochemical (SPEL) properties and thermal analysis of the resulting polymers have been investigated using UV-VIS, Differential Scanning Calorimetry (DSC), and Thermogravimetric Analysis (TGA).

Furthermore, new compounds consisting of bis(2-thienyl) methyl (**I** and **II**) and bis(2-thienyl) ethyl (**III**) units linked by polyether bridges have been synthesized and their electrochemical polymerization was performed via constant potential electrolysis (CPE) in an electrolytic solution containing 0.1 M TBAPF₆ dissolved in CH₃CN. Also, **I** and **II** were polymerized via chemical oxidation

which yielded broken π -conjugated polymers except for **III**. The polymers were characterized using $^1\text{H-NMR}$ and FT-IR spectroscopic techniques. In addition, copolymers of **III** with thiophene (Th) and pyrrole (Py) were studied with cyclic voltammetry (CV). SPEL behaviors of the products were investigated using UV-VIS spectroscopic technique.

Keywords: Electrochemical Polymerization, ESR, SPEL Properties, Poly(DB18C6), Polyether Bridged-Substituted Thiophenes.

ÖZ

TAÇLANDIRILMIS ILETKEN POLİMERLERİN ELEKTROKİMYASAL SENTEZİ: POLİMERLESMEDEN RADİKAL KATYONLARIN DOĞASI VE İLETKENLİK MEKANİZMASI

Cihaner, Atilla

Doktora, Kimya Bölümü

Tez Yöneticisi: Prof. Dr. Ahmet M. Önal

Haziran 2004, 96 Sayfa

Poli(dibenzo-18-taç-6) (Poli(DB18C6)), asetonitril ve diklorometan çözücü karışımında tetrabütülamonyum tetrafloroborat (TBABF₄) veya tetrabütülamonyum hekzaflorofosfat (TBAPF₆) destek elektrolitleri kullanılarak dibenzo-18-taç-6 (DB18C6)'nin elektrokimyasal yükseltgenmesi ile sentezlenmiştir. DB18C6'nin anodik yükseltgenmesi *in-situ* ESR ve *in-situ* UV-VIS spektroskopik teknikleri ile incelenmiştir. Polimerin spektroeletrokimyasal (SPEL) özellikleri ve termal analizleri sırası ile UV-VIS, Diferansiyel Tarama Kalorimetrisi (DSC) ve Termoagırlık Analizi (TGA) ile araştırılmıştır.

Ayrıca, bis(2-tienil) metil (**I** and **II**) ve bis(2-tienil) etil (**III**) birimlerinin polieter köprüleri ile bağlanmış yeni bileşikler sentezlendi ve asetonitril içerisinde 0.1 M TBAPF₆ çözünmüş elektrolitik çözeltisinde sabit potansiyel elektrolizi (CPE) ile polimerleştirilmişlerdir. **III**'den farklı olarak, **I** ve **II**'nin kimyasal yükseltgenmesi kırılmış π -konjuge polimer ürünleri vermiştir.

Polimerler, ¹H-NMR ve FT-IR spektroskopik teknikleri kullanılarak karakterize edilmiştir. Ayrıca, **III**'ün tiyofen (Th) ve pirool (Py) kopolimerleri dönüşümlü voltametre (CV) ile çalışılmış ve ürünlerin SPEL davranımları UV-VIS spektroskopik tekniği ile araştırılmıştır.

Anahtar Kelimeler: Elektrokimyasal Polimerleşme, ESR, SPEL Özellikler, Poli(DB18C6), Polieter Köprülü Tiyofenler,

To My Father, Resit Cihaner

ACKNOWLEDGMENTS

Throughout the journey of life, I have had the honor of being surrounded by exceptional people. Without their guidance and friendship, the completion of this stage would not have been possible. Firstly, I would like to thank my advisor, Professor Dr. Ahmet M. Önal. Without his infinite patience and encouragement, this work would never have been possible. I would also like to thank him for giving me the opportunity to work with him.

I must thank my family, for their love and understanding (and patience!). Also, the greatest acknowledgment goes to them for giving me the intellectual and emotional guidance that made me who I am.

To Elif Göçmen, thanks go for sharing with me every joy and every worry. She has always been very supportive of me. Friendship is a powerful bond and friends truly hold a special place in my heart. Ali Çirpan, Yusuf Güner, Seha Tirkes, Hasan Koyuncu, Ömer Reis and Fatih Algi are such men with whom I have shared countless adventures that will not soon be forgotten. I would also like to thank the staff at METU for their efforts and helps.

Thanks go to Dr. Atef Qasrawi for his help and companionship during my work. I also appreciate the staff of Atilim University for being helpful when I needed it and generally fun to be around. I would also like to thank Dr. Sergey Nesterov for his valuable discussion about ESR studies. Also, I would like to express my gratitude to TUBITAK for financial support. The list could be longer, and I would like to thank anyone whom I have mistakenly omitted.

TABLE OF CONTENTS

PLAGIARISM	iii
ABSTRACT.....	iv
ÖZ.....	vi
ACKNOWLEDGMENTS	ix
TABLE OF CONTENTS	x
LIST OF FIGURES	xiii
ABBREVIATIONS.....	xvii
CHAPTERS	
I. INTRODUCTION	1
1.1 Brief History of Conjugated Polymers.....	1
1.2 Synthesis of CPs.....	3
1.2.1 Electrochemical Polymerization	3
1.2.2 Chemical Polymerization.....	6
1.3 Electrical Conduction in CPs	7
1.3.1 Band Theory.....	7
1.3.2 Origin of Bands p-Conjugated Organic Materials and Optical Transitions in CPs	9
1.3.3 Mechanism of Conductivity in Organic Materials	15
1.4 Applications of CPs.....	18
1.5 CPs Functionalized by Crown Ether (CE) or Polyether Bridges ...	19
1.5.1 Introduction.....	19
1.5.2 Functionalized PThs and Polyphenylenes by CE or Polyether Bridges	20
1.5.2.1 Oligo(oxyethylene)-substituted PThs	21
1.5.2.2 CE-Substituted Polyphenylenes	24

1.6. Aim of This Work	28
II. EXPERIMENTAL	
2.1 Materials	30
2.2 Cyclic voltammetry (CV) and Constant Potential Electrolysis.....	31
2.3 Spectroelectrochemistry.....	32
2.4. Spectroscopic Measurements	32
2.5 Electrical Measurements	32
2.5.1 Resistivity Measurement	33
2.6 Synthesis of Monomers	36
2.7 Polymerization Methods	38
2.7.1 Electrochemical Polymerization	38
2.7.2 Chemical Polymerization.....	38
2.7.2.1 Chemical Polymerization with FeCl_3	38
2.7.2.2 Chemical Polymerization with I_2	39
III. RESULTS AND DISCUSSION	
3.1 Electrochemical Polymerization of DB18C6.....	40
3.2 SPEL Monitoring of the Electrochemical Polymerization.....	42
3.3 Polymer Characterization.....	47
3.4 ESR and UV-VIS SPEL Measurements on Poly(DB18C6) films	49
3.5 Thermal Behavior of Poly(DB18C6)	53
3.6 Electrical, Optical and Photoconductive Properties of Poly(DB18C6).....	56
3.7 2-Substituted Oligo(oxyethylene) Ths	64
3.7.1 Electrochemical Behaviours of Monomers.....	64
3.7.2 Electrochemical Polymerization of I and II	65
3.7.3 Chemical Polymerization of I and II	67
3.7.4 Electrochemical Behavior of III	71
3.7.5 Electrochemical Polymerization of III	71
3.7.6 Chemical Polymerization of III	73

3.7.7 Radical Cation: Mechanism of Polymerization	74
3.7.8 ESR Study of Poly(III) During I ₂ Doping	77
3.7.9 Copolymer of III with Th and Py	78
3.7.9.1 Copolymer of III and Th.....	78
3.7.9.1.1 CV Studies.....	78
3.7.9.1.2 SPEL Behaviors	80
3.7.9.2 Copolymer of III and Py.....	82
3.7.9.2.1 CV studies	82
3.7.9.2.2 SPEL Behaviors	82
IV. CONCLUSION.....	86
REFERENCES	88
VITA	95

LIST OF FIGURES

1.1	Some common CPs	2
1.2	Electropolymerization mechanism. (a) Polymerization of heterocycles (X = S, O, NH) and (b) possible two linkage routes: a-a' and a-β linkages in unsubstituted poly(heterocycles)	5
1.3	Simple band diagrams showing the difference among metals, semiconductors and insulators.	7
1.4	Evolution of the band gap in PA: Schematic representation of the p-molecular orbitals energy levels with increasing chain length in PA.....	10
1.5	Optical transitions for doped conducting polymers. (A) neutral PA, p-doped and n-doped PA all have a mid-gap optical transition. (B) The non degeneracy of poly(heterocycles) causes the charge carriers to be polarons or bipolarons at high doping levels.....	13
1.6	Doping methods in conjugated polymers demonstrated for chemical and electrochemical doping.....	14
1.7	The conductivity range available to CPs spans those common for metals through insulators.	16
1.8	Some examples of CEs and related compounds.....	19
1.9	Some examples of oligo(oxyethylene)-substituted Ths	23
1.10	The structure of poly(DB18C6) and its repeating unit (T).....	25
2.1	Electrical resistivity measurement for the Hall bar samples.....	33
2.2	Setup for the resistivity measurement of van der Pauw samples	35
2.3	Closed cycle refrigeration system	36
3.1	CV of DB18C6 recorded in 0.1 M TBABF ₄ dissolved in CH ₃ CN/CH ₂ Cl ₂ mixture at room temperature (a) single anodic scan, 1.0x10 ⁻² M DB18C6 (b) repetitive cycling, 6.0x10 ⁻² M DB18C6 (voltage scan rate 100 mV/s).....	41

3.2	(a) The changes in the electronic absorption spectrum of 6.0×10^{-2} M DB18C6 in 0.1 M TBABF ₄ dissolved in CH ₃ CN/CH ₂ Cl ₂ mixture during <i>in-situ</i> CPE at 1.4 V. (b) Time traces of specific absorption bands during the CPE and after stopping the electrolysis.	43
3.3	ESR spectrum of 1.0×10^{-2} M DB18C6 recorded at 225 K during the constant current of 200 μ A electrolysis in 0.1 M TBABF ₄ dissolved in CH ₃ CN/CH ₂ Cl ₂ mixture.	45
3.4	(a) Time traces of ESR signal intensity recorded during and after the constant current electrolysis of 1.0×10^{-2} M DB18C6 in 0.1 M TBABF ₄ dissolved in CH ₃ CN/CH ₂ Cl ₂ mixture. (b) The Arrhenius plot according to first order radical decay.	46
3.5	FTIR spectra of (a) DB18C6, (b) BF ₄ ⁻ doped poly(DB18C6), (c) PF ₆ ⁻ doped poly(DB18C6) and (d) PF ₆ ⁻ doped poly(DB18C6) after thermal treatment.	48
3.6	ESR spectrum of poly(DB18C6) film (a) kept under vacuum (b) kept under open air	49
3.7	(a) The changes in the electronic absorption spectrum of poly(DB18C6) film on ITO electrode recorded during the anodic scan from 0.0 V to 0.9 V. (0.1 M TBABF ₄ dissolved in CH ₂ Cl ₂ , voltage scan rate : 20 mV/s). (b) Spectroelectrochemical behaviour of poly(DB18C6). Inset: CV of poly(DB18C6) coated on ITO	50
3.8	CV of poly(DB18C6) coated on Pt electrode recorded in 0.1 M TBABF ₄ dissolved (a) in CH ₂ Cl ₂ , (b) in CH ₃ CN and (c) coated on ITO electrode recorded in 0.1 M TBABF ₄ dissolved in CH ₂ Cl ₂	52
3.9	ESR spectra of oxidized poly(DB18C6) using constant current of 100 μ A in 0.1 M TBABF ₄ dissolved in CH ₂ Cl ₂ at room temperature	52
3.10	DSC thermogram of (a) BF ₄ ⁻ doped poly(DB18C6) and (b) PF ₆ ⁻ doped poly(DB18C6).	54
3.11	TGA thermogram of (a) BF ₄ ⁻ doped poly(DB18C6) and (b) PF ₆ ⁻ doped poly(DB18C6)	55

3.12	Variation of conductivity with temperature for poly(DB18C6) films. The inset shows the I-V characteristics of the films at 300 K.....	57
3.13	Variation of $\ln(s T^{1/2})-T^{-1/4}$ below 260 K.....	59
3.14	Photocurrent spectra of poly(DB18C6) film at 300 K.	60
3.15	$I_{ph}-F$ dependence at 300 K for poly(DB18C6) film. Inset-1 shows the time dependence of I_{ph} Inset-2 is an enlargement of the decay part of inset-1	63
3.16	CV s of Th and 2-substituted oligo(oxyethylene) Ths in 0.1 M TBAPF ₆ in acetonitrile solution vs SCE.	64
3.17	FT-IR spectra of (a) monomer I and (b) its polymer obtained from the anodic polymerization.....	69
3.18	FTIR spectra of the polymer obtained from the chemical polymerization of (a) 2ThMeOH, (b) I (s part) with FeCl ₃ , and (c) I (s part) with I ₂	68
3.19	UV-VIS spectra of monomer I and the polymer obtained from the chemical polymerization of I with I ₂	69
3.20	The assumed structures of the polymers obtained from the chemical polymerization of 2ThMeOH, and I (s part).	70
3.21	FTIR spectra of (a) III , (b) poly(III) by electrochemical polymerization and (c) poly(III) by chemical polymerization	72
3.22	The assumed structures of the polymers obtained from the electrochemical and chemical polymerization of III	73
3.23	ESR spectra of irradiated monomer I (0.07 mole % in Freon 11) (a) at 120 K and (b) at 150 K.....	75
3.24	ESR spectra of irradiated pure monomer I (a) at 77 K and (b) at 220 K (c) at 180 K and (d) monomer I (0.07 mole % in Freon 11) at 150 K.	76
3.25	ESR signal of doped poly(III) with the iodine vapor	77
3.26	CVs of (a) 1.0×10^{-2} M Th and 2.0×10^{-2} M III , (b) 1.0×10^{-2} M Th, (c) Th: III mixture (Th: III ; 50:1) (d) (Th: III ; 25:1) (e) (Th: III ; 12.5:1) and (f) polymer film obtained from the III :Th mixtures.	79

3.27	(a) Electronic absorption spectra of the copolymer obtained from Th: III mixture (50:1) in 0.1 M TBAPF ₆ in CH ₃ CN (b) Comparison of electronic absorption spectra of the copolymer (50:1) and PTh in their neutral (0.0 V vs Ag-wire) and oxidized states (at +1.2 V vs Ag-wire) in 0.1 M TBAPF ₆ in CH ₃ CN.	81
3.28	CVs of (a) 1.0x10 ⁻² M Py and 1.0x10 ⁻² M III (b) 1.0x10 ⁻² M Py, and (c) Py: III mixture (Py: III ; 4:1) (d) (Py: III ; 4:2) (e) (Py: III ; 4:5) (f) polymer films obtained from the Py: III mixtures.	84
3.29	Electronic absorption spectra of (a) PPy, (b) the polymer film obtained from the Py: III (4:5) mixture, and (c) comparison of electronic absorption spectra of the copolymer and PPy in their neutral (0.0 V vs Ag-wire) and oxidized states (at +0.8 V vs Ag-wire) in 0.1 M TBAPF ₆ in CH ₃ CN.	85

ABBREVIATION

CB	Conduction Band
CP	Conducting Polymer
CPE	Constant Potential Electrolysis
CE	Crown Ether
CV	Cyclic Voltammetry
B15C5	Benzo-15-crown-5
DB18C6	Dibenzo-18-crown-6
DSC	Differential Scanning Calorimetry
ESR	Electron Spin Resonance
FTIR	Fourier Transform Infrared
HOMO	Highest Occupied Molecular Orbital
ITO	Indium Tin Oxide
LUMO	Lowest Unoccupied Molecular Orbital
NMR	Nuclear Magnetic Resonance
PA	Polyacetylene
PANI	Polyaniline
PPy	Polypyrrole
Pt	Platinum
PTh	Polythiophene
Py	Pyrrole
PEDOT	Poly(3,4-ethylenedioxythiophene)
Th	Thiophene
TriPh	Triphenylene
RE	Reference Electrode
SPEL	Spectroelectrochemical
SCE	Saturated Calomel Electrode

TBABF ₄	Tetrabutylammonium Tetrafluoroborate
TBAPF ₆	Tetrabutylammonium Hexafluorophosphate
TGA	Thermogravimetric Analysis
VB	Valance Band
WE	Working Electrode

CHAPTER I

INTRODUCTION

1.1 Brief History of Conjugated Polymers

Many conducting polymers (CPs) were well known in their (non)conducting forms much before their conductivity, but not well characterized. For example, well-defined polyacetylene (PA) have been described since 1971 [1]. Chemical polymerization of aniline in sulphuric acid solution was reported by Letheby in 1862 [2], and pyrrole (Py) was known as a conductive “Py black” by spontaneous polymerization in air [3].

The main developments in the CPs containing conjugated $-\text{CH}=\text{CH}-$ bonds begin with oxidative coupling of heterocycles such as Py, thiophene (Th), furan [4] and aniline [5]. As early as 1968, electropolymerization of polypyrrole (PPy) was reported [6]. Thus, CPs are “rediscovered” materials.

The development of importance in CPs originated with the discovery in a collaborative effort between the Shirakawa and Heeger/MacDiarmid groups that PA exposed to iodine vapors develops very high and well characterized conductivities [7]. Therefore, these researchers launched a new era in polymeric materials and in 2000 the Nobel Prize in Chemistry was awarded to them for their discovery [7,8].

PA was initially the most studied CP both in scientific and practical applications. However, due to the limitations of PA, alternative “synthetic metals” were developed to improve solubility and processing properties. Several electron-rich CPs including PPy [9-11], polythiophene (PTh) [12,13], poly(3,4-ethylenedioxythiophene) (PEDOT) [14-16], and polyfuran [17], as well as other aromatic polymers such as polycarbazole [18], polyfluorene [19], polyaniline (PANI) [20], poly(*p*-phenylene vinylene) [21], and poly(*p*-phenylene) [22] were developed and extensively investigated as alternative CPs (Figure 1.1). Polymers such as PTh and PPy are two of the most studied CPs due to their conductivity and stable doped forms. Also, these structures are more easily modified than PA, allowing for designing new structures [23-25].

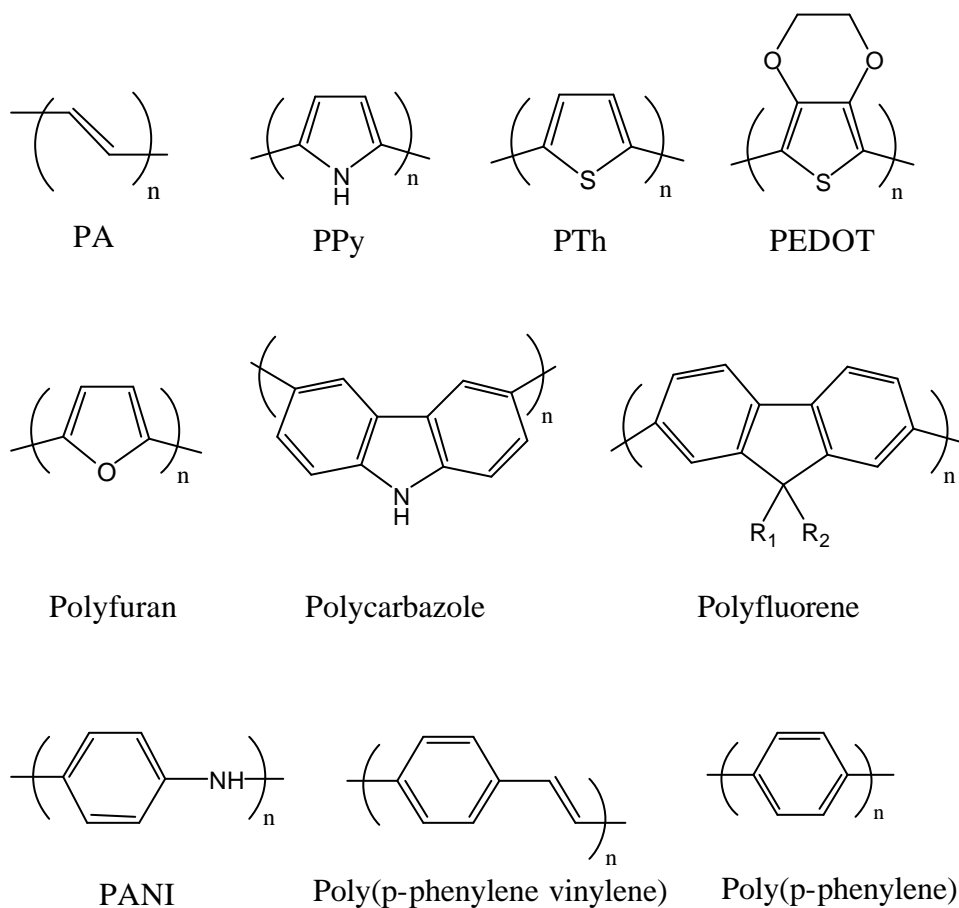


Figure 1.1. Some common CPs.

Among these so-called “first generation” conducting polymers, PTh has a considerable interest, mainly due to its structural versatility and stability. However, due to the “PTh paradox” (overoxidation during electropolymerization), some strategies were developed to control the properties of PThs and to eliminate overoxidation by designing different derivatives of the monomer structure [23,26]. For example, 3,4-ethylenedioxy derivative of PTh (PEDOT) includes low monomer oxidation potential, high stability in the doped form and an ease of derivatization at the ethylenedioxy ring. Also, PEDOT is a processable polymer with a high degree of order due to the lack of α - β and β - β' couplings. Therefore, PEDOT is as an excellent candidate for use in industrial applications such as an antistatic layer in photographic films, electrochromic devices, LEDs, capacitors and sensors [16, 27, 28].

1.2 Synthesis of CPs

1.2.1 Electrochemical Polymerization

Electrochemical synthesis of CPs involves the anodic oxidation of a monomer dissolved in a suitable electrolytic medium by applying an external potential, usually the monomer oxidation potential, to form reactive radical cations. The initial oxidation of monomer is followed by one of the two possible routes. The first route involves coupling of a monomer radical with a neutral monomer. A neutral dimer is formed after the second oxidation and loss of two protons [29, 30]. On the other hand, the second route involves the coupling of two radical cations followed by the loss of two protons to yield neutral dimer [31-34]. Then, the neutral dimer is oxidized and the process is repeated. Due to extended conjugation over two rings, the dimer has a lower oxidation potential than the monomer itself, and therefore it is oxidized easily to form the radical cation. As chain length increases, resulting oligomers become insoluble in the electrolytic medium and an electroactive polymer film is deposited onto the working

electrode. Because of the oxidative nature of electropolymerization, the deposited polymer is typically in its oxidized state and the positive charges along the polymer backbone are compensated by the supporting electrolyte anion. A proposed polymerization mechanism for heterocycles was given in Figure 1.2 (a). During the polymerization, a-a' couplings mainly afford a linear polymer backbone with electrical properties. On the other hand, the possible occurrence of a-β linkage causes the formation of branching and more defects in a given chain and therefore modifies its electronic distribution (Figure 1.2 (b)). This is consistent with the considerable increase in the content of disorder as well as the decrease in conductivity as the polymerization proceeds. It is known that the a and β positions have about 95/5 relative reactivity for Th and decreases as the polymerization proceeds, leading to an increase in the number of undesired couplings and consequently to a decrease in the polymer effective mean conjugation length [33].

Undesired a-β and β-β' couplings can be eliminated by “blocking” the 3- and 4-positions of the monomer by the attachment of various alkyl and alkoxy groups. For example, in EDOT, both β positions are substituted and the polymerization proceeds exclusively through the desired a-a' couplings and a soluble material is obtained with an enhanced degree of order.

Despite the facile nature of electrochemical polymerization, the obtained insoluble polymer via electropolymerization method prevents the analysis of primary structure using common techniques. Because of this limitation, chemical polymerization methods have gained popularity for synthesizing novel soluble conjugated polymers.

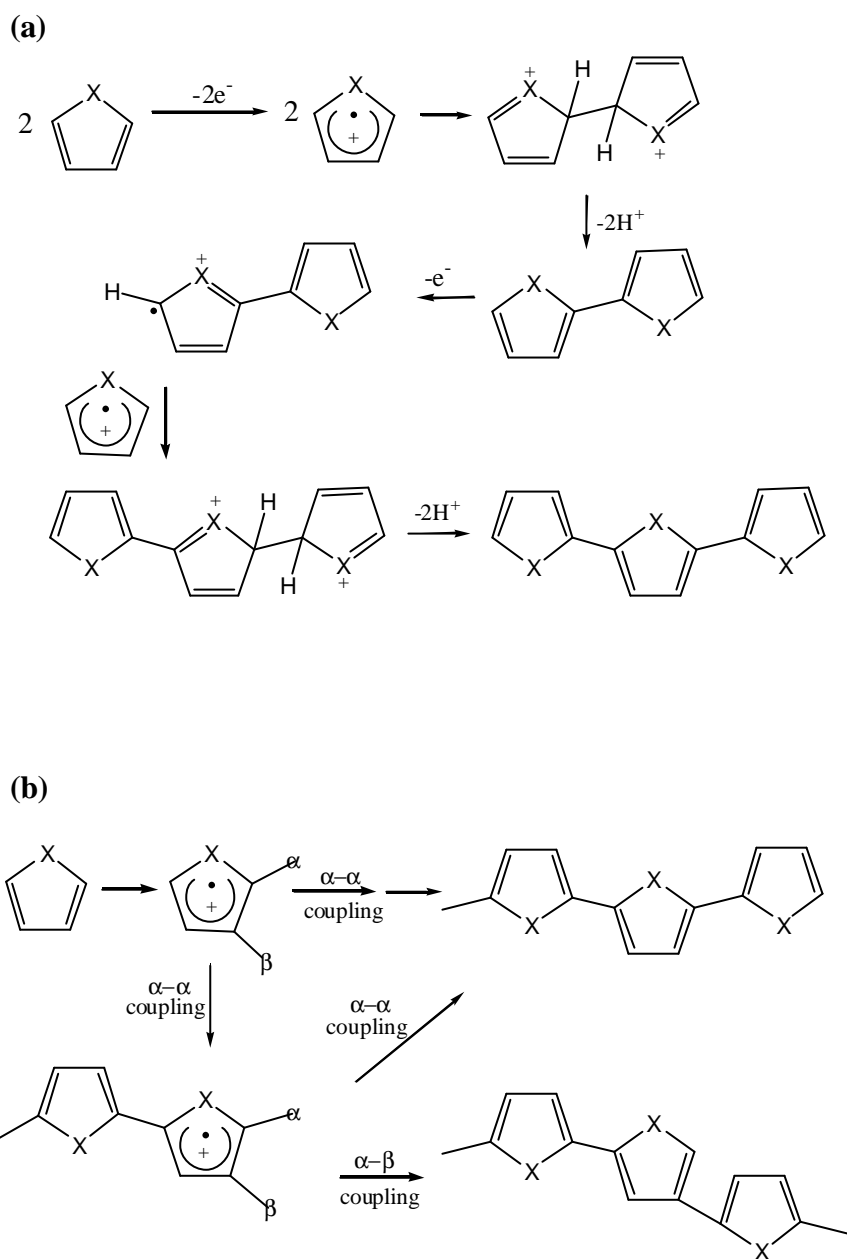


Figure 1.2. Electropolymerization mechanism. (a) Polymerization of heterocycles ($X = S, O, NH$), (b) Possible two linkage routes: $\alpha-\alpha'$ and $\alpha-\beta$ linkages in unsubstituted poly(heterocycles).

1.2.2 Chemical Polymerization

Chemical polymerization represents the least expensive and most widely exploited method for the preparation of conjugated polymers [35]. The mechanism of chemical and electrochemical polymerizations is thought to be very similar. Instead of an external potential, chemical polymerizations are carried out by exposing the monomer to a two-electron stoichiometric amount of oxidizing agent, resulting in the formation of the polymer in its doped and conducting state. For example, Th and its derivatives are typically polymerized in the presence of anhydrous FeCl_3 [36-38], although other Lewis acids can also be used [39].

The most important advantage of chemical polymerizations is that, unlike unsubstituted heterocycles that form insoluble powders, properly substituted heterocyclic and other aromatic monomers form highly soluble polymers. Therefore, these polymers can be analyzed using common characterization techniques to determine their primary structure. Also, the polymerization conditions can be easily scaled-up and yields large quantities of polymer.

However, chemical polymerizations have several disadvantages that often result in poor quality polymers. As stated earlier, Lewis acid catalyzed polymerizations yield the more rigid oxidized polymer [40] resulting in its precipitation in the polymerization medium, limiting the degree of polymerization. Also, the use of strong oxidizing agents may cause the overoxidation and eventual decomposition of the polymer, this disadvantage can be eliminated by using electrochemical methods by controlling the monomer oxidation potential [41-43].

1.3 Electrical Conduction in CPs

1.3.1 Band Theory

According to the band theory, the electrical properties of a material are the direct consequence of the energy difference (the band gap, E_g) between the highest occupied molecular orbital (HOMO) and the lowest unoccupied molecular orbital (LUMO). There are five classes of materials that can be identified and are largely differentiated by their conductivity magnitude and temperature dependence. These are metals, semimetals, semiconductors, insulators, and superconductors. Of these, three can be easily explained by simple band diagrams (Figure 1.3).

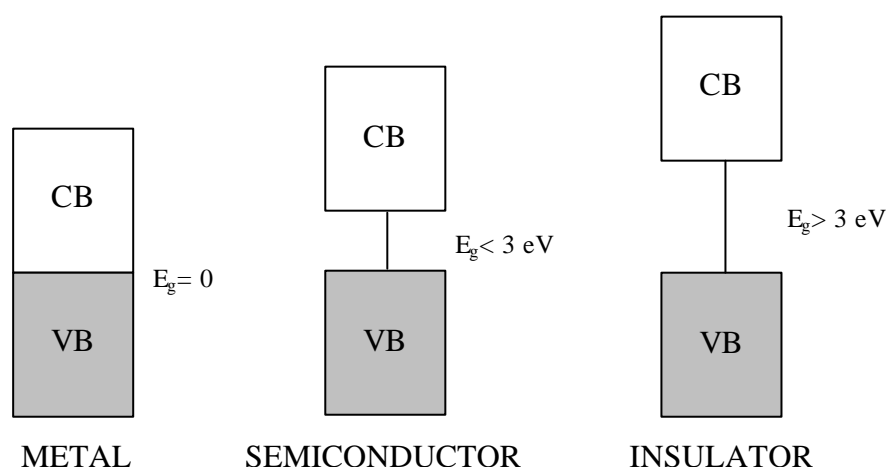


Figure 1.3. Simple band diagrams showing the difference among metals, semiconductors and insulators.

Metals are the most familiar conducting materials and are characterized by a zero band gap originating from a partially filled band (whereas this band is filled in semiconductors and insulators) or, alternatively, a contacting valence band, (VB) and conduction band (CB). In addition, the number of charge carriers contributing to conductivity is constant at all temperatures, due to the lack of a

band gap between HOMO and LUMO. The mobility of charge carriers, and consequently the conductivity of a metal, increases as the temperature approaches absolute zero.

Semiconductors have filled VBs and empty CBs. The gap energy is small as compared to the larger gap in insulators. For intrinsic semiconductors, electrons in the VB can be thermally activated into the CB, and the density of such electrons follows Arrhenius law. During the activation process, a corresponding hole is created in the VB and both free electrons and free holes contribute equally to the conductivity. These semiconductors have a positive temperature dependence of the conductivity. Even though the carrier mobility is affected by the same scattering process as in a metal, the number of charge carriers at the certain temperature dominates the overall temperature dependence of the conductivity. In addition, the room temperature conductivity of semiconductors is lower than the conductivity of metals due to a reduced charge carrier density. In extrinsic semiconductors, the number of charge carriers can be increased by introduction of impurities (dopants). In these materials, the carrier density is affected more by dopant nature and concentration than by the temperature.

The vast majority of CPs exhibit semiconductor or insulator-like conductivity. The conductivity magnitude is determined by the temperature and the size of the band gap. In neutral conjugated polymers band gap refers to the onset energy of the π - π^* transition from which the E_g of conjugated polymers can be approximated. In their neutral form, conjugated polymers are semiconducting, but on oxidation (p-doping) or reduction (n-doping), interband transitions form between the VB and CB, lowering the effective band gap, and resulting in the formation of charge carriers along the polymer backbone. The difference between a semiconductor and an insulator is rather arbitrarily determined at a band gap of 3 eV in most cases.

In insulators, the electrons are strongly localized between the atoms, forming chemical bonds. There is no significant overlap between p-orbitals of adjacent atoms and the VB is completely filled. Furthermore, a large gap separates it from the CB, which is not accessible by thermal excitation. For example, polymers having only s bonds are good insulators.

1.3.2 Origin of Bands in p-Conjugated Organic Materials and Optical Transitions in CPs

The simple chemical structure of PA, $-(\text{CH}_2)_x-$, implies that each carbon contributes a single p_z electron to the p band (HOMO). As a result, this band would be half filled, leading to a one-dimensional metal-like conduction along a neutral PA chain. Figure 1.4 shows the increase in the p orbital overlap as the length of the PA chain increases [44]. However, *cis*-PA was found to be an insulator with a conductivity of ca. 10^{-13} S cm⁻¹ and *trans*-PA has a neutral conductivity of 10^{-5} - 10^{-6} S cm⁻¹. Doubly degenerate ground state of *trans*-PA is unstable and dimerizes by a Peierls distortion opening up a band gap (1.48 eV by photoconductivity) at the Fermi level. Because of this, PA must be doped to either partially fill the CB by adding electrons (n-type doping) or partially vacate the VB by oxidation (p-type doping). This doping process, while possible and quite effective at improving the conductivity to a maximum of 2×10^4 S cm⁻¹, does not result in an air stable material and caused chemists to look elsewhere for other polymers that could be doped more easily. In the case of *cis*-PA, the ground state structure is non-degenerate and the VB is filled. Evolution of the band structure from monomer to polymer for conjugated heterocycles is similar to the one sketched in Figure 1.4 [45].

PA is unique among CPs because it has a degenerate ground state. Neutral PA has one allowed optical transition from the VB to CB as shown in Figure 1.5 A. There are three possible routes for creating charge carriers on a PA chain. In *trans*-PA with an odd number of electrons, a neutral soliton forms from the odd p

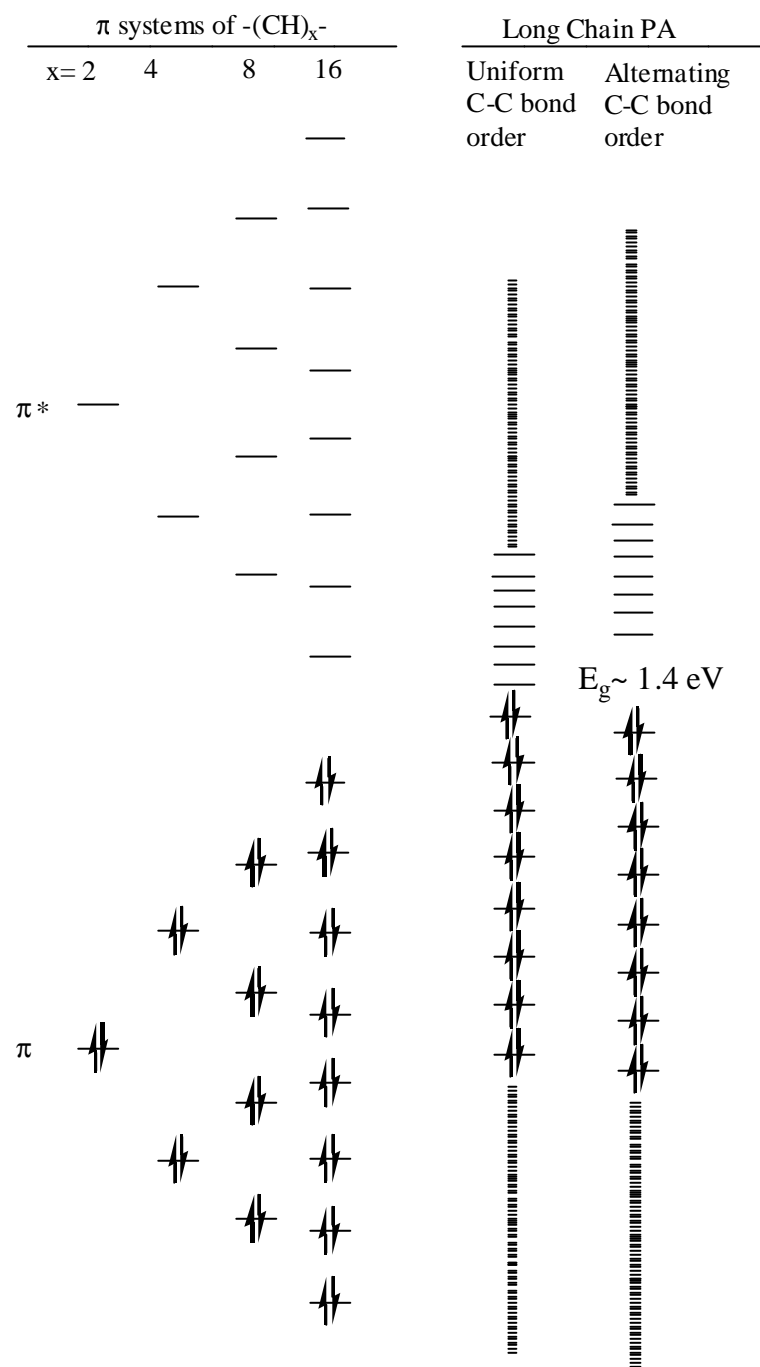


Figure 1.4. Evolution of the band gap in PA: Schematic representation of the p-molecular orbitals energy levels with increasing chain length in PA [45].

orbital and single p-electron. Oxidation creates an empty state and reduction creates a doubly occupied state at mid-gap, all of which are spectroscopically observed.

On the other hand, all CPs other than PA have nondegenerate ground state due to the energy difference between the aromatic form and quinoidal form of poly(heterocycles) which necessitates different charge carriers and thus optical responses. The quinoid structures have a lower ionization potential and a larger affinity than the aromatic structure [46].

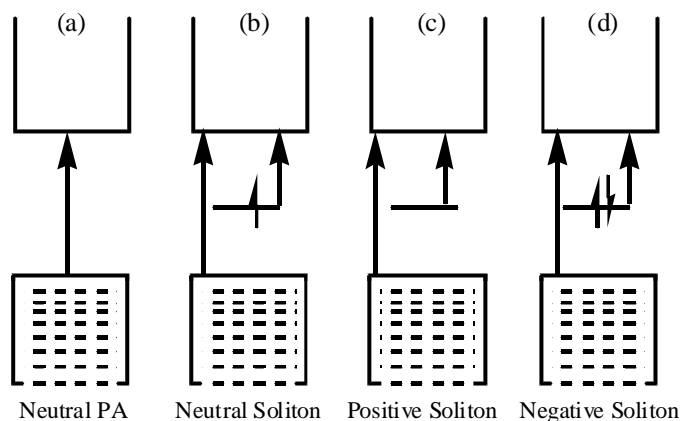
At a hypothetical zero doping level, the polymer is neutral, and its band structure is that of a standard semiconductor, with a band gap of 3.2 eV in the case of PPy (Figure 1.5 B (a)). Removal of one electron from the CP chain produces a polaron as shown in Figure 1.5 B (b), with the two polaron levels about 0.5 eV from the CB and VB edges. According to Bredas and Street [47], on removal of an electron, a bipolaron is produced (Figure 1.5 B (c)), with now the bipolaron levels being further removed from the VB and CB. It is important to note that in an actual CP structure, the entire CP chain would first have to become nearly saturated with polarons before bipolarons formation would commence. This is also supported by spectroelectrochemical (SPEL) studies; at low doping levels, spectra corresponding to polarons are first seen, before bipolaron spectra occur.

As one progress further to very high doping level (a maximum of about 35 % is experimentally achievable in PPy), the individual bipolaron states of Figure 1.5 B (c) coalesce into bipolaron bands (Figure 1.5 B (d)) [48]. It is also important to note that these bipolaron bands arise from electronic states “scavenged” from the VB and CB edges, and the gap between these bands consequently increases; this band gap increases from 3.2 eV for a nearly neutral polymer to 3.6 eV for highly doped one. At these high dopant concentrations, the bipolarons, which are spinless, can become mobile under the application of an electrical field, thus giving rise to the high conductivity observed in CPs concomitant with absence of unpaired spins detectable by ESR or other measurements.

It is also evident from the discussion above that if one were able to achieve even higher doping levels, the two bipolaron bands would gradually broaden enough to coalesce into the VB and CB, producing metal-like conduction due to the lower, half-filled valence/bipolaron band (Figure 1.5 B (e)). This could occur at hypothetical, higher doping levels, near 100 %, or if the intrinsic π - π^* band gap of the CP was low. This is said not to happen in PPy, with a fairly high band gap (3.2 eV, 388 nm) and maximum experimentally observed doping level of 35 %, but evidence has been put forth for its occurrence in other CPs, notably PTh, which has a lower band gap (2.0 eV, 620 nm).

There are also negatively charged polarons and bipolarons, which forms during “n-doping” or reduction. It is to be noted that apart from these positively and negatively charged polarons and bipolarons, the neutral polarons and bipolarons are just the corresponding structural distortion before removal of electrons, and can be said to exist only hypothetically. The theory presented above is based on the seminal work of Fesser, Bishop, and Campbell, whose FBC theory is one of the most widely cited by scientists attempting to interpret optical transitions in their conjugated polymers.

A. POSSIBLE OPTICAL TRANSITIONS FOR PA



B. POSSIBLE OPTICAL TRANSITIONS FOR A NON-DEGENERATE POLY(HETEROCYCLE)

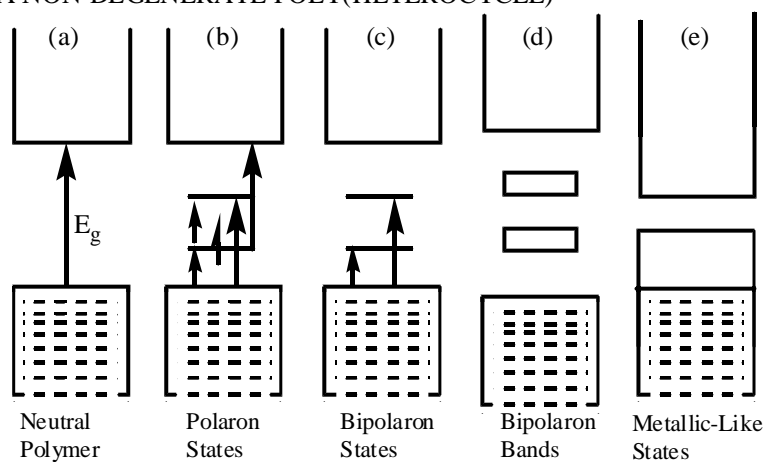
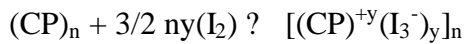


Figure 1.5. Optical transitions for doped CPs. (A) neutral PA, p-doped and n-doped PA all have a mid-gap optical transition. (B) The non degeneracy of poly(heterocycles) causes the charge carriers to be polarons or bipolarons at high doping levels.

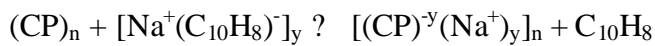
Doping can be accomplished in several ways depending on the polymer nature and its intended application. The initial discovery of the ability to dope conjugated polymers involved chemical doping by charge transfer redox chemistry [7,8]. Oxidation (p-doping) was accomplished by exposing the polymer to iodine vapors, whereas reduction (n-doping) involved treatment with sodium naphthalenide (Figure 1.6 A).

A. CHEMICAL DOPING

(a) p-type doping

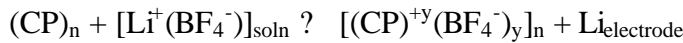


(b) n-type doping



B. ELECTROCHEMICAL DOPING

(a) p-type doping



(b) n-type doping

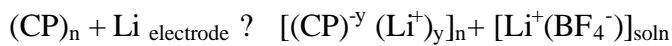


Figure 1.6. Doping methods in conjugated polymers demonstrated for chemical and electrochemical doping.

In this case, complete doping results in high quality materials with metallic-like conductivities. Another unique chemical doping procedure is protonation of PANI by acid-base chemistry. This leads to an internal redox reaction converting the semiconducting form of PANI (emeraldine base) to a metal (emeraldine salt) [49]. Although chemical doping is an efficient process, controlling the level of dopant ions is rather difficult. Attempts to reach intermediate doping levels resulted in inhomogeneous doping. As an alternative, electrochemical doping allows fine tuning of the doping level by simply adjusting

the potential between the working (WE) and reference electrodes (RE) (Figure 1.6 B) [50]. The WE supplies the redox charge to the CP, while ions diffuse in or out of the electroactive film to compensate the electronic charge. Thus any doping level can be achieved by setting the electrochemical cell to a desired potential and waiting for the system to attain an equilibrium state. This type of doping is permanent, meaning that the charge carriers remain in the film unless neutralization potential is purposely applied.

1.3.3 Mechanism of Conductivity in Organic Materials

CPs offer a unique property in that their conductivity can be tuned over 8 or more orders of magnitude in the same material. Several different conductivity mechanisms are available for electrically conducting CPs depending on their structure. Figure 1.7 shows the typical conductivity ranges for materials commonly considered metals, semiconductors and insulators although the factor that determines this classification is really the temperature dependence of conductivity rather than the conductivity magnitude. The three most common CPs shown in Figure 1.7 span the range of conductivities from metal to insulator depending on doping level. This property is unique to CPs. Neutral polymers tend to be semiconductors or, less frequently, insulators since the band gap is generally < 3 eV yet is too high for efficient population of the CB by kT . Doping by introducing charge carriers (positive or negative) has a drastic effect on conductivity as noted in Figure 1.7 and the details of this are important for designing new materials.

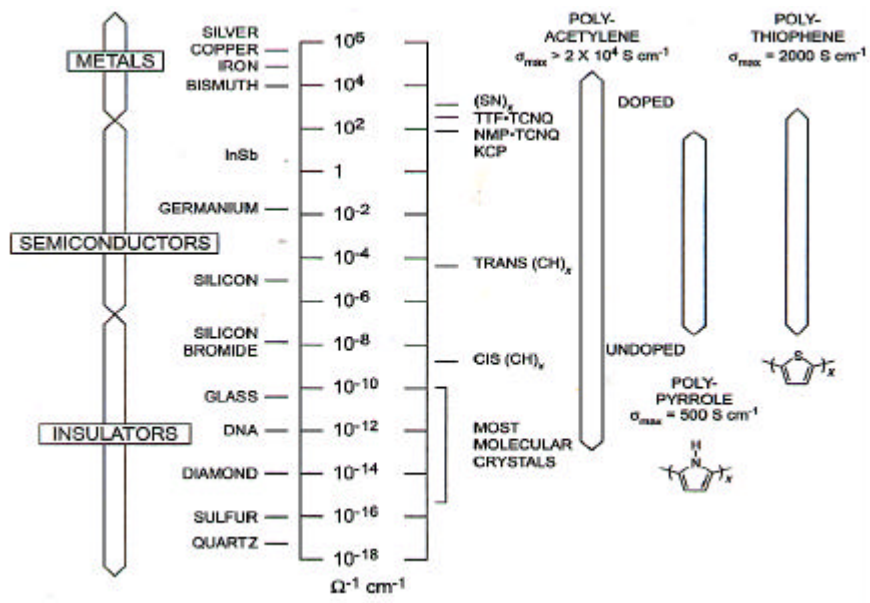


Figure 1.7. The conductivity range available to CPs spans those common for metals through insulators [32].

The conductivity, σ , in any semiconductor is given by,

$$\sigma = nq\mu_n + pq\mu_p$$

where μ_n and μ_p are the electron and hole drift mobilities, respectively.

In particular the conductivity of most elements and compounds is dominated by one carrier type because usually $n \gg p$ or $n \ll p$ for a specific material. For a p-type conduction only, the electrical conductivity can simply be written as the product of the hole density p , the charge of individual carrier q , and the carrier mobility μ as

$$\sigma = pq\mu$$

All three quantities that determine conductivity have different temperature dependences and it is the competition between these quantities that determines the overall relationship between σ and T . The charge carrier mobility is related to T and decreases with increasing temperature because of scattering. For doped PPy, the conductivity increases with temperature due to increasing thermal population of the CB [51].

The process of carrier conduction by hopping established by Mott [52] is different from conventional conduction process in that the conduction takes place in localized energy region within the energy gap of the material and not in the CB. Therefore, to obtain hopping conduction it is necessary to have a normally insulating, or semiconducting material exhibiting a few intrinsic thermal free carriers at least over a limited energy region, a large density of sites through which charge transfer can take place.

Fermi energy lies in the range of energies where states are localized. At low temperatures, the conductivity activation energy related to the thermionic emission conduction tends to zero and the thermally activated hopping conduction by electrons in states near the Fermi level energy dominates. The rate determining process is the hopping of an electron from a state below the Fermi level to one above. The conductivity is obtained as,

$$\sigma = \sigma_0 \exp\left(-\frac{T_0}{T}\right)^{1/4}$$

where σ_0 and T_0 are the pre-exponential factor and the degree of disorder, respectively.

1.4 Applications of CPs

CPs exhibit novel properties not typically available in other materials and these unique properties enable a large number of applications. These numerous applications can be split into three main classes. The first use conjugated polymers in their neutral form, and take advantage of their semi-conducting and luminescent properties. Examples of applications that use neutral polymers are conjugated polymers as semiconducting materials for field effect transistors [53] and as the active material in an electroluminescent device [54]. The second category of applications involves using the polymer in its doped or conducting form, and some representative applications in this category are electrostatic charge dissipation and EMI shielding [14,55], selective anionic membranes and as electrode materials for capacitors [16]. The third category uses the ability of the polymer to reversibly switch between its conducting and reduced forms. Upon switching between these two states, the polymer undergoes color, conductivity, and volume changes. Applications that use these properties include battery electrodes [56], mechanical actuators [57], sensors [58], drug delivery [59], and electrochromics [60].

1.5 CPs Functionalized by Crown Ether (CE) or Polyether Bridges

1.5.1 Introduction

The monocyclic polyethers called CEs were discovered in 1967 by Pedersen [61,62] and can be defined as uncharged macroheterocycles containing the repeat unit $(-O-CH_2-CH_2-)_n$ (Figure 1.8). They are designed as molecular hosts able to complex alkali and alkaline earth cations, transition metal cations and ammonium cations. Since then, other ligands such as the cryptands [63,64], the spherands and the chiral CEs [65] have been synthesized and their complexing properties have been extensively studied.

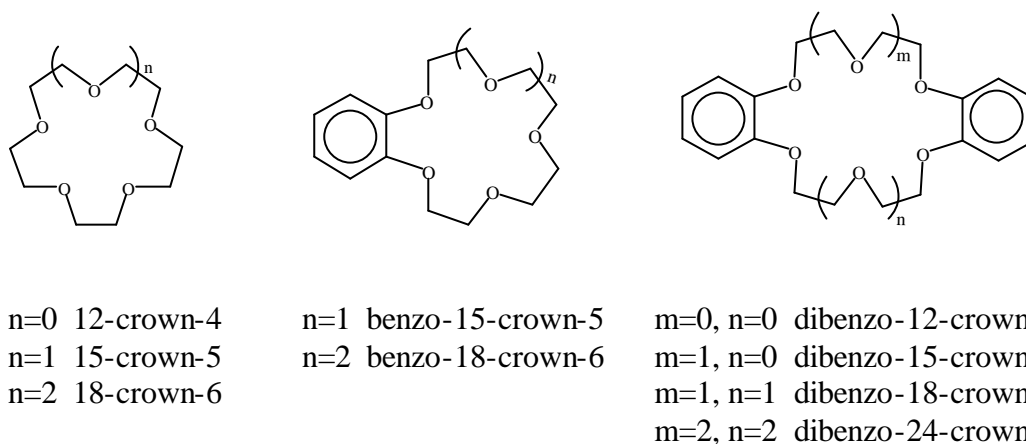


Figure 1.8. Some examples of CEs and related compounds.

Important review papers devoted to the chemistry of the CEs [66-68] and their analytical, chemical and biological applications have been published [69]. It has been also demonstrated that the introduction of functional groups provided more ample applications in analytical chemistry and related fields [70].

CE complexing properties are well known, and depend on the physical properties of both the CE and the ion being complexed. Several factors influence the complexing properties of a given CE towards a cation [61]:

- the relative sizes of the ions and the hole in crown cavity,
- the number and type of heteroatoms in the ring
- the physical placement of the binding sites
- any steric hindrance in the ring
- the tendency of the ion to associate with the solvent
- the electrical charge of the ions

Generally, the most stable complexes are formed when the ionic diameter is closely equal to the crown diameter [71,72]. In this case, the stoichiometry of the complex is frequently 1:1 with the cation assumed to be located inside the cavity of the polyether ring. When the cation is larger than the cavity, 1:2 and 2:3 complexes are formed.

1.5.2 Functionalized PThs and Polyphenylenes by CE or Polyether Bridges

The functionalized CPs are generally obtained from the oxidation of the starting monomer substituted by a group containing polyether or CE ligands. In the class of the conjugated polymers, functionalized PThs and polyphenylenes can be used for constructing cation-responsive electrodes. So, it is conceivable that the host-guest interaction between the ligand and a given cation may be “recognized” by the polymer. Accordingly, some of these polymers were successfully used for the recognition and the extraction of a large variety of cations including alkali, heavy and precious metal cations.

1.5.2.1 Oligo(oxyethylene)-substituted PThs

The substitution of PTh films by linear oligo(oxyethylene) (polyether) chains has great interest not only due to their complexing properties towards cations but also due to their enhanced solubility and high hydrophilic character [23]. The electrochemical synthesis of such functionalized polymers can be successfully achieved when two principal conditions are fulfilled. Firstly, two or more CH₂ groups must be used as a spacer between the Th ring and the first oxygen atom in order to neutralize the electron-withdrawing effect of ether groups on the conjugated system [73]. When only one methylene group separates the first oxygen atom from the heterocycle, the conjugation and the electronic conductivity of the corresponding polymer was seen to decrease owing to an enhancement of the oxidation potential of the monomer. Secondly, the impediment of the electropolymerization reaction caused by the steric bulkiness of the functional group should be avoided if the polyether chain is not too long. As reported by Lemaire et al. [73], above seven ether groups, the electrosynthesis of the substituted PTh was unsuccessful.

In the case where these two conditions are fulfilled, the electropolymerization of polyether-substituted Ths could be potentiostatically or galvanostatically achieved to obtain good electroactive films, and also it was reported for PThs that the most homogeneous and conducting films were obtained in galvanostatic conditions [23]. The electrosynthesis medium was generally acetonitrile or nitrobenzene containing tetrafluoroborate, perchlorate or hexafluorophosphate salts as the supporting electrolyte.

An interesting polymer **1** (Figure 1.9) with original properties associated with the oligo(oxyethylene) side chain is produced by anodic coupling. A considerable increase in hydrophilicity has been observed and the polymer remains electroactive in aqueous media, in contrast to poly(alkylTh)s [73,74]. This was said to be the first conjugated polymer system with a covalently attached

functional group for ion complexation. Furthermore, this polymer exhibits a specific electrochemical response to lithium ions.

On the other hand, an original approach developed by some authors consisted in the electroformation of complexing macrocyclic cavities from the oxidation of the Th derivatives substituted with acyclic polyether chains. In this context, symmetrical monomers possessing two Th units linked together by a polyether subunit have been synthesized and their electrochemical behavior has been investigated [75-77]. Electrochemical polymerization of **2b** (Figure 1.9) conducted in the presence of Li^+ in an effort to template intramolecular coupling and macrocycle closure. Nevertheless, a significant amount of crosslinking probably occurred. Conductivities of only 10^{-2} S/cm were reported for electropolymerized films. However, its structure and its sensing properties were not determined [75]. The properties of complexation of different undoped poly(**2**) toward inorganic cations (Ag^+ , Mn^{2+} , Co^{2+} and Sb^{3+}) have been investigated. It can be seen that these polymers exhibit a binding power which is much stronger towards Mn^{2+} and Co^{2+} than towards Sb^{3+} [78].

Simonet and co-workers have recently synthesized new Th derivatives **3** (Figure 1.9) substituted in the 2 position by acyclic polyether chains. Contrary to the Ths functionalized in the 3 position, the oxidation of such compounds led to unconjugated, redox-type polymer films, except for **3e** and **3f** which did not electropolymerize. These were expected to consist in the succession of biTh units separated by the carbon atom bearing the R group and the polyether chain. The oxidation potential of the monomers was found to be dependent on the electronic character of the R. Therefore, owing to the presence of the electron-withdrawing nitro group, **3d** was oxidized at a potential higher than **3a**, whereas inversely **3e** and **3f** were oxidized at a lower potential than **3a**.

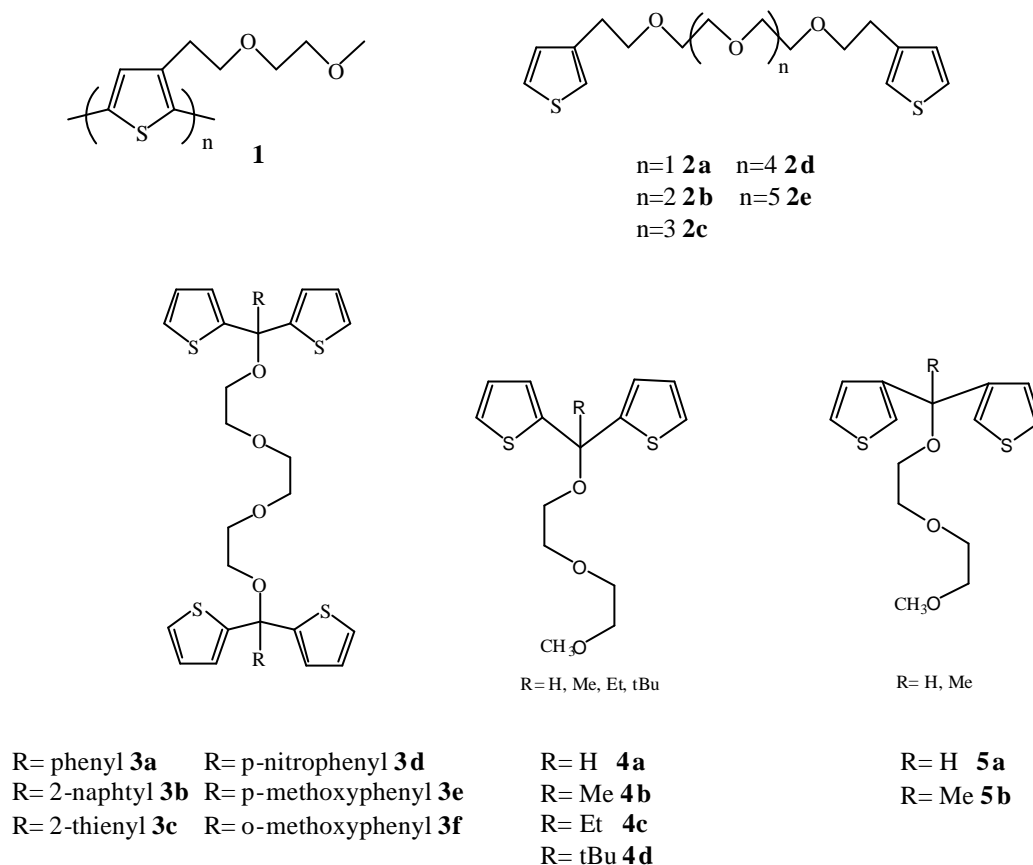


Figure 1.9. Some examples of oligo(oxyethylene)-substituted Ths.

On the other hand, Marrec et al [79] investigated the electrochemical and chemical properties of the compounds **4** and **5** (Figure 1.9). Unexpectedly high rates of sulphur found by elemental analysis in the resulting polymer obtained from **4** after the electrolysis. This was explained by a possible cleavage of the ether chain because electrochemical oxidation weakens the benzylic carbon-oxygen bond at the stage of the radical cation (assistance of sulphur lone pairs undergoing intramolecular electron transfer from the sulphur lone pairs to oxygen atom lone pairs , hence leading to C-O bond cleavage) and thus a β -elimination reaction occurs. On the other hand, oxidation of both monomers of **5** took place at 1.7 vs 0.1 M Ag^+/Ag and electroactive deposits grew on the electrode surface while cycling, without any cleavage.

All the electrogenerated polymers exhibited two reversible redox systems corresponding to the n-doping and p-doping processes. They could be cycled between the two states without apparent decrease in their electroactivity. Although the potential complexation properties towards some cations have not yet been investigated, this type of polymers, capable of being negatively and positively charged, should be of great interest for the development of chemically reversible ionic sensors. Indeed, the cation binding should be enhanced when the polymer is in its n-doped state and disfavored when it is in its p-doped state.

1.5.2.2 CE-Substituted Polyphenylenes

The functionalization of this class of polymers by polyethers or CEs has been principally developed by Simonet's group. Such electroactive polymers could be electrogenerated from the oxidation of CE-substituted benzenes as well as oligo(oxyethylene)-substituted benzenes.

When the substituents of the two aromatic rings were placed in the ortho position, specific trimerizations on each ring occurred and gave rise to electroactive polymers possessing TriPh moieties [80,81]. For example, trimerization reactions were reported for most of the benzo- and dibenzo-CEs. Accordingly, new tricyclic molecules could be electrogenerated from the oxidation of benzo-15-crown-5 (B15C5) [82] and benzo-18-crown-6 [83]. As a matter of fact, the anodic coupling of the benzo-CE led directly to the corresponding trimer radical cation which was found to be stable and reversibly reducible into the neutral species in CH₃CN. Finally, this type of electron donor molecules could be very interesting for the formation of charge transfer complexes with acceptor organic or inorganic compounds [84,85].

The synthesis of electroactive polyTriPhs has been achieved from the anodic oxidation of dibenzo-CEs. The TriPh moieties were presumably two-

dimensionally linked via polyether bridges (Figure 1.10). The structure of these poly(dibenzo-CE)s has been established [86] by means of different physicochemical methods, such as scanning electron microscopy, infrared, UV-visible, ESR and solid state ^{13}C -NMR [87] spectroscopic techniques.

The film exhibits very low conductivity and its surface morphology is quite compact and fibrous in the doped form. Cauliflower-like surface evolves upon chemical or electrochemical dedoping. The polymer also acted as an oxidizing agent. These films may be considered to be redox-polymers with the TriPh unit acting as the redox center.

The large number of papers devoted to poly(dibenzo-CE)s and especially to poly(dibenzo-18-crown-6) (poly(DB18C6)) has demonstrated that such electroactive polymers exhibited remarkable structural, electrochemical and complexing properties. Poly(DB12C4), poly(DB15C5) and poly(DB18C6) could be obtained as a film coating an electrode surface from the oxidation of the monomer in dried CH_2Cl_2 or a $\text{CH}_2\text{Cl}_2 + \text{CH}_3\text{CN}$ mixture containing Bu_4NBF_4 or Bu_4NPF_6 as the supporting electrolyte [88,89].

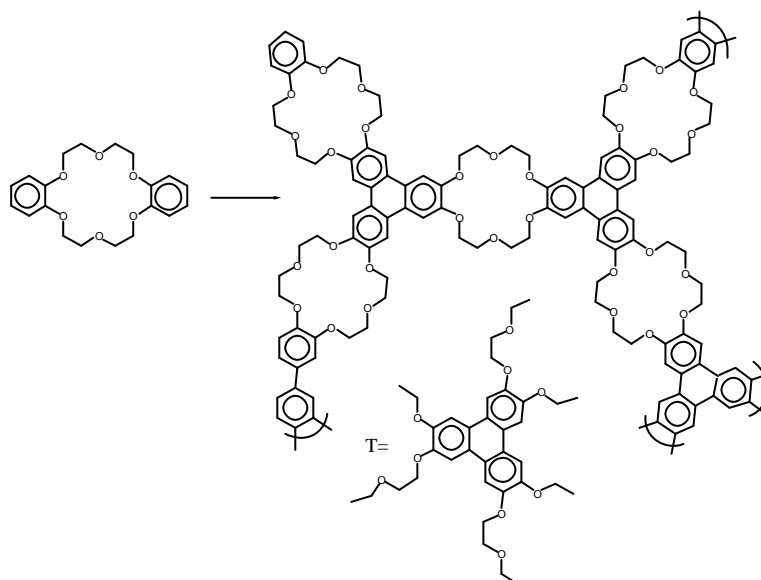
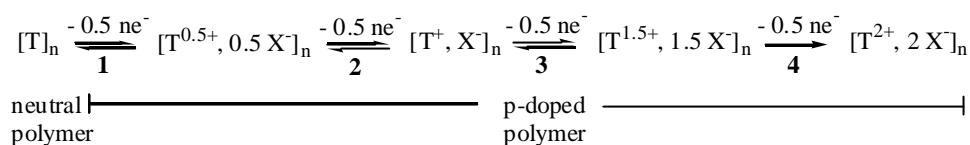


Figure 1.10. The structure of poly(DB18C6) and its repeating unit (T).

The electropolymerization was performed either by repeated potential linear scanning or by electrolysis at a constant potential. The electrochemical behavior of DB24C8 was somewhat similar but no tractable deposit was obtained from its oxidation.

The electrochemical behavior of poly(DB18C6) shows that this polymer exhibited three fully reversible steps followed by an irreversible one, each one corresponding to a 0.5 electron redox exchange.



where T symbolizes the electroactive hexasubstituted TriPh unit and X⁻ is the doping anion ensuring the electroneutrality of the material. From the elemental analysis and voltammetric data, the most stable structure of the p-doped polymer films was thought to be [T^{0.5+}, 0.5X⁻]_n. The four different oxidation states correspond to 50%, 100%, 150%, and 200% doping. Scanning above the first step, however, results in rapid film overoxidation and loss of response. Also, the doping anion was more strongly retained in the polymer structure when X⁻=BF₄⁻, ClO₄⁻ or SCN⁻ [90].

The ionophoric properties of the poly(dibenzo-CE)s have been investigated in their p-doped, oxidized form as well as in their undoped, neutral form. Their undoping could be quickly and efficiently achieved by a chemical treatment of the p-doped polymer with a reducing agent, such as the electrogenerated superoxide anion O₂⁻, primary and tertiary amines in acetonitrile or tetraalkylammonium hydroxide [91]. The total dedoping process can be seen by cyclic voltammetry at a potential of slightly below -3 V.

Qualitatively, the behavior of BF_4^- -doped poly(DB15C5) and poly(DB18C6) towards alkali cations was very close to that observed in solution with the monomers, i.e. the strongest affinity was obtained with K^+ and Na^+ in the case of poly(DB18C6) and with Li^+ for poly(DB15C5) [91]. Also, the complexing properties of poly(dibenzo-CE)s are dependent on the affinity of the CE towards a given cation, the oxidation level of the polymer, the undoping method used, the nature of the counter-anion associated to the complexed cation and the nature of the solvent. The affinity of the polymer towards heavy metal and precious metal cations was greatly improved when the polymer was previously undoped [92-96]. For example, the ratio of one cation per two TriPh units could be reached with cations like K^+ , Cs^+ , Rb^+ , Hg^+ , Ni^{2+} and Pd^{2+} [94,95]. Additionally, poly(DB18C6) exhibited a moderate selectivity when several cations were mixed [94,96]. Ag^+ , Sr^{2+} , Ba^{2+} , Ca^{2+} , Hg^{2+} , Ni^{2+} and La^{3+} were found to be more efficiently extracted from H_2O whereas K^+ and Rb^+ were more efficiently extracted from CH_3CN . Moreover, the effect of the counter-anion was also unclear [97,98].

As reported by De Backer et al., the reduction of the TriPh units could be performed when the polymer was treated with alkali metals. By this treatment, undoped poly(DB18C6) was converted into a new n-doped material similar to polyelectride [99]. Also, Lunsford et al. reported that the polymer films obtained from the oxidation of benzo- and dibenzo-CEs can be used as modified electrodes for the amperometric or potentiometric detection of catechols and catecholamines (e.g. dopamine) [100-102]. However, it seems very likely that the polymers electrosynthesized by these authors were electroinactive and insulating because a strongly positive electropolymerization potential (3.2 V vs Ag/AgCl, in CH_3CN) was used. Moreover, the possibility of a degradation of the CE at such a potential value could not be ruled out, although it has been reported that 18-crown-6 was not oxidizable up to 2 V (vs SCE) [103].

1.6. Aim of This Work

Although synthesis of poly(DB18C6) was well documented [91,103,104], information about its SPEL, ESR and thermal properties are still lacking. In this work, the anodic polymerization of DB18C6 under extra dry conditions was firstly monitored by using *in-situ* ESR and *in-situ* UV-VIS spectroscopic techniques. Furthermore, the SPEL and thermal properties of the resulting polymer films were also studied by conventional methods.

On the other hand, regarding these materials and the above mentioned applications, -up to our knowledge- no works have been investigated to consider their electrical and photoelectronic technological applications like, using these materials as memory cells, switching devices, photoconductors, radiation sensors, etc. These technological applications require the knowledge of the structural, optical, electrical, photoconduction and radiation properties of the material before subjecting it to instrumental designing. Therefore, one aim of this work is to report the electrical, optical and photoconduction properties of the conducting poly(DB18C6) films hoping that this information would help the researchers toward applying this material in electronic technological applications. The study of such characteristics allowed us to investigate, the band gap, the impurity and /or localized levels distributed in the band gap and the absorption bands of the material. In addition the photoconduction characteristics as function of time and illumination intensity are being investigated.

The functionalized conducting polymers are generally obtained from the oxidation of the starting monomer substituted by a group containing alkyl, crown ether or polyether bridges [23,105-108]. The latter two are of special interest because of their importance in the field of ionophoric resins. In this respect, recently two electropolymerizable groups linked by a flexible polyether chain at their α - and β - positions were synthesized (Figure 1.9) [75,77-79,81].

On the basis of these information, we tried to synthesize bis(2-thienyl) methyl and bis(2-thienyl) ethyl units linked by polyether bridges. By the polymerization of related monomer, regular polymers consisting of pseudo-polyether cages were prepared. In addition, electrochemical and spectroelectrochemical behaviors of the conducting copolymers of the related monomer with thiophene and pyrrole were studied.

CHAPTER II

EXPERIMENTAL

2.1 Materials

The monomer, DB18C6 (Fluka), was used without any further purification. The supporting electrolytes tetrabutylammonium hexafluorophosphate (TBAPF₆) (Aldrich) was used without further purification and tetrabutylammonium tetrafluoroborate (TBABF₄) (Aldrich) was recrystallized two times from methanol + water (1:1) and dried under vacuum. Acetonitrile was firstly dried over CaH₂ and distilled once from P₂O₅ under Ar_(g) and stored over molecular sieves. Dichloromethane was also dried over CaH₂ and distilled over CaH₂ under nitrogen. Two solvents were treated with freshly activated alumina prior to use. Tetrahydrofuran (THF) was refluxed with sodium/benzophenone and distilled under Ar_(g) atmosphere. NaH (Riedel-de Haen, 60% suspension in oil), (2-thienyl) methanol (Aldrich) and (2-thienyl) ethanol (Aldrich) were used as received. Th was dried over CaH₂ and distilled once from CaH₂ under Ar_(g). The molecular sieves (4 Å) and alumina were activated at 250 °C and 450 °C, respectively, for several hours. Polished platinum electrodes were used as WE and counter electrodes. For SPEL studies indium tin oxide coated quartz glass (ITO) (Delta Tech. 8-12 Ω), was used as WE. Solvent mixture was purged with Ar_(g) for 30 min prior to SPEL studies and the measurements were done under Ar_(g) atmosphere. In order to avoid the diffusion of water, Ag-wire was preferred as RE for electrochemical polymerization and for CV, respectively.

2.2 Cyclic Voltammetry (CV) and Constant Potential Electrolysis (CPE)

A large variety of electroanalytical methods can be applied to the study of conducting polymers. Among these methods, to study redox behaviour of a monomer or a polymer, CV has becoming increasingly popular due to its simplicity and versatility. Furthermore, CV reveals information regarding the stability of the product during multiple redox cycles.

This method sweeps the potential of an electrode, immersed in an unstirred solution, and measuring the resulting current at the WE. Therefore, the obtained voltammogram is a display of current (vertical axis) vs. potential (horizontal axis).

The reducing or oxidizing strength of the WE is precisely controlled by the applied potential. Continuous deposition of the polymer onto the WE can be monitored by the increase in the polymer's anodic and cathodic peak currents, while the polymer redox properties are characterized by the magnitudes of its peak potentials.

CV and electrolysis experiments were carried out by a HEKA IEEE-488 potentiostat/ galvanostat, utilizing a three-electrode configuration. Oxygen removal from the reaction medium is carried out by bubbling $\text{Ar}_{(g)}$ prior to electropolymerization, whereas maintaining the cell oxygen-free during an experiment is accomplished by passing $\text{Ar}_{(g)}$ over the solution.

Following electropolymerization, the electrode is removed from the monomer solution and carefully rinsed with monomer-free electrolyte solution. The rinsed electrode is then placed in another three-electrode cell filled with monomer-free electrolyte solution to study the redox behaviour of the polymer film.

2.3 Spectroelectrochemistry

SPEL measurements provide information about the material's band gap and intraband states created upon doping as well as gives electrochromic properties of CPs at various applied potentials.

Measurements were carried out with a HP 8453A diode array UV-VIS spectrometer using a specially designed three-electrode cell to allow potential application while monitoring the absorption spectra. The WE is an ITO fitting a SPEL cuvette (0.7 cm wide). Ag-wire pseudo reference is used as a RE and a Pt wire is used as a counter electrode. For potential control, all three electrodes were connected to a HEKA IEEE-488 potentiostat/ galvanostat.

2.4 Spectroscopic Measurements

Varian E12 ESR spectrometer was used for investigating paramagnetic behavior of the polymers and also for *in-situ* studies. FTIR spectra and ^{13}C -, ^1H -NMR spectra of the polymers were recorded on a Nicolet 510 FT-spectrophotometer and a Bruker Instrument-NMR Spectrometer (DPX-400), respectively. Thermal characterization of polymers was carried out using a Perkin Elmer TGA system and a DSC 910S/TA 2000 under air. A constant heating rate of 10 °C/min was used during DSC experiments.

2.5 Electrical Measurements

Among available conductivity techniques, four-probe method has several advantages for measuring electrical properties of conducting polymers. First, four-probe technique eliminate errors caused by contact resistance, since the two

contacts measuring the voltage drop are different from the contacts applying the current across the sample. Second, this technique allows for conductivity measurements over a broad range of applied currents, usually varying between 1 μA and 1mA for conducting polymers studied in this work. These current values produce potential differences ranging from 10 μV to 10 V, depending on the resistance and thickness of the sample. For the electrical characterization of thin films, dc resistivity and Hall measurements were performed at room temperature and also in the temperature range of 200-550 K. The details of the measurement techniques are described in the following section.

2.5.1 Resistivity Measurement

The resistivity of thin films was measured by applying the standard dc-technique on Hall bar samples and van der Pauw method on Maltese cross samples. The temperature variation of resistivity in between 200-550 K range was studied by placing the samples in a closed cycle (CTI-cryogenics model 22 refrigerator) helium cryostat. For the electrical measurements the constant current was applied to the samples by using a Keithley 220 programmable current source and the voltage drops were measured by a Keithley 618 electrometer. The circuit diagram and experimental set up are given in Figure 2.1. The constant current was applied through the sample and the voltage drops across the contacts 2 and 4 (V_{24}), and that between 6 and 8 (V_{68}) were measured.

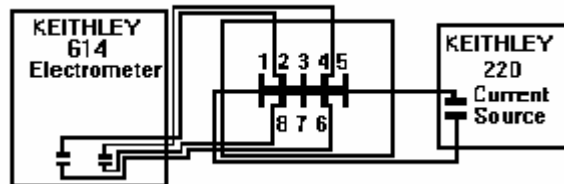


Figure 2.1. Electrical resistivity measurement for the Hall bar samples.

The variation of the current range depends on the total resistivity of the sample studied, the electrical resistivity was obtained by using the following expression

$$\rho = \frac{wtV}{LI}$$

, where w is the width of the thin film, t is the thickness, L is the spacing of the contacts across which the voltage is measured and V/I is the inverse slope of I-V characteristics. Note that the current I_{15} versus the voltage V_{24} and V_{68} are plotted separately and the average of both slopes is taken as the slope of I-V characteristics. The Equation is not valid unless the contacts are ohmic, therefore the ohmicity of contacts must be checked by plotting the logarithmic I-V characteristics where the slope has to be around unity for both polarities, which means that the voltage current relationship is linear satisfying the Ohm's law.

The circuit diagram of the experimental set up used for the electrical resistivity measurement of van der Pauw samples is given in Figure 2.2. Two successive measurements by shifting the current and voltage probes either clockwise or counterclockwise direction to reduce the asymmetry of the samples have been done. First, the resistance between the probes 3 and 4 (R_a), and that between the probes 2 and 3 (R_b) were measured. A constant current is applied through the contacts 1 and 2 and the voltage drop between 3 and 4 is measured. The voltage to current ratio is taken as $R_a = V_{34}/I_{12}$. Then the current is applied through the contacts 1 and 4 and the potential drop across the contacts 2 and 3 is measured giving the second resistance $R_b = V_{23}/I_{14}$. The exchange of the probes on the contact was made by a switch box connected to the measuring system. The measured values of R_a and R_b , together with the thickness of the sample, are used to obtain the resistivity through the relation

$$\rho = \frac{\pi t(R_a + R_b)}{2 \ln 2} f\left(\frac{R_a}{R_b}\right)$$

where $f(R_a/R_b)$ is a function of the ratio of the potential difference V_{34} and V_{23} known as the correction factor or van der Pauw function. If the contacts are symmetrical about a line through any pair of any non adjacent contacts then $f(R_a/R_b)$ or V_{34}/V_{23} should be equal to one.

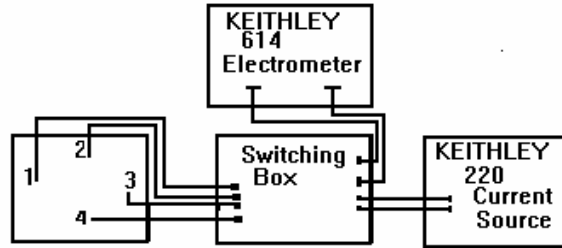


Figure 2.2. Setup for the resistivity measurement of van der Pauw samples.

The temperature dependence of resistivity has been studied by the measurements performed on the samples placed in CTI-cryogenics model 22 closed cycled Helium cryostat and Lake Shore DRC-91C temperature controller in the temperature range of 200-550 K. The schematic of the system is shown in Figure 2.3.

The Hall bar sample was mounted to the sample holder in the second stage of the cryostat and this holder is surrounded by heater wire. A silicon diode sensor was connected to the Lake Shore DRC-91C temperature controller. The resistivity measuring circuit is connected to the sample through the electrical feed through of the cryostat. Measurements were performed when the sample temperature was stabilized at a certain temperature up 550 K with 10 K intervals.

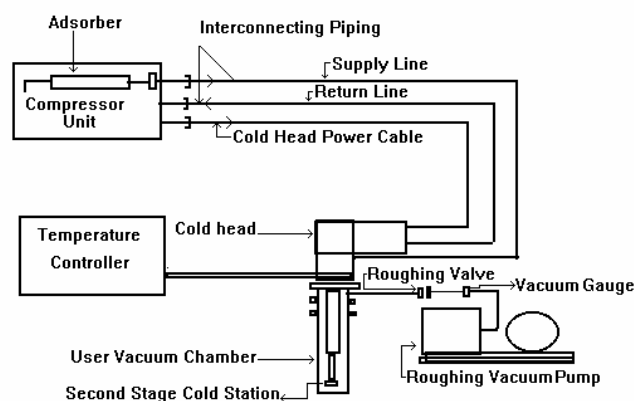
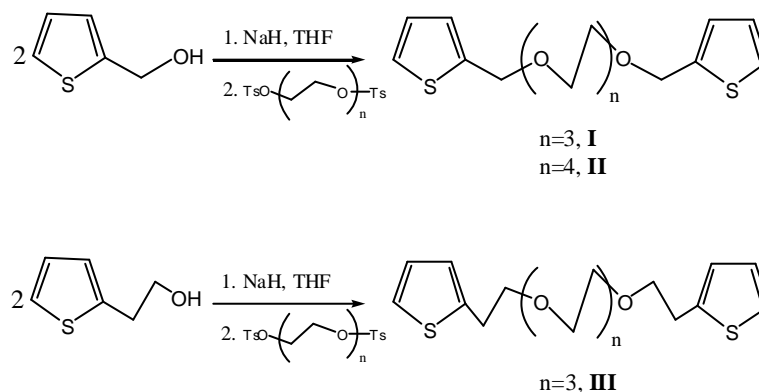


Figure 2.3. Closed cycle refrigeration system.

2.6 Synthesis of Monomers



The monomers were synthesized according to a general procedure already described [77]. 20 mmol of (2-thienyl) methanol (or (2-thienyl) ethanol) and excess NaH were mixed in 200 mL of dry THF under $\text{Ar}_{(g)}$ atmosphere for 30 min at room temperature. 19.5 mmol of ditosylate (with the appropriate chain length) were added dropwise over an hour and the solution was refluxed for 24 hours. Then, the hot solution was cooled to room temperature and neutralized using 0.1 M HCl until obtaining a clear yellow solution. The solution was extracted using

diethyl ether and washed with water. The organic phase was dried over MgSO_4 and evaporated under vacuum. After work up, the oily residue was purified on packed silica gel using hexane/ethyl acetate (6:1) as an eluent to afford monomers as yellowish oil. ^1H - and ^{13}C -NMR spectra were recorded in CDCl_3 and are given in ppm referred to TMS.

1,12-bis(2-thienyl)-2,5,8,11-tetraoxadodecane (I)

Clear yellowish oil. Yield ~ 70 %. ^1H -NMR (400 MHz in CDCl_3) d/ppm: (m, J (Hz)): 3.54-3.56 (m, 16 H), 4.62 (s, 4 H), 6.85-6.89 (m, 4 H), 7.11-7.17 (dd, J= 5 Hz, 2 H) ^{13}C -NMR 100 MHz (CDCl_3) d/ppm: 141.46, 126.88, 126.70, 126.02, 71.09, 71.04, 69.45, 68.01.

1,15-bis(2-thienyl)-2,5,8,11,15-pentaoxapentadecane (II)

Clear yellowish oil. Yield ~ 75 %. ^1H -NMR (400 MHz in CDCl_3) d/ppm: (m, J (Hz)): 3.74-3.80 (m, 16 H), 4.92 (s, 4 H), 7.07-7.12 (m, 4 H), 7.39 (dd, J= 5 Hz, 2 H) ^{13}C -NMR 100 MHz (CDCl_3) d/ppm: 141.50, 126.88, 126.68, 126.02, 71.09, 71.05, 69.46, 68.02.

1,14-bis(2-thienyl)-3,6,9,12-tetraoxatetradecane (III)

Reddish brown oil. Yield ~ 70 %. ^1H -NMR (400 MHz in CDCl_3) d/ppm: (m, J (Hz)): 3.01 (t, J= 6.82 Hz, 4 H), 3.52-3.58 (m, 12 H), 3.61 (t, J=6.91, 4 H), 6.74 (dd, J= 0.7 Hz, 2 H), 6.81 (dd, J= 1.65 Hz, 2 H), 7.00 (dd, J= 1.12 Hz, 2 H) ^{13}C -NMR 100 MHz (CDCl_3) d/ppm: 141.48, 126.95, 125.40, 123.83, 72.34, 71.10, 71.00, 70.78.

2.7. Polymerization Methods

2.7.1 Electrochemical Polymerization

Electrochemical polymerization was performed in a classical three-electrode cell. The WE and counter electrode were rectangular platinum sheets (1 cm²) and RE was a Ag-wire. All polymer samples were grown using constant potential electrolysis (oxidation potential of related monomer) in 0.1 M TBABF₄ or TBAPF₆ dissolved in CH₃CN or CH₂Cl₂ containing 0.05 M of monomer in the presence of activated alumina to eliminate residual traces of water. Samples were peeled off from the WE, washed with CH₂Cl₂ and then dried under vacuum at 50 °C for 12 h.

2.7.2 Chemical Polymerization

2.7.2.1 Chemical Polymerization with FeCl₃

The polymers were synthesized according to a general procedure [109]. The monomer was dissolved in dry CHCl₃ (dried over MgSO₄) and a suspension of anhydrous FeCl₃ in CHCl₃ of equal volume was added to the monomer solution for 1 h at 0 °C under Ar_(g) atmosphere used to remove the generated HCl as well as keep the iron catalyst in its active Fe³⁺ oxidation state. The final concentration for the monomer and FeCl₃ was 0.05 M and 0.2 M, respectively. When the addition was complete, the mixture was stirred for 24 h at room temperature and the reaction mixture was poured into methanol, and a precipitate formed. This was filtered and washed with methanol and ether, respectively. The solid was dried under vacuum at 50 °C.

2.7.2.2. Chemical Polymerization with I₂

The polymers were synthesized according to a general procedure [110]. The monomer (0.7 mmol, 0.28 g) was dissolved in dry CH₂Cl₂ and I₂ (0.14 mmol, 0.035 g) in CH₂Cl₂ was added drop wise to the monomer solution. When the addition was complete, the mixture was refluxed for 24 h and the reaction mixture was poured into methanol, and a precipitate was formed. This was filtered and washed with methanol. The precipitate and methanol soluble part were dried under vacuum at 60 °C.

CHAPTER III

RESULTS AND DISCUSSION

3.1 Electrochemical Polymerization of DB18C6

Since it is reported that satisfactory synthesis of CP films require anhydrous conditions to avoid the rapid inhibition of the anodic oxidation [91], all solvent-supporting electrolyte solutions were treated with freshly activated neutral alumina prior to use and CPE was conducted in the presence of freshly activated neutral alumina. In fact, water reacts with crown ether radical cation and leads to the formation quinone units which prevent polymerization.

Electrochemical behaviour of the monomer, DB18C6, was investigated using CV in TBABF₄ dissolved in a solvent mixture of CH₂Cl₂ and CH₃CN (1:1) in the presence of freshly activated alumina prior to CPE.

As shown in Figure 3.1 (a), during the first anodic scan an oxidation peak appears at + 1.65 V vs Ag-wire (0.95 vs Fc/Fc⁺) and during the second cycle a new reversible peak appeared at 1.10 V vs Ag-wire (0.40 vs Fc/Fc⁺). It is observed that the intensity of the reversible peak increases during successive anodic scans, which is characteristic of conducting polymer deposits (see Figure 3.1 (b)). A conducting film also forms on the electrode surface during the successive cycling. However, its formation on the electrode surface totally passivated the electrode after a certain number of sweeps due to the inhibition of the system.

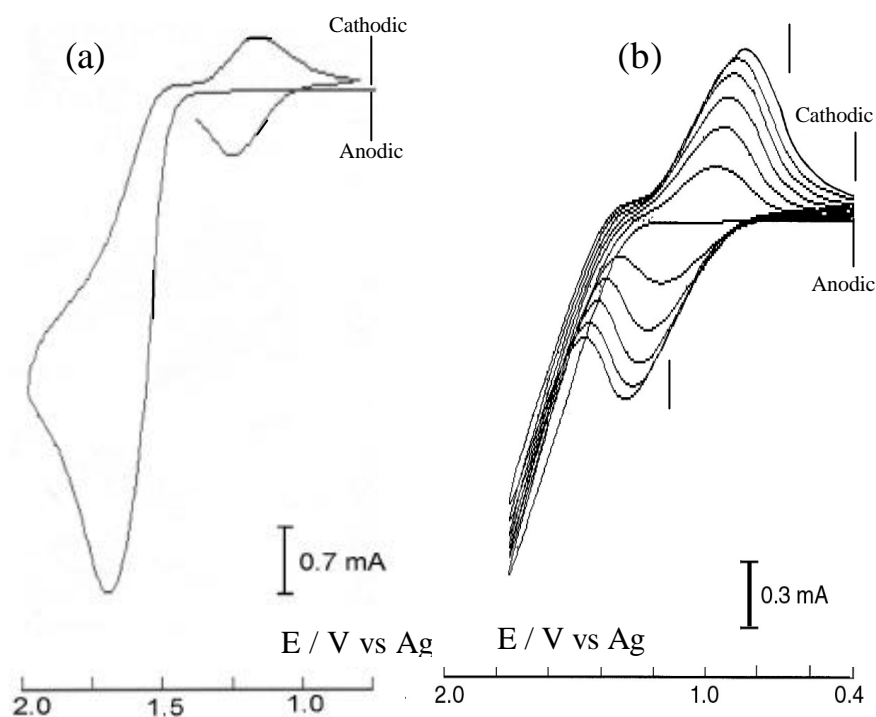


Figure 3.1. CV of DB18C6 recorded in 0.1 M TBABF₄ dissolved in CH₃CN/CH₂Cl₂ mixture at room temperature (a) single anodic scan, 1.0x10⁻² M DB18C6 and (b) repetitive cycling, 6.0x10⁻² M DB18C6 (voltage scan rate 100 mV/s).

On the basis of these informations, the anodic oxidation of DB18C6 was carried out in a mixture of CH₂Cl₂ and CH₃CN (1:1) and TBABF₄ or TBAPF₆ in the presence of freshly activated alumina at 1.4 V vs Ag-wire corresponding to the foot of the main oxidation peak. The bright black film formed at the end of CPE (2 C/cm²) was peeled off from the working electrode surface and dried under vacuum after washing with CH₂Cl₂. The average thickness of the polymer films was measured using micrometer and found to be 10 μm.

3.2 SPEL Monitoring of the Electrochemical Polymerization

The course of CPE at 1.40 V vs Ag-wire was followed by *in-situ* monitoring the changes in the electronic absorption spectra of the monomer solution. The study was carried out in a solution of DB18C6 and WE in the UV cell. Prior to use, solvent-electrolyte mixture was treated with freshly activated alumina; however, alumina was not used during *in-situ* CPE to avoid scattering of light. Although CH₃CN solution of DB18C6 exhibits two absorption bands at 230 and 275 nm due to $\pi \rightarrow \pi^*$ transition, the changes in these bands can not be monitored since the available window for ITO WE is above 300 nm. However, upon starting the CPE, a new broad band centered about 770 nm starts to intensify, which is accompanied with the formation of a green colored thin film, Figure 3.2 (a).

Also, two absorption bands were observed in the higher energy region between 300 and 500 nm; the one that appears around 320 nm is ill-defined due to its closeness to the cut-off region of ITO, the other band appears at 420 nm. These bands are due to the $\pi \rightarrow \pi^*$ transition of the triphenylene moiety [111]; however, the 770 nm band is related to the cation radical. V. Le Berre et al also reported similar observations during the synthesis of tris(crown ether) triphenylene from B15C5 [82]. A comparison of the electronic absorption spectrum obtained during the CPE of DB18C6 solution with that of tris(crown ether)triphenylene showed that λ_{\max} values are red shifted in the case of DB18C6 which can be ascribed to the formation of polymer film on ITO surface.

The changes in the electronic absorption spectrum of the electrolysis solution were also monitored both during the CPE (60 s, 100 mC/ cm²) and after stopping the electrolysis (240 s). Time traces of the characteristic bands are given in Figure 3.2 (b). As seen from the figure, the intensities of all the bands increase almost linearly as the film grows on ITO surface. However, more surprisingly, the intensity of the bands does not remain constant after stopping CPE, indeed they all

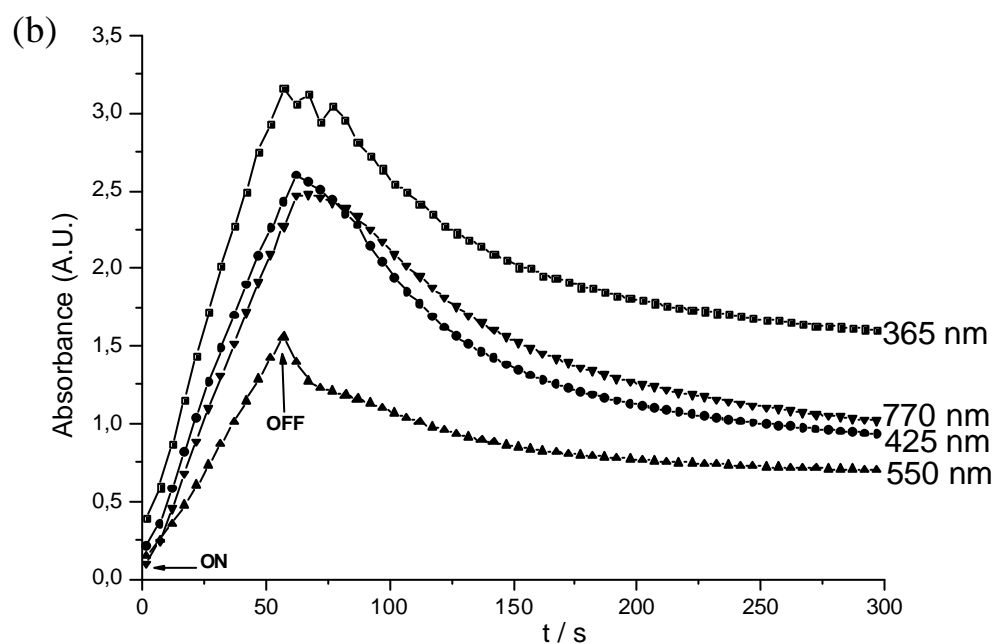
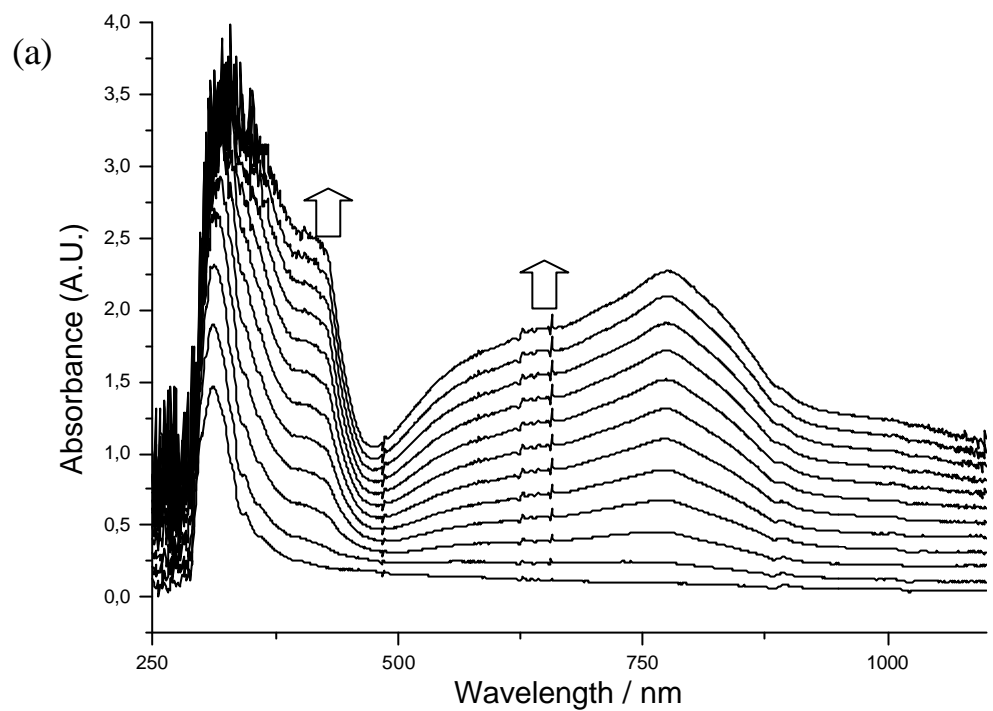


Figure 3.2. (a) The changes in the electronic absorption spectrum of 6.0×10^{-2} M DB18C6 in 0.1 M TBABF₄ dissolved in CH₃CN/CH₂Cl₂ mixture during *in-situ* CPE at 1.4 V. (b) Time traces of specific absorption bands during the CPE and after stopping the electrolysis.

decrease exponentially, which indicates that thin poly(DB18C6) film is not stable in its oxidized state, but it is more stable in its neutral state.

Formation of radical-cation was also monitored by *in-situ* recording of the ESR spectrum of the solution containing DB18C6 during constant current electrolysis at 225 K. The cell used for *in-situ* ESR studies described previously [112]. Upon starting the electrolysis using a constant current of 200 μA , a broad singlet appeared immediately, indicating the formation of radical-cations. This broad singlet can be resolved to a spectrum consisting of 13 lines (Figure 3.3) with $\Delta H = 0.06$ mT and $a_{\text{H}} = 0.11$ mT. The total width of the spectrum was 1.54 mT. The smaller linewidth of the radical cation (0.06 mT) compared to that of benzene radical cation (0.19 mT) [113] also indicates the formation of polyaromatic structure since the decrease in the spin density causes smaller linewidths. Although, a seven line spectrum is consistent with the triphenylene radical cation, presence of 13 lines led us to think the formation of a triphenylene radical cation-radical cation π -stacked dimer (a salt like structure) or triplet state di(radical cation) in the triphenylene moiety. In fact, V. Le Berre et al, also reported the formation of such salts from B15C5 [82].

The decay of ESR signal was also measured at various temperatures after stopping the electrolysis and it is found that decay of the signal better fits to a first order kinetics. Apparent activation energy for the decay was found to be 0.2 J/mol from the Arrhenious plot (Figure 3.4 (a) and (b)). This low value of activation energy is consistent with the first order radical decay and its half life at -8 °C is 131 s.

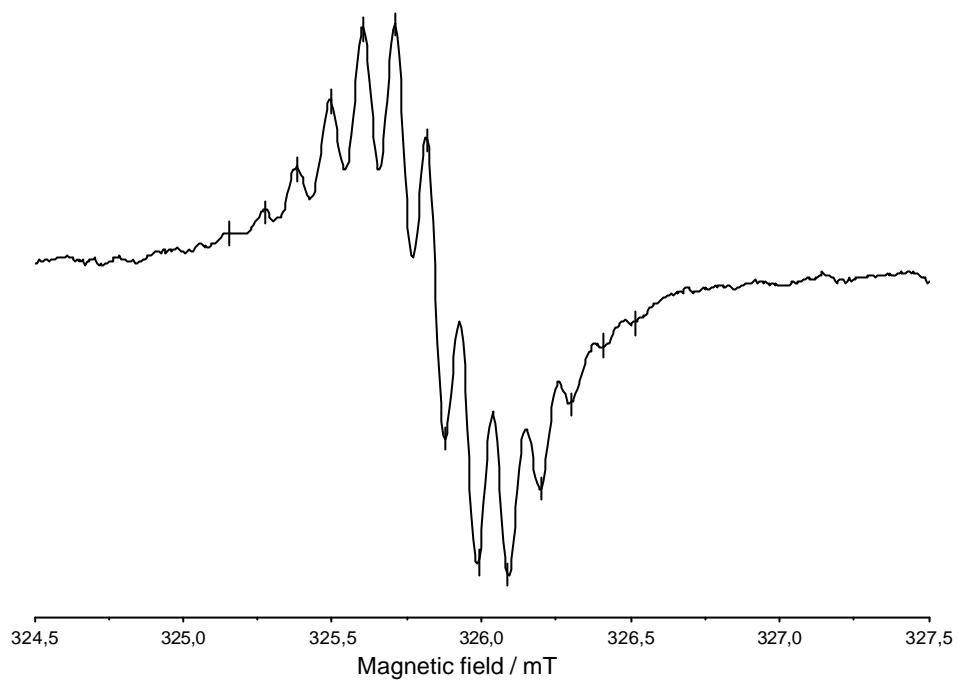


Figure 3.3. ESR spectrum of 1.0×10^{-2} M DB18C6 recorded at 225 K during the constant current of 200 μ A electrolysis in 0.1 M TBABF₄ dissolved in CH₃CN/CH₂Cl₂ mixture.

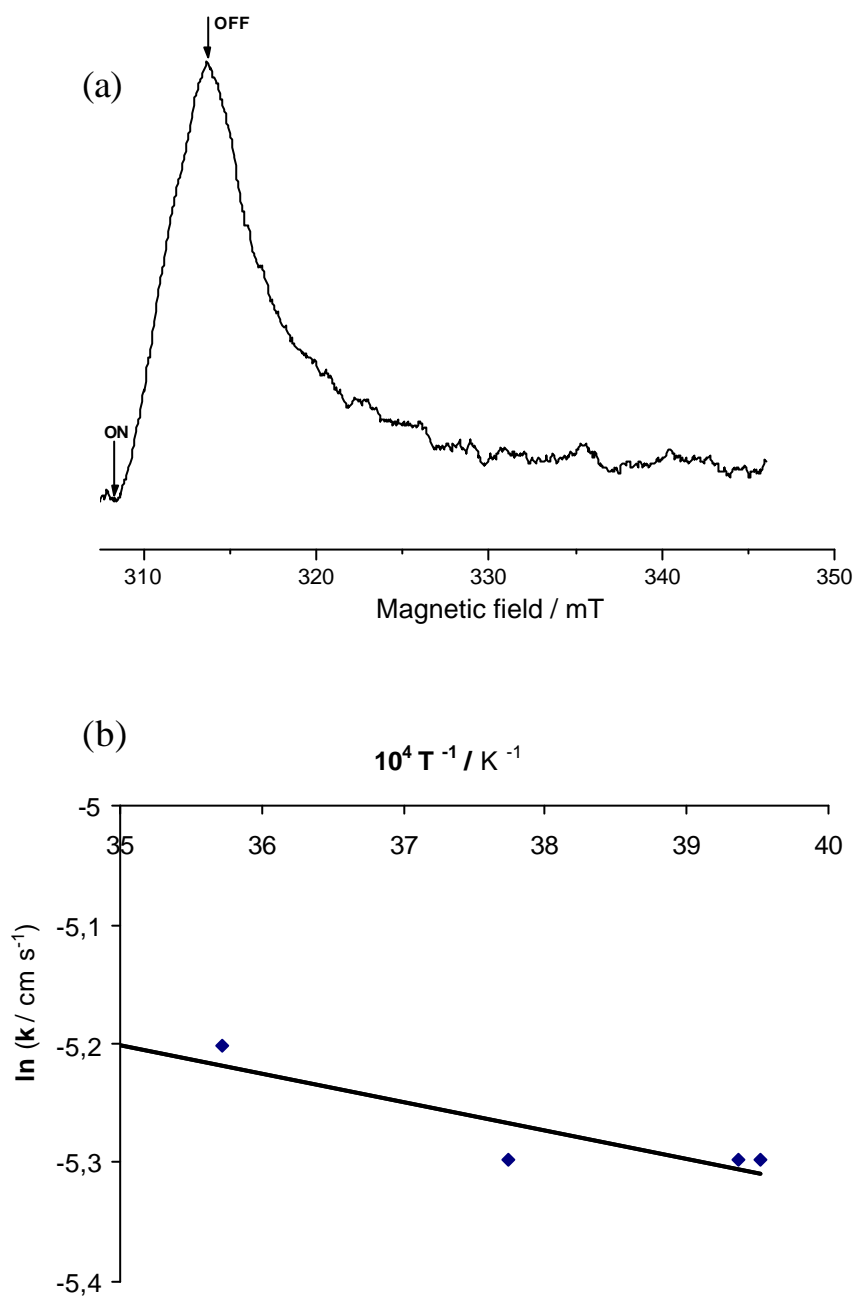


Figure 3.4. (a) Time traces of ESR signal intensity recorded during and after the constant current electrolysis of 1.0×10^{-2} M DB18C6 in 0.1 M TBABF₄ dissolved in CH₃CN/CH₂Cl₂ mixture. (b) The Arrhenius plot according to first order radical decay.

3.3. Polymer Characterization

Characterization of the resulting polymers was carried out using FTIR spectroscopy. Figure 3.5 (b) and (c) depict the FT-IR spectra of BF_4^- and PF_6^- doped poly(DB18C6) films, respectively. FT-IR spectrum of the monomer, DB18C6, is also given in Figure 3.5 (a) for comparison.

The absorption bands attributed to dopant BF_4^- counter-anion are hidden by the polymer etheric bands. In contrast, in the case of PF_6^- , the absorption band at 840 cm^{-1} related to this anion.

The conductivity of poly(DB18C6) film was measured using two-probe technique and it is observed that the resistance value increases in time when the film is kept in contact with air. However, there was no change in the resistance value when the film is kept under vacuum. This observation was also confirmed by ESR measurements conducted on the films. Although it is reported that poly(DB18C6) film exhibits a symmetric singlet [86], we observed an ESR signal with a Dynosian and asymmetric ($A/B=2.5$) line shape for the polymer film kept under vacuum (see Figure 3.6 (a)). However, in the presence of air, the signal shows almost symmetric behavior ($A/B=1.1$) (see Figure 3.6 (b)). This behaviour and the increase in the resistance are due to the loss of conductivity. Such decay in conductivity is usually explained due to the oxidation of polymer films during storage. However, poly(DB18C6) is known as an oxidizing polymer [103]. Thus, the decay in the conductivity and the change in the line shape could be most probably due to moisture.

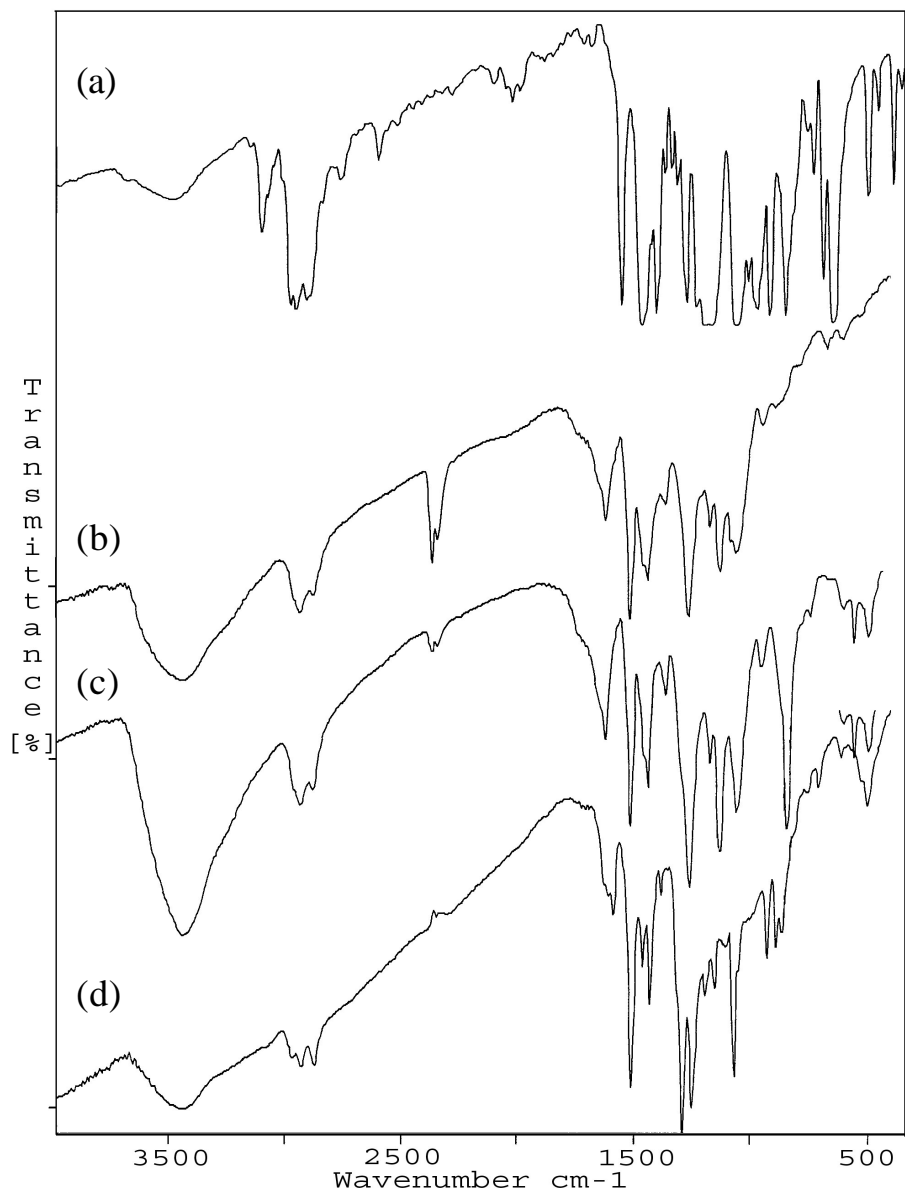


Figure 3.5. FTIR spectra of (a) DB18C6, (b) BF_4^- doped poly(DB18C6), (c) PF_6^- doped poly(DB18C6) and (d) PF_6^- doped poly(DB18C6) after thermal treatment.

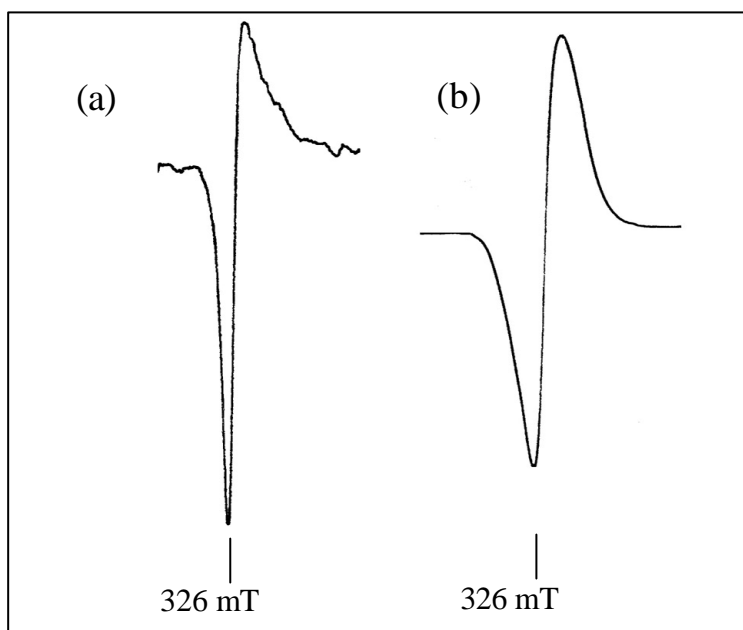


Figure 3.6. ESR spectrum of poly(DB18C6) film (a) kept under vacuum (b) kept under open air.

V. Le Berre et al [86] reported that the decay of ESR signal was not due to nucleophilic species like water present in the matrix of the polymer but instead due to indirect oxidation of electrolyte. Since the decay of ESR signal was not observed for the polymer film kept under vacuum, the role of nucleophilic species should not be ruled out.

3.4 ESR and UV-VIS SPEL Measurements on Poly(DB18C6) Films

Electronic absorption spectrum of the polymer film deposited on ITO by CPE at 1.40 V (100 mC/cm²) was monitored during *in-situ* CV studies in CH₂Cl₂-TBABF₄ solvent electrolyte couple and the results are given in Figure 3.7 (a). As seen from the figure, one ill-defined absorption band at 320 nm ($\pi \rightarrow \pi^*$ transition) and two bands at 420 nm ($\pi \rightarrow \pi^*$ transition) and 770 nm (radical cation) intensify during the anodic scan from 0.0 V to 0.9 V vs Ag-wire.

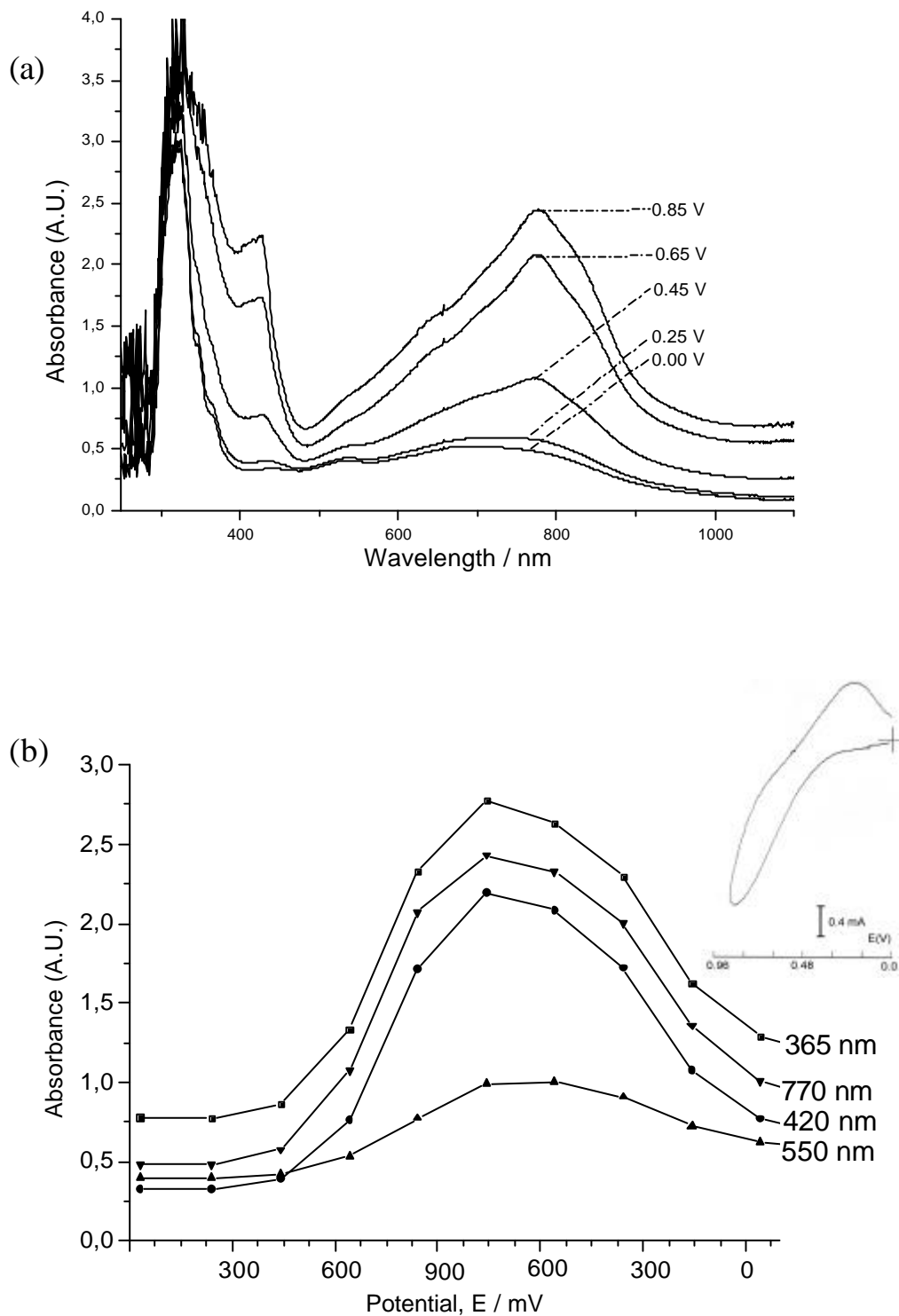


Figure 3.7. (a) The changes in the electronic absorption spectrum of poly(DB18C6) film on ITO electrode recorded during the anodic scan from 0.0 V to 0.9 V. (0.1 M TBABF₄ dissolved in CH₂Cl₂, voltage scan rate : 20 mV/s). (b) Spectroelectrochromic behaviour of poly(DB18C6). Inset: CV of poly(DB18C6) coated on ITO.

These bands lose intensity during the reverse scan (0.90 V to 0.0 V). The spectrovoltametric behaviours of these bands are also given in Figure 3.7 (b) together with CV of the film on ITO (inset of Figure 3.7 (b)). These spectral changes are also accompanied with a color change from light blue to green during the anodic scan.

Although poly(DB18C6) films on Pt WE surface can be cycled reversibly between 0.3 V and 1.85 V in CH_2Cl_2 (see Figure 3.8 (a)) and between 0.3 V and 1.3 V in CH_3CN (see Figure 3.8 (b)), further oxidation beyond the given upper limits diminishes the reversibility, it can be cycled reversibly up to 0.9 V when the film is on the ITO surface (Figure 3.8 (c)). The electronic absorption spectrum of the neutral form of the polymer film exhibits only the 320 nm band and from its commencement on the low energy end, the band gap was found to be 3.9 eV [111,114]. This value is relatively high when compared to common conducting polymers; however, it is consistent with the low conductivity of the polymer film.

The changes in the ESR spectrum of the film during its oxidation (doping) and reduction (dedoping) were also monitored. Poly(DB18C6) film was coated on a thin Pt wire (0.5 mm x 2 mm) that was used as WE of the ESR cell. The oxidation and reduction of polymer film was followed in the monomer free solution containing TBABF_4 as supporting electrolyte. The thin film exhibits an asymmetric signal which intensifies during oxidation with a constant current of 100 μA and it decreases during the reduction using the same current density (Figure 3.9). However, the same asymmetric signal starts to intensify immediately upon reversal of polarity (i.e., during oxidation), which indicates the reversibility of doping-dedoping processes.

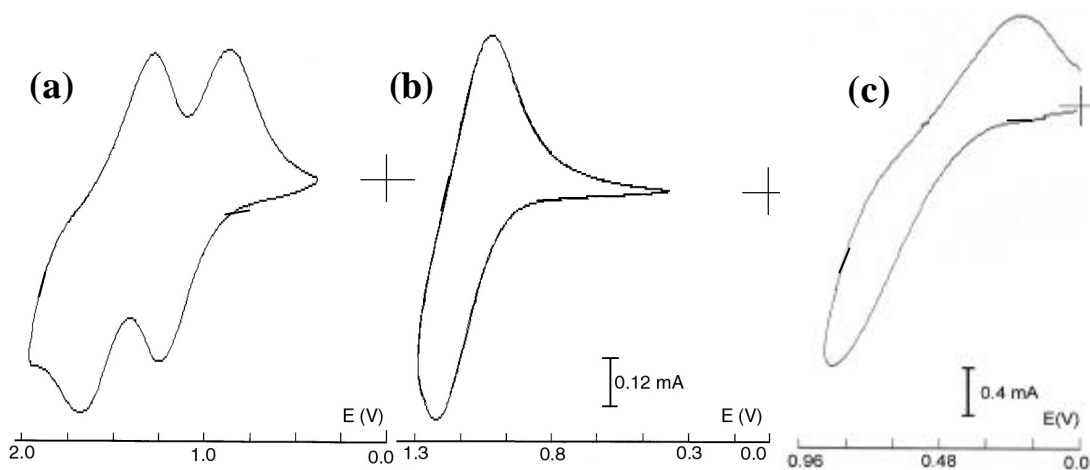


Figure 3.8. CV of poly(DB18C6) coated on Pt electrode recorded in 0.1 M TBABF₄ dissolved (a) in CH₂Cl₂, (b) in CH₃CN and (c) coated on ITO electrode recorded in 0.1 M TBABF₄ dissolved in CH₂Cl₂.

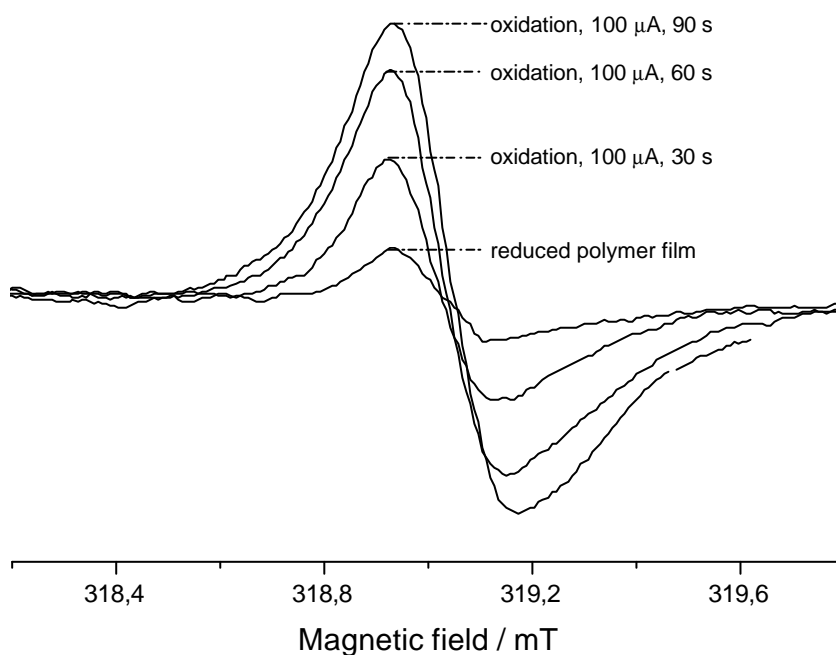


Figure 3.9. ESR spectra of oxidized poly(DB18C6) using constant current of 100 μ A in 0.1 M TBABF₄ dissolved in CH₂Cl₂ at room temperature.

3.5 Thermal Behavior of Poly(DB18C6)

Thermal stability of poly(DB18C6) was investigated using DSC and TGA. As shown in Figure 3.10 (a), in DSC thermograms, the polymer film doped by BF_4^- shows an endothermic transition at about 74 °C due to the removal of the solvent, especially CH_3CN , and it has also a glass transition temperature (T_g) at about 220 °C. Moreover, a sharp exothermic transition appears at 378 °C. Since this exotherm is not followed by a corresponding melting endotherm, the exotherm could be due to an organizational process which is accompanied by dopant loss and during this process polymer film starts to decompose slightly. As shown in Figure 3.10 (a), repeated cycling shows that only the transition corresponding to T_g at about 217 °C remains with no exothermic transition. Dopant loss was also confirmed using FTIR spectroscopy. For this reason, poly(DB18C6) was prepared using TBAPF_6 as supporting electrolyte since PF_6^- dopant has a specific band at 840 cm^{-1} which is not hidden by the polymer film. The polymer film doped by PF_6^- has a T_g at about 144 °C and shows an exotherm at about 312 °C (see Figure 3.10 (b)) at which dopant loss was confirmed by the disappearance of the absorption band related to PF_6^- dopant in FTIR in Figure 3.5 (d). Notice that, during dopant loss, the polymer film decomposition starts immediately, especially in the structure of the polyoxochains. DSC thermograms show that dopant species affect both the T_g and thermal stability of the polymer film. It is observed that BF_4^- doped polymer film has a higher stability and a higher T_g value than that of polymer film doped by PF_6^- . This may be due to the plastisizer effect of PF_6^- dopant in the polymer matrix.

TGA was also used to confirm DSC measurements. TGA thermograms for the polymer doped by PF_6^- show a maximum weight loss at 342 °C and then also a slight weight loss appears at 474 °C, which are related to dopant loss and decomposition of polyoxochains, respectively (Figure 3.11 (b)). At 830 °C the polymer loses about 45% of its weight and the rest consists of mainly triphenylene moiety. The similar behaviour was observed for the polymer doped by BF_4^- in Figure 3.11 (a).

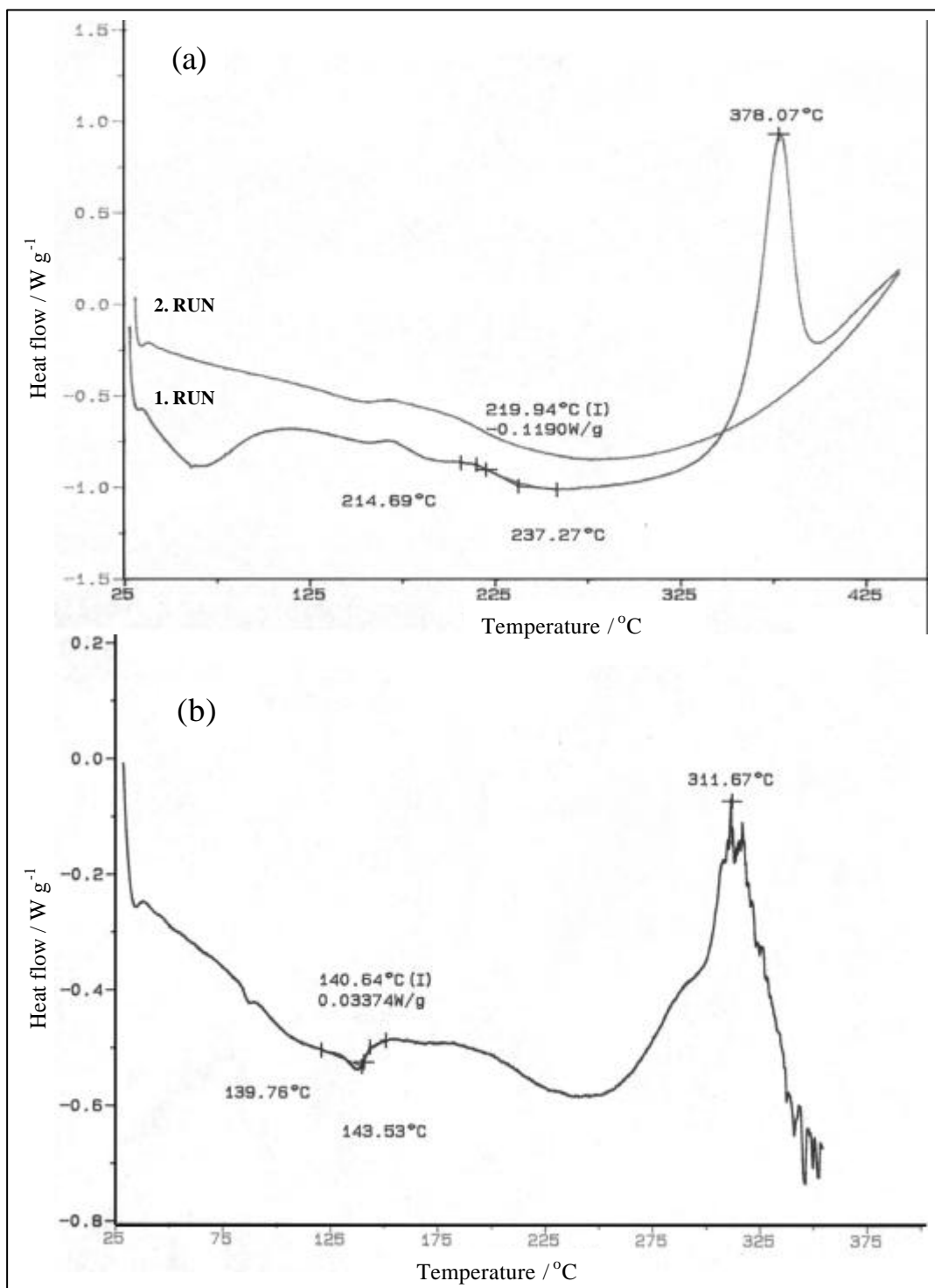


Figure 3.10. DSC thermogram of (a) BF_4^- doped poly(DB18C6) and (b) PF_6^- doped poly(DB18C6).

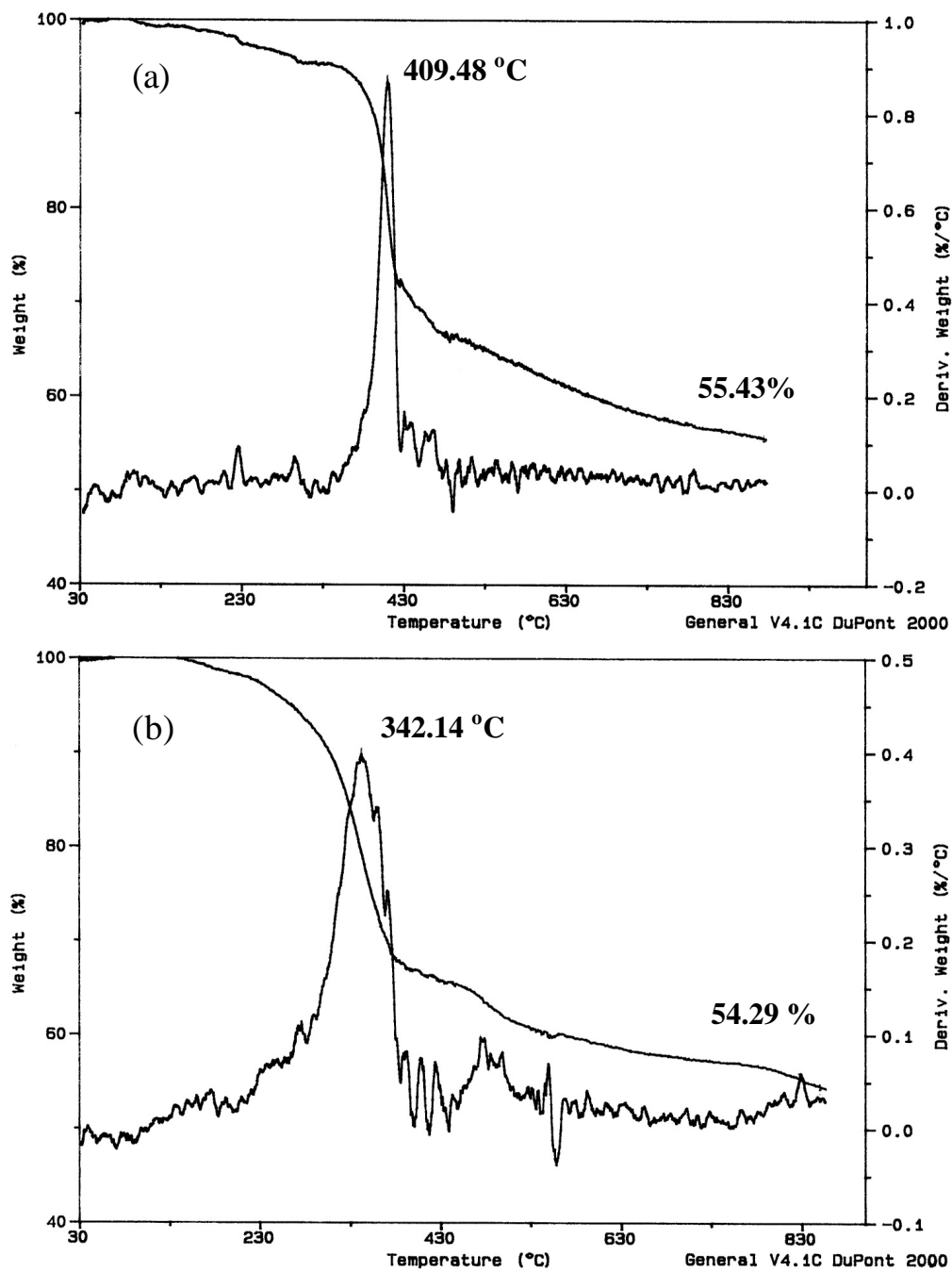


Figure 3.11. TGA thermogram of (a) BF_4^- doped poly(DB18C6) and (b) PF_6^- doped poly(DB18C6).

3.6 Electrical, Optical and Photoconductive Properties of Poly(DB18C6)

The room temperature conductivity (σ) value of poly(DB18C6) film is found to be $6.2 \times 10^{-5} \text{ S cm}^{-1}$. In order to find out the dominant carrier transport mechanism in the films, the temperature dependence of the dark electrical conductivity was examined in the temperature range of 200-550 K. Below 200 K, the sample resistance exceeds $10^{10} \Omega$ and electrical measurements could not be carried out due to instrumental limitations. Variation of the dark electrical conductivity as a function of reciprocal temperature is given in Figure 3.12. In general, the conductivity decreases exponentially with decreasing temperature at higher rates in the high temperature region (above 420 K).

In the amorphous materials, if the main conduction is due to the carriers excited beyond the mobility edge into non-localized or extended states which tends to occur at high temperatures, the conductivity is observed to follow the relation [52],

$$\mathbf{s} = \mathbf{s}_{0i} \exp\left(-\frac{E_{si}}{kT}\right) \quad (1)$$

where s_{0i} is the pre-exponential factor and E_{si} is the conductivity activation energy level in a specific temperature range (denoted by the letter i). The values of E_{s1} , E_{s2} and E_{s3} calculated from the linear slopes of $\ln(s)T^{-1}$ using Eqn. (1) (see the solid lines of Figure 3.12) are found to be 0.93, 0.32 and 0.76 eV in the temperature ranges of 550-420 K ($i=1$), 410-320 K ($i=2$) and 310-260 K ($i=3$), respectively.

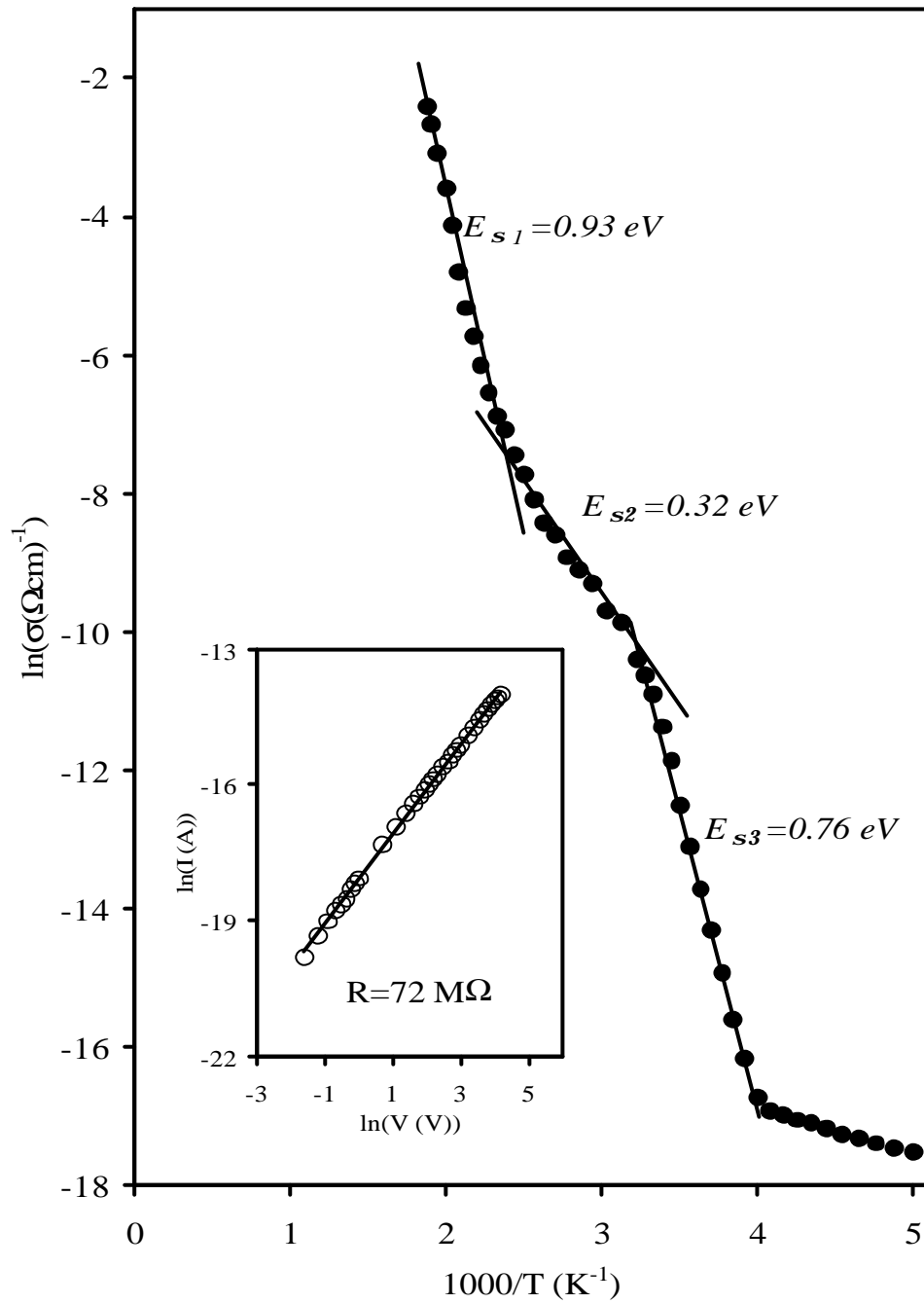


Figure 3.12. Variation of conductivity with temperature for poly(DB18C6) films. Inset shows the I-V characteristics of the films at 300 K.

The value 0.93 eV energy level is also observed as a broadening in the photocurrent spectra located at ~1350 nm. The calculated activation energies are less than $E_g/2$, implying that not the intrinsic but the tail states conduction is the dominant conduction mechanism above 260 K. Below 260 K the $\ln(s)T^{-1}$ variation is very weak with an activation energy slightly changing with temperature indicating the weak temperature dependence of activation energy. The mean value of the conductivity activation energy in this range is ~ 0.06 eV. As it is clear from the above calculations the activation energy exhibits a sudden change from 0.72 to ~0.06 eV. The presence of the weak temperature dependent activation energy and the sharp decrease in its value below 260 K implies that the conduction mechanism due to excitation of charge carriers into the mobility edge and/or the localized states at the band edge may have changed.

Due to the above mentioned reasons, the s - T data was analyzed according to Mott's hopping mechanism [52]. The expression for the conductivity with the correction for the temperature dependence of the effective density of states [52,115] is,

$$s\sqrt{T} = s_2 \exp\left(-\left(\frac{T_0}{T}\right)^{1/4}\right) \quad (2)$$

In the low temperature region (below 260 K), $sT^{1/2}$ was plotted as a function of $T^{-1/4}$ on a semi-logarithmic scale and the variation is observed to exhibit linear behavior as illustrated in Figure 3.13. Thus, below 260 K, variable range hopping is probably the transport mechanism in the amorphous poly(DB18C6) films. The ratio (T_0/T) which represents the degree of disorder in the samples around a specific temperature is of the order of 10^4 indicating that the films are of amorphous nature.

Variation of photocurrent (I_{ph}) was investigated by applying different light intensities (F) at room temperature. The photocurrent was measured along the layer, while the light was incident perpendicular to the layer. The illumination was done using a halogen lamp with the light being filtered using high resolution neutral discrete filters. The resolution of the filters was better than 2 meV. Figure 3.14 illustrates the photocurrent spectra of the film at 300 K being studied in the photon wavelength range of 1550-214 nm (0.8-5.8 eV). The photocurrent has a response over a wide range and has a main peak at 320 nm which should correspond to a band gap of 3.9 eV.

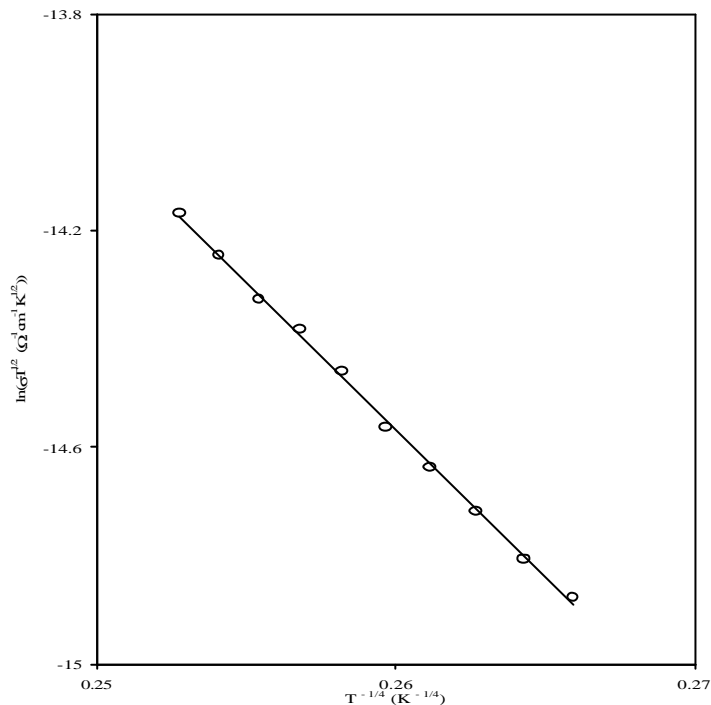


Figure 3.13. Variation of $\ln(s T^{1/2}) - T^{-1/4}$ below 260 K.

As it's clear from the spectral response of the photocurrent, the poly(DB18C6) film has six peaks located at 320, 425, 550, 770, 950, 1050 nm and a broadening at 1350 nm (0.93 eV). Most of these peaks were also observed in the electronic absorption spectra of the film (see the inset of Figure 3.14) recorded in

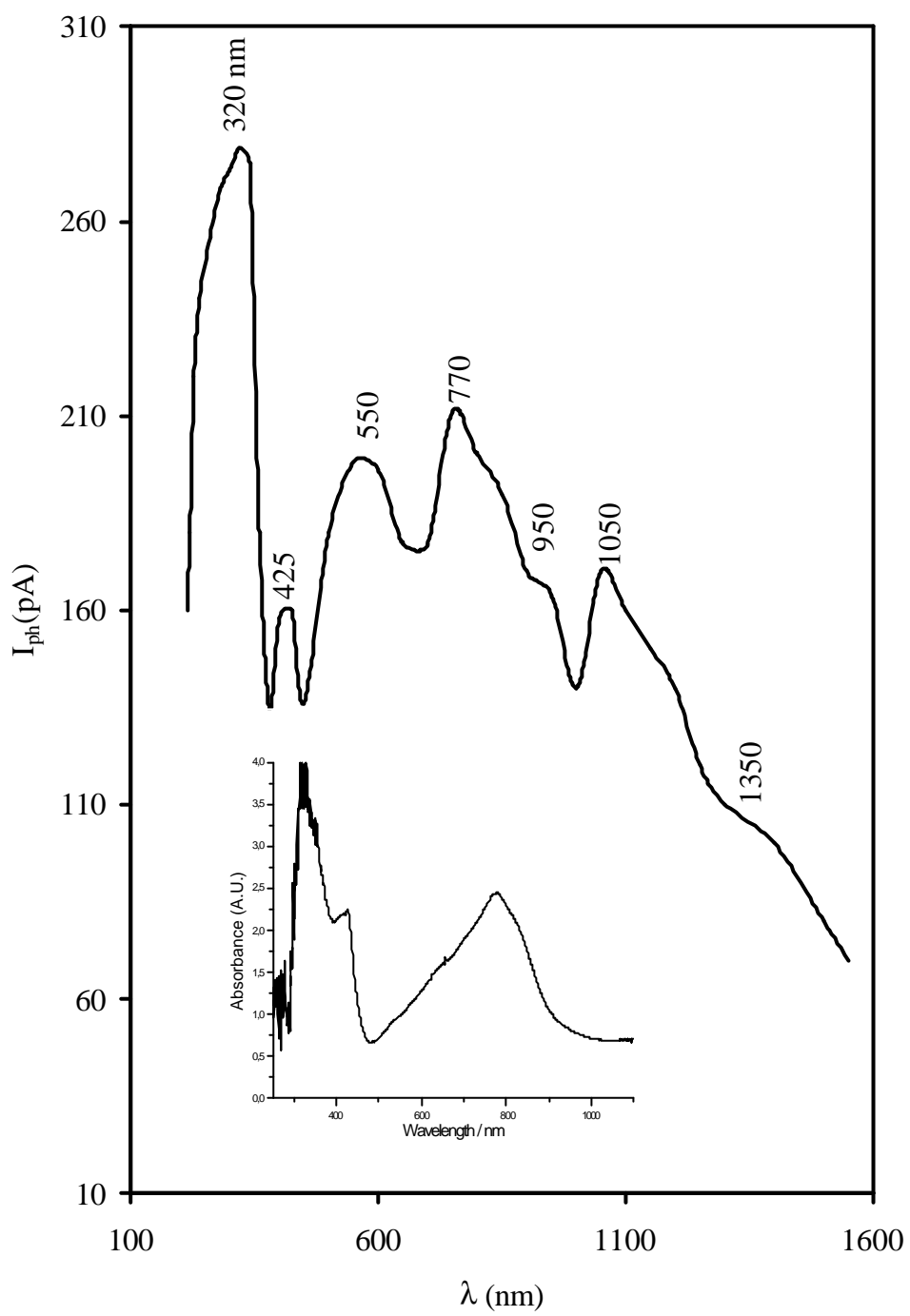


Figure 3.14. Photocurrent spectrum of poly(DB18C6) film at 300 K.

a solution of anhydrous CH_2Cl_2 with TBABF_4 . The first two intense peaks are related to the $p \rightarrow p^*$ transition of the triphenylene moiety and the other peaks are related to the radical cations [82].

Figure 3.15 illustrates the variation of I_{ph} as a function of illumination intensity. The photocurrent is found to increase with increasing illumination intensity. The variation of I_{ph} with F could be divided into three distinct regions: the low, $32 < F_{lo} < 60$; intermediate, $63 < F_{md} < 122$; and high $125 < F_{hi} < 155 \text{ mWcm}^{-2}$, intensity regions. In general, $I_{ph} \propto F^g$ and g is found to have three different values in the three intensity regions. In the low intensity region, g_{lo} is 0.5 indicating bimolecular recombination (sublinear recombination) at the surface, the intermediate region, g_{md} is 1.0 (linear) pointing out the a strong recombination at the surface and the high intensity region, g_{hi} is 1.7 (supralinear) indicating a stronger recombination at the surface [116]. Recalling that the free carrier life time, t may itself be a function of excitation rate following the relation

$$t \propto F^{g-1} \quad (3)$$

, then $g = 1.0$ regime is an indication of the free electron life time being constant with illumination intensity. For $g < 1.0$, the life time decreases with increasing illumination intensity. For $g > 1.0$, the life time increases with increasing illumination intensity showing the supralinear character. Thus, Figure 3.15 illustrates the regions where the free carrier life time is changing and/or remaining constant with illumination intensity at room temperature.

For the aid of technological applications and the confirmation of I_{ph} - F data analysis, the time dependence of the photocurrent was measured at $F = 63$ (F_{md} region, $g_{md} = 1.0$, constant life time). Inset-1 of Figure 3.15 shows the growth and decay of the photocurrent in poly(DB18C6) film recorded at 300 K. After the light is turned on, the photocurrent readily reaches a stationary level that is practically independent of the previous poling. Current relaxation is also clearly evidenced,

showing an initial drop by 44 times of magnitude in few seconds, which is followed by a gradual decay in which the current remains constant for several hours. Inset-2 of Figure 3.15 illustrates the semi-logarithmic plot of I_{ph} as function of decay time.

The plot of $\ln(I_{ph})-t$ is linear with a slope of 0.039. Recalling that the response time, t_{res} , of the photocurrent is the time required to reach $1/e$ of the original value and represented by the relation [117],

$$I_{ph} = I_0 \exp(-t/t_{res}) \quad (4)$$

with I_0 being the maximum value of photocurrent before the light is turned off, then in accordance with Eqn. (4) and the slope calculated from inset-2 of Figure 3.15, t_{res} is 25.6 s. This parameter plays an important role in determining the modulation frequency of a time dependent working device in technological applications.

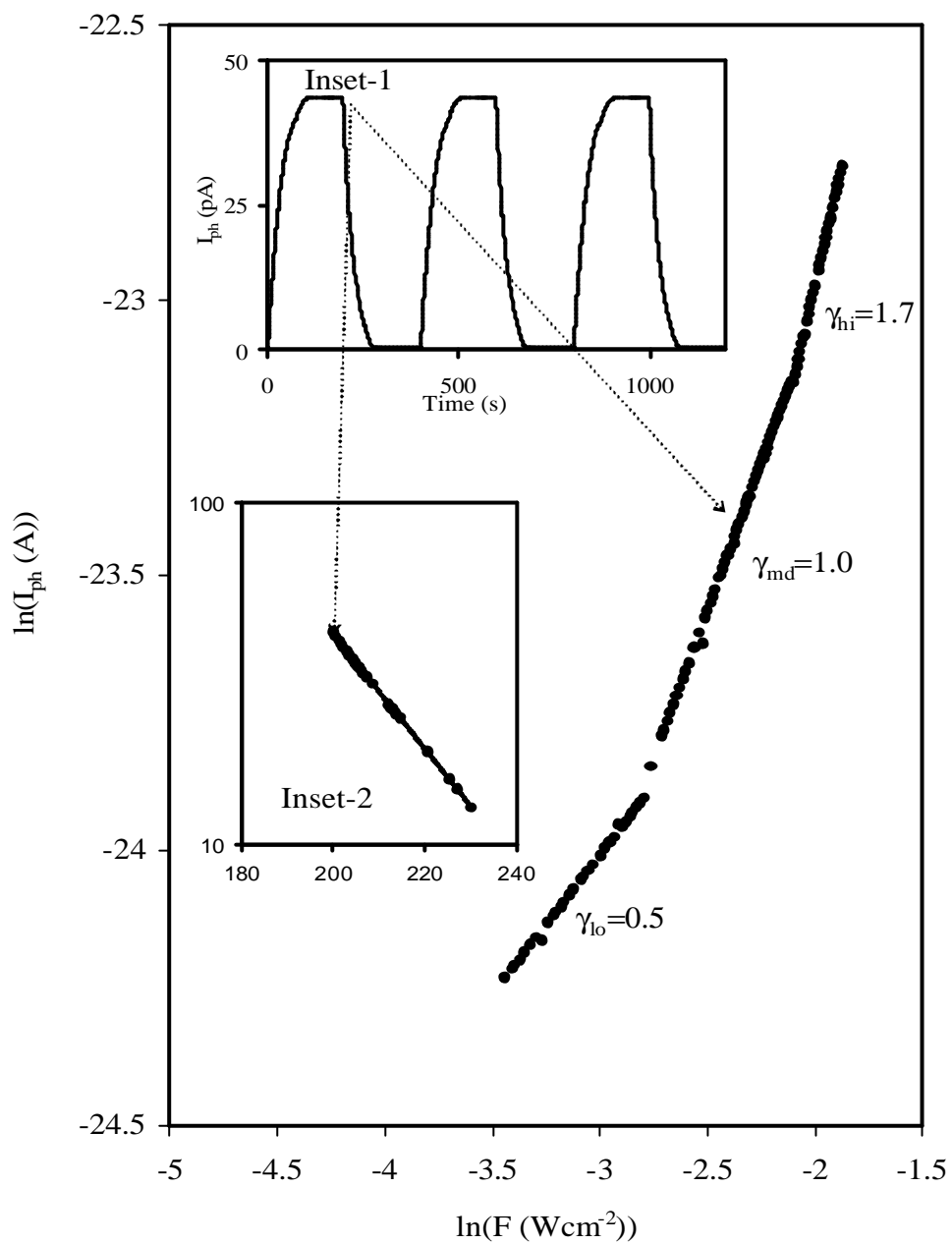


Figure 3.15. I_{ph} - F dependence at 300 K for poly(DB18C6) film. Inset-1 shows the time dependence of I_{ph} . Inset-2 is an enlargement of the decay part of inset-1.

It can be seen that the length of polyether spacer has little effect upon the anodic peak potential values for monomers, which is in agreement with the electrochemical results obtained for other polyether functionalized monomers, such as Py [118] and fluorene [119]. Since the polyether unit is known to be electrochemically inert up to 2.0 V, the first anodic peak is most probably due to the electron loss from the Th ring [103].

3.7.2 Electrochemical Polymerization of I and II

In the light of CV studies, the anodic electropolymerization of **I** and **II** was first tried at 2.0 V vs Ag-wire. However, it is observed that products that form on the WE surface diffuse into the electrolytic medium at this potential. Although, other solvents like propylene carbonate and CH_2Cl_2 were also tried, they were all found to be ineffective to prevent diffusion. Therefore, CPE of **I** and **II** was tried at a higher potential (i.e., 2.5 V vs Ag-wire). Upon starting CPE at this potential, the film formation and passivation of the electrode was observed after a certain time. The polymer film was washed with CH_2Cl_2 , peeled off from the electrode surface and dried under vacuum at 60 °C for 12 h. A dark brown electroinactive polymer film was obtained and characterized using FTIR spectroscopy.

Figure 3.17 (a) and (b) depict the FTIR spectra of monomer **I** and its polymer obtained via CPE at 2.5 V, respectively. A close inspection of Figure 3.17 clearly shows the disappearance of the peak at 2866 cm^{-1} attributed to methylene, $-\text{CH}_2-$, groups of polyetheric bridge between two Th rings. Furthermore there is a sharp decrease in the intensity of the peak at 1093 cm^{-1} corresponding to $-\text{C}-\text{O}-\text{C}-$ stretching of the polyether bridge. The sharp peak at 840 cm^{-1} is due to PF_6^- dopant anion and clearly indicates incorporation of the dopant anion into polymer matrix. The presence of 802 cm^{-1} indicates a-a' coupling which is also confirmed by the absence of the peaks at 820 and 730 cm^{-1} due to a- β coupling.

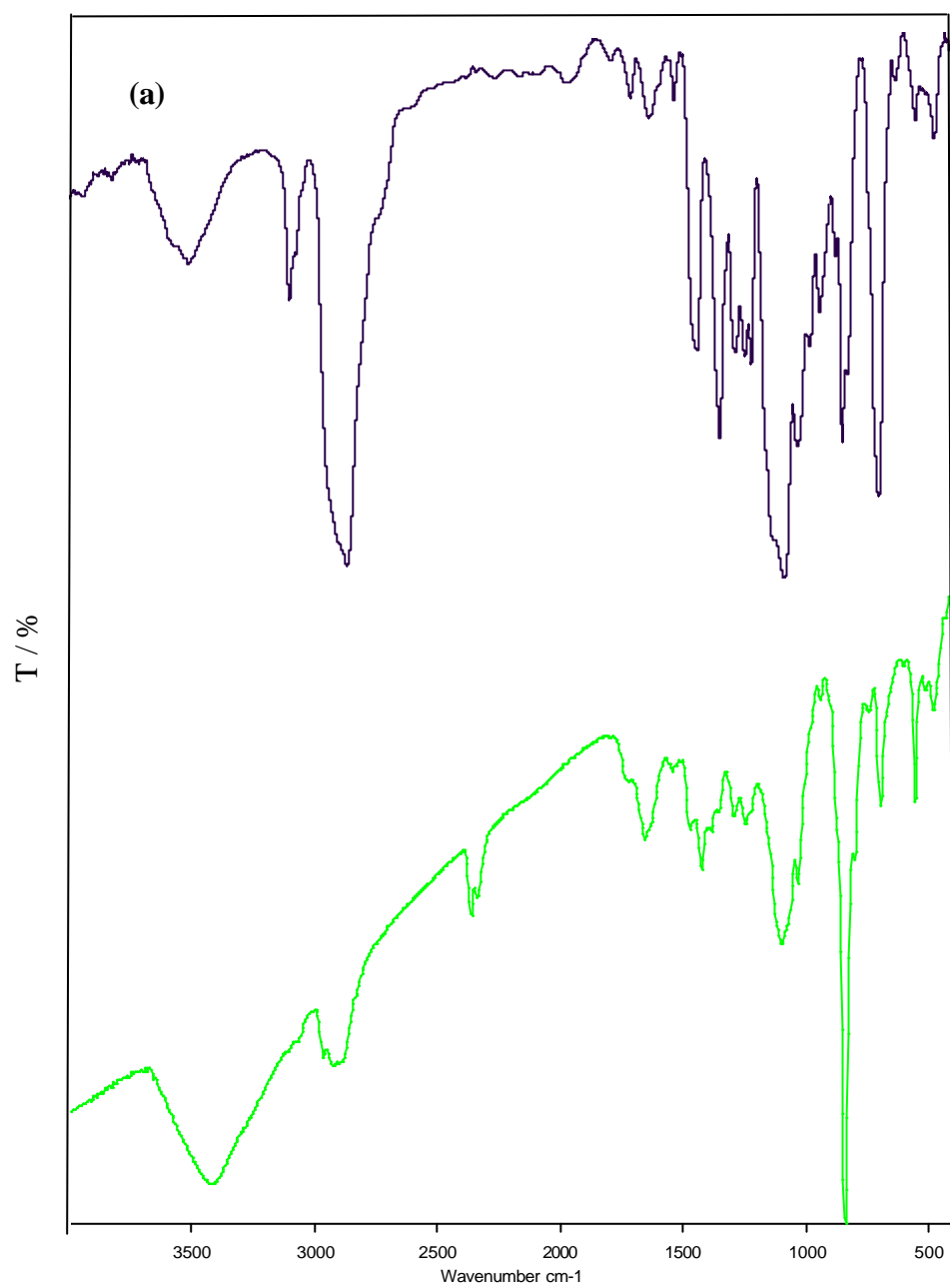


Figure 3.17. FT-IR spectra of (a) monomer **I** and (b) its polymer obtained from the anodic polymerization.

3.7.3 Chemical Polymerization of I and II

To compare the results of electrochemical polymerization, chemical polymerization was performed using FeCl_3 in CHCl_3 . After precipitation with MeOH, the precipitate was washed with CH_2Cl_2 and fractionated into two parts as CH_2Cl_2 soluble (**s**) and CH_2Cl_2 insoluble (**is**) products. The soluble (**s**) and insoluble (**is**) parts were characterized using $^1\text{H-NMR}$ spectroscopic technique. $^1\text{H-NMR}$ spectra of **s** and **is** parts were recorded in CDCl_3 and in DMSO, respectively. $^1\text{H-NMR}$ spectrum of **s** part has two broad bands between 6.5 and 7.5 ppm (Th rings) and between 3.6 and 4.2 ppm (2-substituted methylene groups (for the monomer **I**, 2-substituted methylene groups are at about 4.8 ppm)), whereas that of **is** part in DMSO has three broad bands between 1 and 4 ppm due to the methylene groups of polyetheric structure. Also, the FTIR spectra of **is** part and the polyethyleneglycol in the literature are the same when compared.

In order to predict the structure of polymeric product, monomer **I** and its precursor, 2-thiophenemethanol (2ThMeOH), was also polymerized by using I_2 as chemical oxidizing agent. Chemical polymerization of 2ThMeOH and monomer **I** was carried out in I_2 dissolved in CH_2Cl_2 by refluxing the solution for 24 h. In the case of 2ThMeOH, the insoluble shiny black polymer was obtained after washing with CH_2Cl_2 . On the other hand, the solution was poured into MeOH to precipitate the polymer in the case of monomer **I**. Then the precipitated product and MeOH soluble part were dried under vacuum and characterized by FTIR spectroscopic technique. The FTIR spectrum of product obtained from chemical oxidation of 2ThMeOH, **I** (s part) with FeCl_3 and **I** (precipitate) with I_2 is given in Figure 3.18.

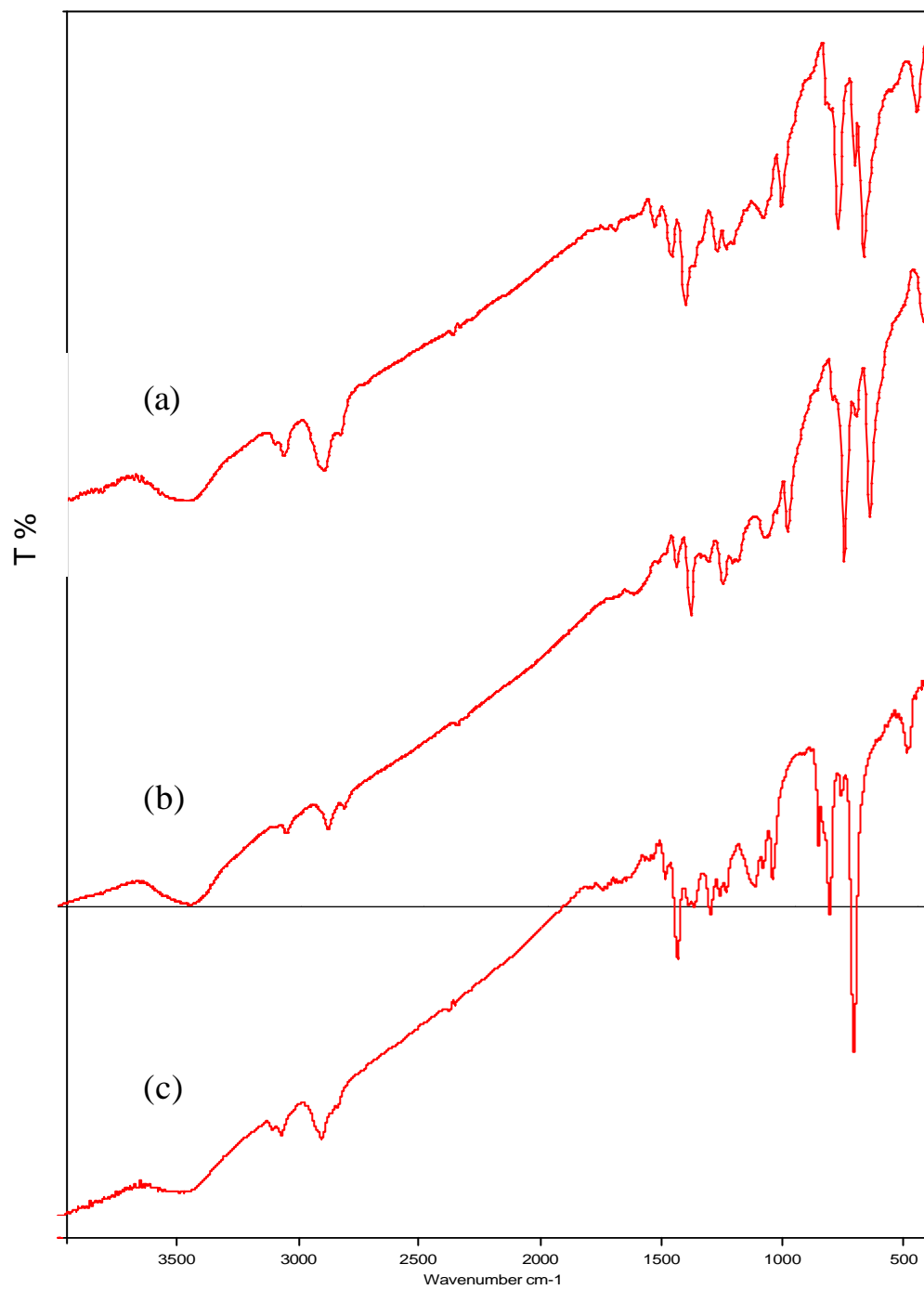


Figure 3.18. FTIR spectra of the products obtained from the chemical polymerization of (a) 2ThMeOH, (b) **I** (s part) with FeCl₃, and (c) **I** (s part) with I₂.

As seen from the Figure 3.18, these three polymers have very similar FT-IR spectra, which indicates that chemical oxidation of monomer **I** and **II** gives poly(2,2'-bithiophenemethylene)s as a main product due to the cleavage of polyether bridges.

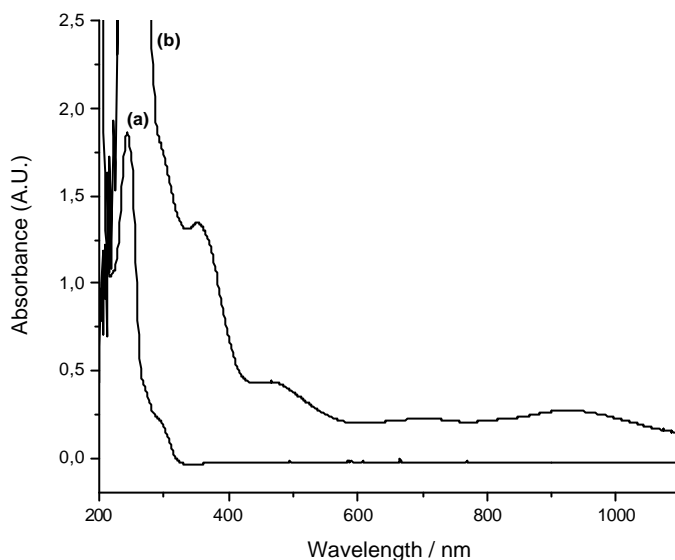


Figure 3.19. UV-VIS spectra of (a) monomer **I** and (b) the polymer obtained from the chemical polymerization of **I** with I_2 .

Figure 3.19 shows the electronic absorption spectrum of CH_2Cl_2 solution of the polymer obtained from the chemical oxidation of **I** with I_2 . The band at 255 nm is associated with the $\pi-\pi^*$ transition of the aromatic Th ring, resembling the same transition as for the monomer. The band at 352 nm corresponds to the $\pi-\pi^*$ transition of the aromatic biTh moiety. Interestingly, there exist also broad bands beyond 440 nm. The presence of it would not agree with structures consisting of isolated, repeating biTh units. Thus, analysis of the electronic absorption spectrum of the polymer indicated that the polymer may contain not only segments with broken π -conjugation, but also quinoidal segments [120,121]. Since quinoidal structures dramatically shift UV-VIS absorptions to longer wavelengths [120-122], the observed red shift of the bands at 255 and 352 nm with respect to Th and

biTh is also in accordance with the presence of extended quinoidal segments in the polymer structure.

As already demonstrated for 2-thienyl carbinols [123-125], polyetheric substituted Ths would be very susceptible to acid catalyzed elimination. On the basis of this information, chemical polymerization of **I** and 2ThMeOH was also carried out using $\text{BF}_3 \cdot \text{Et}_2\text{O}$ in CH_2Cl_2 . The products were washed with CH_2Cl_2 and insoluble brown polymers were obtained. FTIR spectra of these polymers gave the same spectrum with the previous polymers obtained via chemical polymerization. The band at 1100 cm^{-1} is due to the BF_4^- dopant anion in the polymer matrix. Also, a series of poly(2,2'-bithiophenemethylene) was obtained (see Figure 3.20).

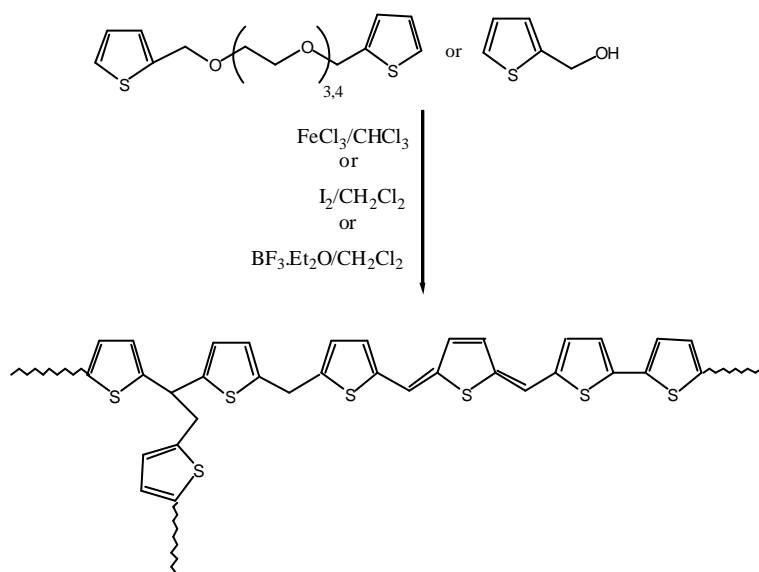


Figure 3.20. The assumed structures of the polymers obtained from the chemical polymerization of 2ThMeOH, and **I** (s part).

3.7.4 Electrochemical Behavior of **III**

As already demonstrated by Roncali et al. [126], at least two methylene bridges must be located between the Th ring and the first oxygen atom in order to neutralize the electron-withdrawing effect of ether groups on the conjugated system. For this purpose, monomer **III** was synthesized.

The electrochemical behavior of **III** was investigated in TBAPF₆ dissolved in CH₃CN using CV technique. Only one irreversible oxidation peak at 1.85 V vs SCE was observed during the anodic scan (see Figure 1.16). It is found that the intensity of this peak decreases during repetitive cyclings. Comparison with **I** and **II**, it shows that the observed oxidation peak is accounted for the formation of the Th radical cations. Also, 2-ethylene oxyethylene Th is more easily oxidized than Th and its 2-methylene oxyethylene substituted derivatives.

3.7.5 Electrochemical Polymerization of **III**

Electrochemical polymerization was carried out via CPE at 1.85 V vs SCE in 0.1 M TBAPF₆ dissolved in CH₃CN in the presence of 0.05 M **III**. The WE was coated with a flexible black polymer film. Since no new reversible peak for the doping and dedoping of the polymer was observed during repetitive cycling between 0.0 and 1.5 V in a monomer free electrolytic medium, the polymer obtained via CPE at 1.85 V is most probably a non-conducting polymer.

Coated WE was washed with CH₂Cl₂, peeled off from the electrode surface and dried under vacuum at 60 °C for 12 h. FT-IR spectrum of the polymer film was compared with that of the monomer **III** (Figure 3.21). Presence of bands at 2866 and 1093 cm⁻¹, attributed to the polyetheric groups, in the FT-IR spectrum of poly(**III**)

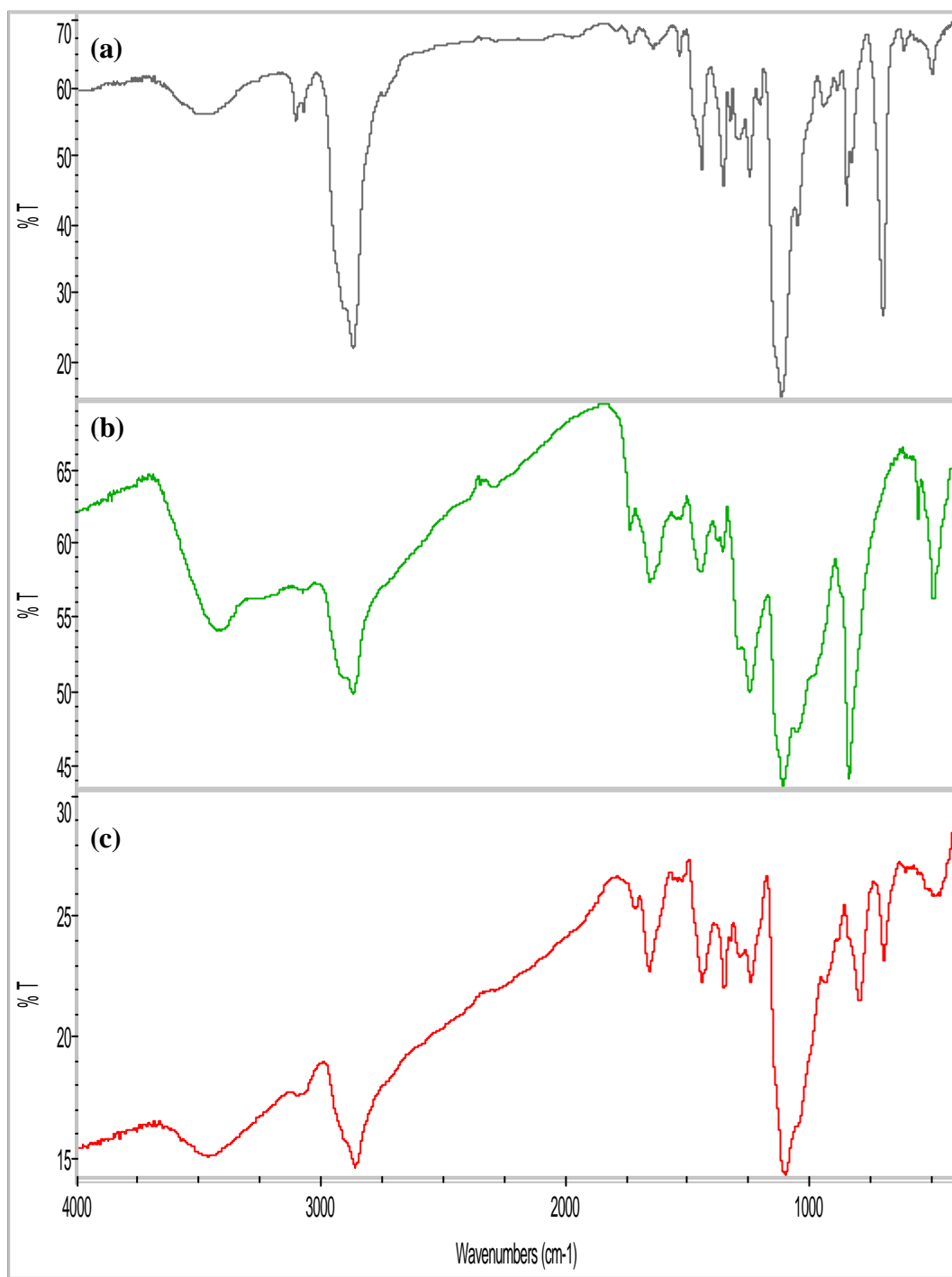


Figure 3.21. FTIR spectra of (a) **III**, (b) poly(**III**) by electrochemical polymerization and (c) poly(**III**) by chemical polymerization.

indicated that the polyetheric bridges between Th rings were not broken. Moreover, the peak due to the presence of dopant anion PF_6^- can be seen at 840 cm^{-1} .

3.7.6 Chemical Polymerization of **III**

The polymer was synthesized via FeCl_3 oxidative polymerization method and an insoluble black polymer film (not powder) was obtained. Comparison of the FTIR spectra of monomer **III** and its polymer (Figure 3.21 (a) and (c)) shows that polymerization was carried out from the 2-5 coupling (a-a' coupling) without any side reactions like a- β coupling. It is known that the α and β positions have about 95/5 relative reactivity for Th and decreases with the increasing number of attached Th along the polymer chain, but during the polymerization of **III**, only two Th ring can attach to each other. Therefore, This structure is anticipated, as coupling at the 5-position of Ths is electronically preferred to the 4-position so during the polymerization mislinkages at the 4-position were eliminated [109].

On the basis of this information, by the polymerization of related monomer, a regular polymer consisting of pseudo-polyether cages was obtained. The polymer structure in Figure 3.22 can be proposed for the polymers obtained from monomer **III** via chemical and electrochemical oxidation

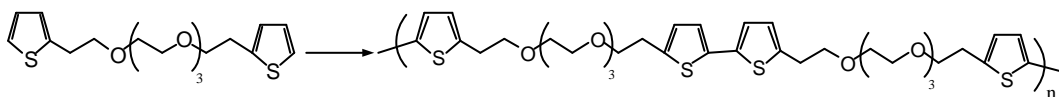


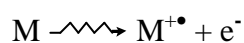
Figure 3.22. The assumed structures of the polymers obtained from the electrochemical and chemical polymerization of **III**.

3.7.7 Radical Cation: Mechanism of Polymerization

As it is explained in part 1.2.1, there are two possible routes for the formation of polymer during its electrooxidation. In order to get further information about the nature of the radical cations formed and their subsequent reactions, we have also irradiated monomer **I** and **II** both in pure form or by using Freon 113 /or Freon 11 as the matrix. The irradiation was carried out at 77 K using a total dose of 1 Mrad. The ESR spectra of the irradiated samples were recorded at various temperature ranging from 77 K to 150 K.

In the case of thio-derivatives **I** and **II**, the spectra obtained in F-113 and F-11 are similar and present the superposition, at least 2 signals—singlet in the central part and 2 pairs of outer lines with splitting about 13-16 G (arrows M: monomeric and D: dimeric, Figure 3.23). With the increasing temperature the singlet starts to resolve a spectrum of multiplet consisting of a sextet with 7-11 G splitting, e.g. at 150 K. These signals correspond to radical cations in monomer (M) and dimer (D) form. Hyperfine splitting for dimeric radical cation is about half of monomeric value.

Increasing the temperature up to 150 K in the case of F-11 leads to disappearance of monomeric signal (right parts of the spectrum, arrows M - e.g., spectra **I** at 150 K in Figure 3.23) due to reaction:



and this transformation presents an additional argument of correct interpretation. Interpretation of line C is absent at present. This signal might be due to neutral radical with H-atom addition to Th ring.

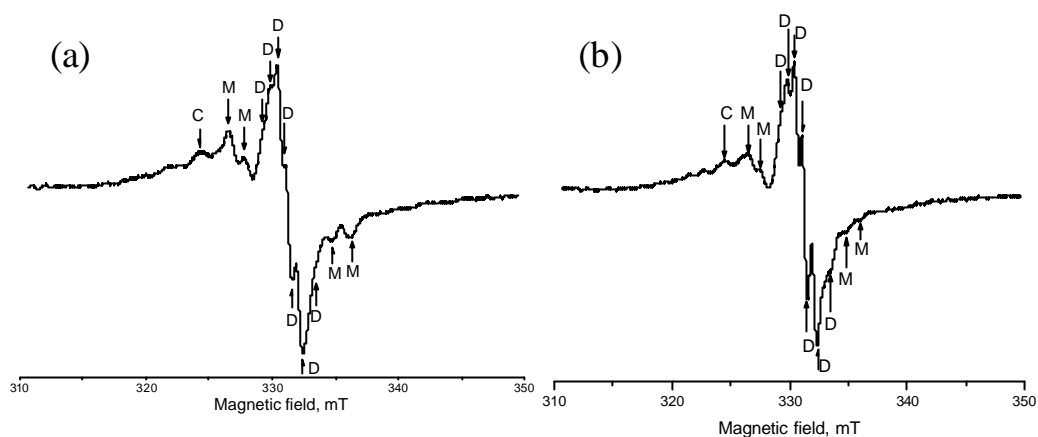
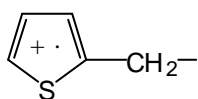
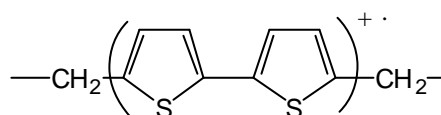


Figure 3.23. ESR spectra of irradiated monomer **I** (0.07 mole % in Freon 11) (a) at 120 K and (b) at 150 K.

Spectra of pure monomer **I** (Figure 3.24) at 77 K and 220 K most probably correspond to dimeric radical cations (sextet at 180 K corresponds to central part of spectra at 150 K in Figure 3.23). Upon thermal annealing, dimeric radical cations change to dimer radical with approximately the same constants of hyperfine splitting (7-11 G). So the main products both in freon matrix and in pure samples are dimers. The general formulas of these species are:



monomeric radical cation



dimeric radical cation

Thus, in the light of ESR measurements, monomeric radical cations are formed due to electron ejection from the monomer. These radicals react with the monomer molecules present in their vicinity and form dimer radical cations.

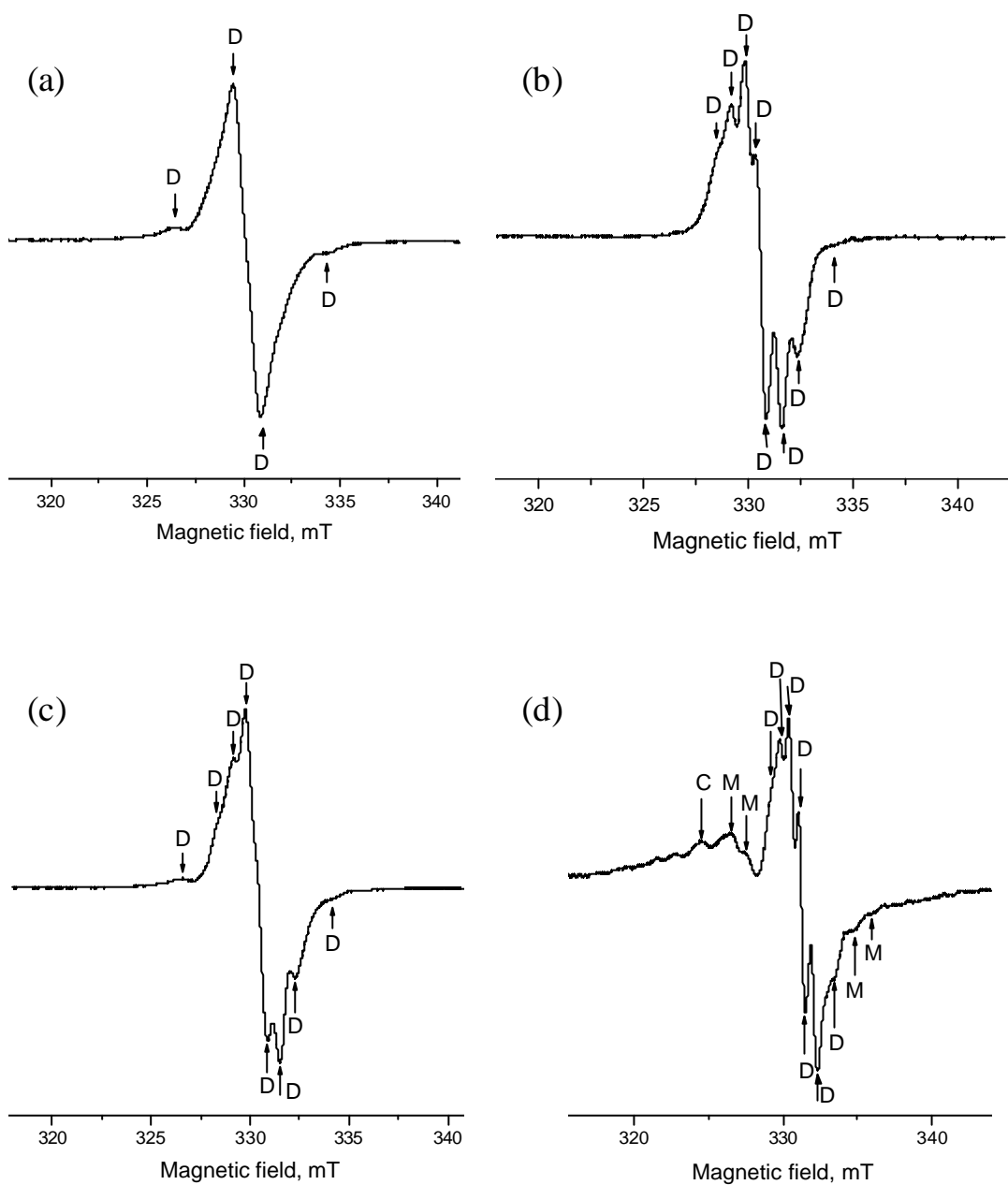


Figure 3.24. ESR spectra of irradiated pure monomer I (a) at 77 K and (b) at 220 K (c) at 180 K and (d) monomer I (0.07 mole % in Freon-11) at 150 K.

3.7.8 ESR Study of Poly(III) During I₂ Doping

The poly(III) obtained via chemical or electrochemical polymerization methods is a semiconductor with very low conductivity. On the other hand, it gains conductivity by exposing to iodine vapor and its conductivity becomes about $10^{-2} \text{ S cm}^{-1}$ after iodine doping and this doping process can be successfully monitored using ESR spectroscopy. As it can be seen from the Figure 3.25, duration of the doping process the intensity of ESR signal increases with time and it shows the formation of polarons and increasing conductivity. Unfortunately, the intensity of the signal begins to decrease slowly with the turning off the iodine vapor exposure.

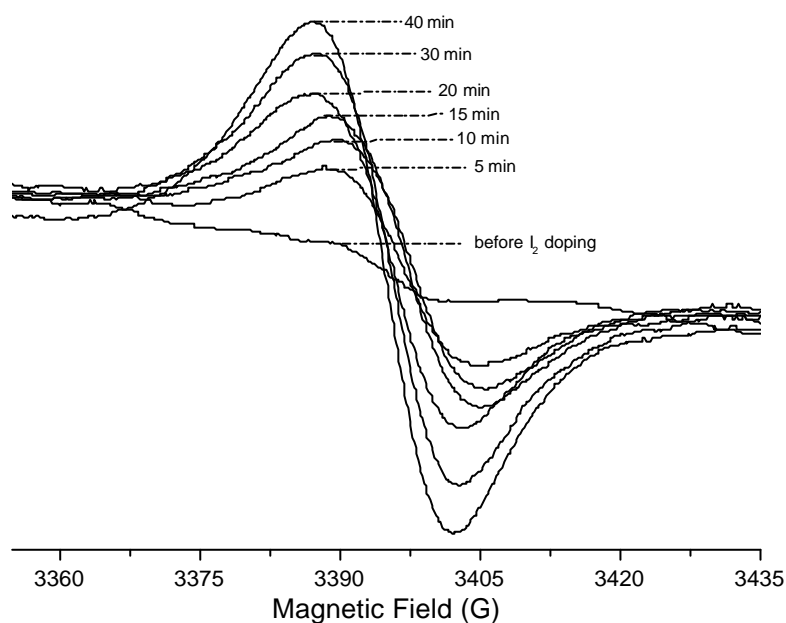


Figure 3.25. ESR signal of doped poly(III) with the iodine vapor.

3.7.9 Copolymer of **III** with Th and Py

Since polymerization of monomer **I** and **II** yielded p-broken chains and polymerization of monomer **III** resulted in the formation of a semiconductor with a very low conductivity, we investigated the copolymerization of **III** with Py and Th to enhance its conductivity.

3.7.9.1 Copolymer of **III** and Th

3.7.9.1.1 CV Studies

First of all, redox behavior of **III** and Th was carried out and compared in an electrolytic solution containing 0.1 M TBAPF₆ in CH₃CN using CV (see Figure 3.26). As seen from Figure 3.26 (a), oxidation of monomer **III** is easier than that of Th. The relative small difference (i.e. 0.15 V) in their oxidation potentials might allow random copolymerization of both monomers via CPE or successive cycling. The effect of increasing ratio of monomer **III** to Th was also investigated and results are depicted in Figure 3.26 (b)–(e).

Although CV of Th shows that the intensity of reversible redox peak of the polymer film formed on the WE increases after each cycling, the intensity of reversible peak decreases or diminishes after a certain number of cycling in the CVs of the mixtures. Also, the redox behavior of the obtained polymer films was performed in the same monomer free electrolytic solution in Figure 3.26 (f). As it can be seen from the CVs, the electroactivity of the polymer film diminishes with the increasing amount of the monomer **III** in the mixture and after a certain ratio the obtained polymer films lost its electroactivity.

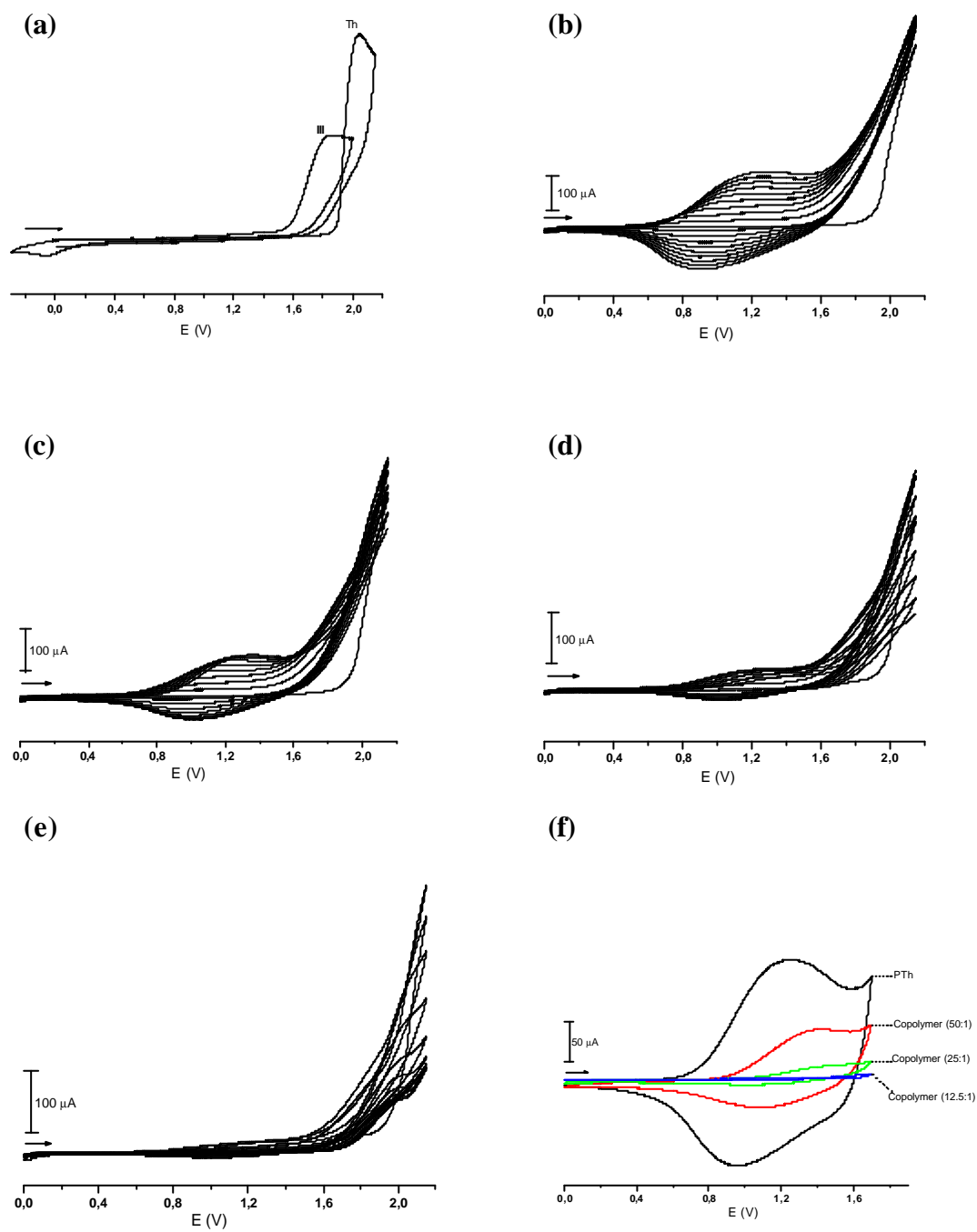


Figure 3.26. CVs of (a) 1.0×10^{-2} M Th and 2.0×10^{-2} M **III**, (b) 1.0×10^{-2} M Th, (c) **III**:Th mixture (Th:**III**; 50:1) (d) (Th:**III**; 25:1) (e) (Th:**III**; 12.5:1) and (f) polymer film obtained from the **III**:Th mixtures.

3.7.9.1.2 SPEL Behaviors

SPEL behavior of the copolymer film obtained from the mixture of **III** and Th via CPE at 2.0 V vs Ag-wire on ITO WE was investigated. The absorption spectra of the polymer film were monitored at various potential values between 0.0 V to 1.6 V vs Ag-wire in monomer free electrolytic solution (Figure 3.27 (a)). Oxidized state of the film has a reddish-orange color and the neutral state has a greenish blue color. Also, the film is stable in its neutral state because when the film was oxidized, it immediately goes to the neutral state and this behavior was also observed in the inert atmosphere.

The comparison of the SPEL behaviors of the copolymer film obtained from the **III** and Th mixture and the PTh are different: PTh was more easily oxidized and it has lower E_g value as shown in Figure 3.27 (b). In addition, the polymers obtained from the **III** and Th mixture via chemical (the obtained polymer is powder) or electrochemical polymerization methods are semiconductor with low conductivity and by exposing to iodine vapor its conductivity is enhanced. Finally, on the basis of these informations, it can be said that the obtained polymer via chemical and electrochemical methods is a random copolymer of **III** and Th mixture.

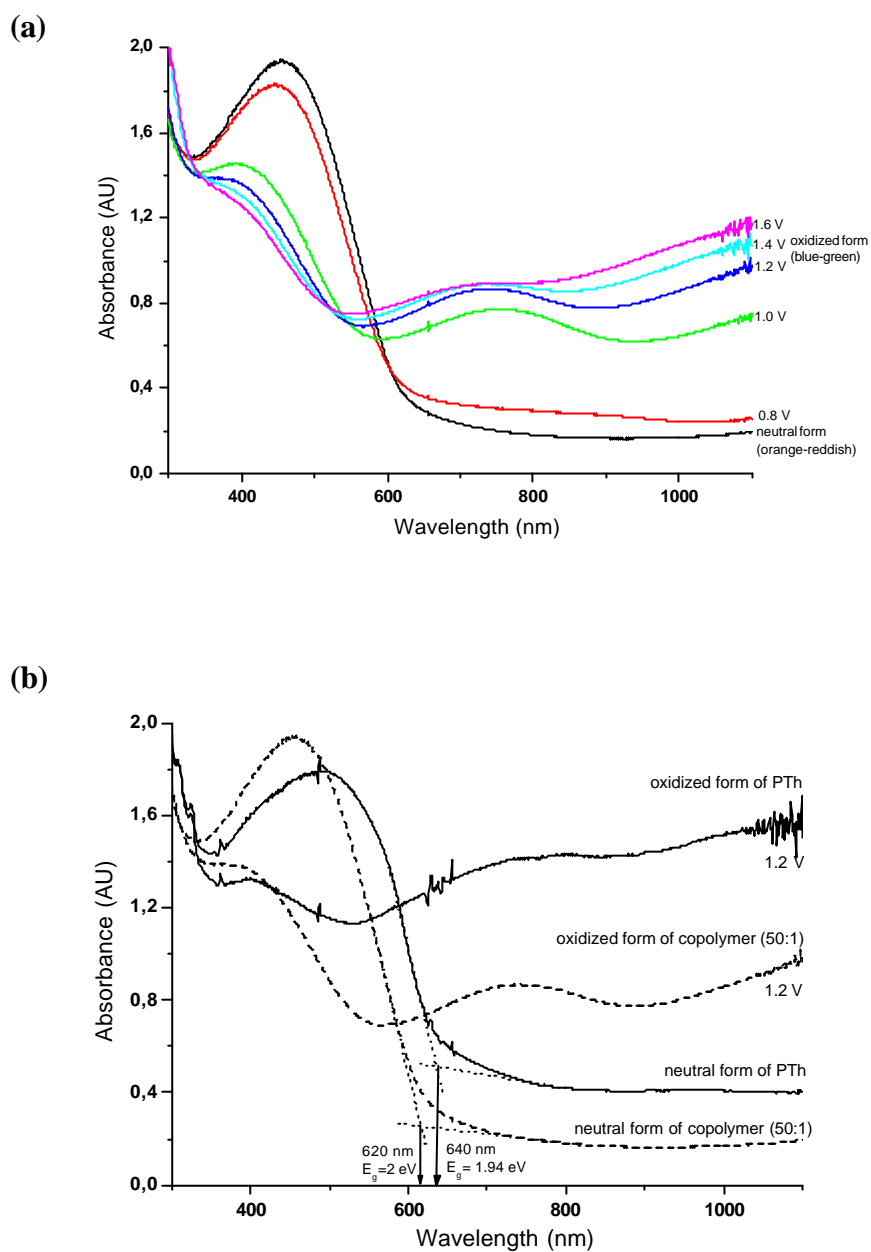


Figure 3.27. (a) Electronic absorption spectra of the copolymer obtained from Th:III mixture (50:1) in 0.1 M TBAPF₆ in CH₃CN (b) Comparison of electronic absorption spectra of the copolymer (50:1) and PTh in their neutral (0.0 V vs Ag-wire) and oxidized states (at +1.2 V vs Ag-wire) in 0.1 M TBAPF₆ in CH₃CN.

3.7.9.2 Copolymer of **III** and Py

3.7.9.2.1 CV studies

Redox behavior of Py was compared with that of **III** in the same electrolytic medium. Figure 3.28 (a) shows that Py is more easily oxidized than **III** (1.35 V for Py and 1.85 V for **III** vs SCE). After that, the CVs of PPy and the various ratios of **III** and Py mixture were compared with each other while cycling between -0.4 V and 1.3 V vs SCE. The formation of PPy can be easily seen with the increasing intensity of reversible redox peak at 0.28 V (Figure 3.28 (b)). However, with the addition of **III**, the intensity of reversible peaks increases more during the cycling compared to pure Py in Figure 3.28 (c)-(e). Also, electrochemical behaviors of the polymer films obtained from the **III** and Py mixture were studied in the monomer free electrolytic solution and compared with that of PPy. It shows that redox potential values of polymer film obtained from Py and **III** mixture were shifted to higher potential value than that of the PPy film, indicating formation of a copolymer.

3.7.9.2.2 SPEL Behaviors

In order to get further support for the formation of copolymer from **III** and Py, the change in the electronic absorption spectrum of polymer film prepared via CPE at +1.3 V and the polymer film obtained from pure Py are recorded in 0.1 M TBAPF₆ in CH₃CN. As seen from Figure 3.29 (a), during potential scanning from 0.0 V to 0.8 V, the polaron band centered at 522 nm loses intensity whereas the broader bipolaron absorption centered at 980 nm gains intensity. However, in the case of polymer film obtained from **III** and Py, the intensity of polaron band centered at 516 nm first increases during potential scanning from 0.0 V to 0.4 V, then starts to decrease with increasing potential and finally disappears. Also, with the increasing potential from 0.0 V to 0.8 V a broad bipolaron absorption band was observed beyond 700 nm (Figure 3.29 (b)).

In addition, SPEL studies showed that the E_g value (3.37 eV) of the polymer film obtained from the **III** and Py mixture is higher than that of PPy (3.2 eV) in Figure 3.29 (c) and also the conductivity of PPy (20 S cm^{-1}) is higher than that of the polymer film ($10^{-2} \text{ S cm}^{-1}$).

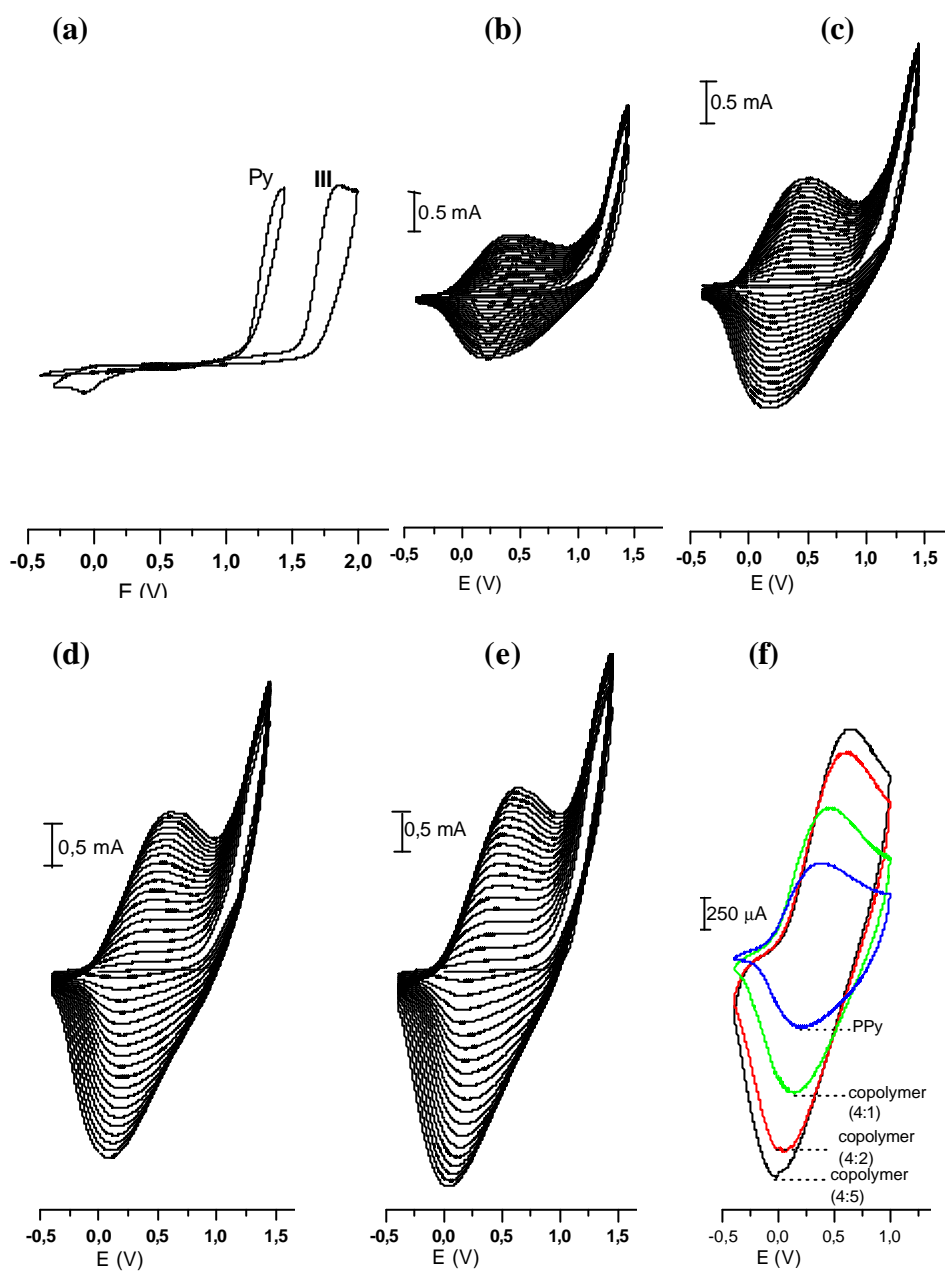


Figure 3.28. CVs of (a) 1.0×10^{-2} M Py and 1.0×10^{-2} M III (b) 1.0×10^{-2} M Py, and (c) Py:III mixture (Py:III; 4:1) (d) (Py:III; 4:2) (e) (Py:III; 4:5) (f) polymer films obtained from the Py:III mixtures.

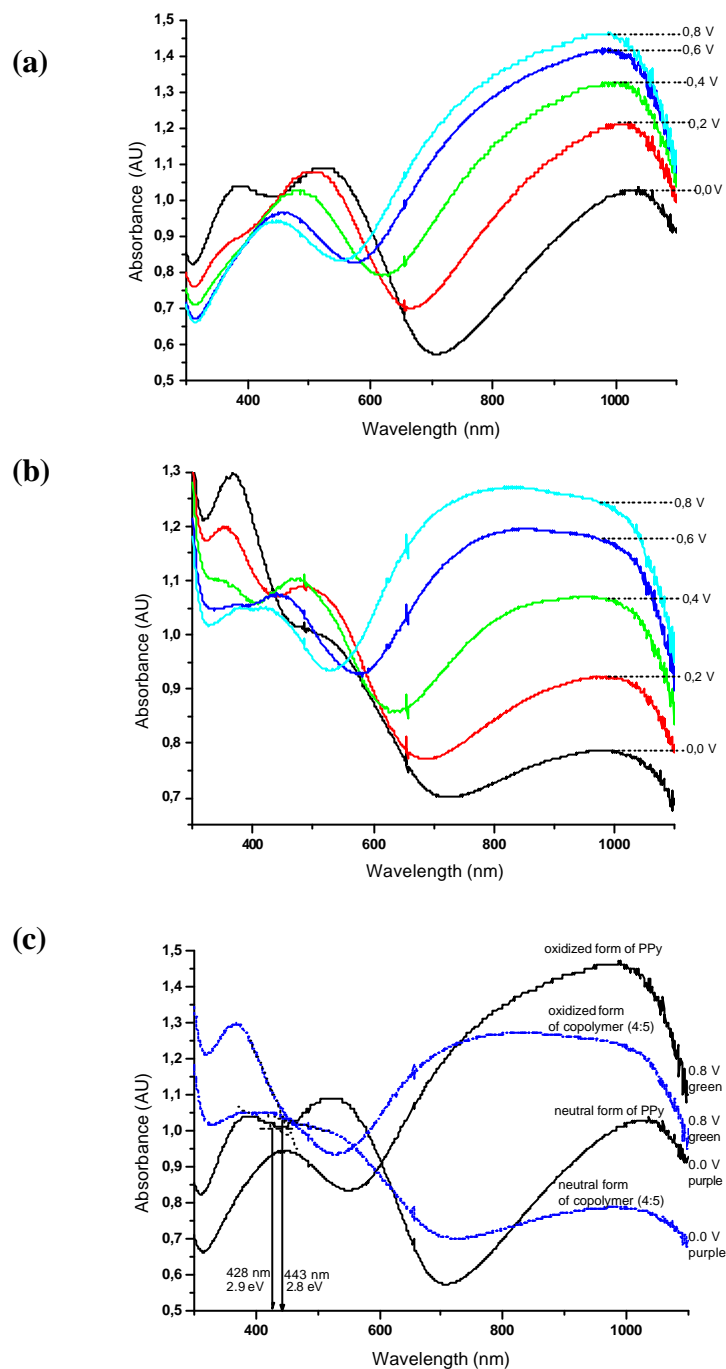


Figure 3.29. Electronic absorption spectra of (a) PPy, (b) the polymer film obtained from the Py:III (4:5) mixture, and (c) comparison of electronic absorption spectra of the copolymer and PPy in their neutral (0.0 V vs Ag-wire) and oxidized states (at +0.8 V vs Ag-wire) in 0.1 M TBAPF₆ in CH₃CN.

CHAPTER IV

CONCLUSION

In this work amorphous semiconducting polymer films were prepared by electrochemical oxidation of DB18C6 in a mixture of CH₃CN and CH₂Cl₂ as solvent at room temperature. Both *in-situ* ESR and UV-VIS spectroscopic measurements revealed the formation of triphenylene radical cation during the electrochemical polymerization. UV-VIS and CV measurements confirmed that polymer film on ITO can be reversibly cycled between 0.0 V and 0.9 V. The band gap, E_g, of the polymer was found to be 3.9 eV from electronic absorption spectrum of the neutral form of the film. ESR and conductivity measurements showed that the conductivity of polymer decreases in time due to further interaction of the film with nucleophilic impurities present in the matrix. Thermal analysis of the polymer film showed that the polymer has a high T_g value which changes depending on the dopant ion. It is also found that thermal treatment of the film causes dopant loss above 300 °C, which was also confirmed by FTIR measurements.

The temperature dependence of dark electrical conductivity in the temperature range of 550-200 K, reflects the extrinsic type of conduction with energy levels located at 0.93, 0.37 and 0.76 eV below the conduction band tail states in the temperature regions of 550-420, 410-320, and 310-260 K, respectively. The transport mechanism is dominated by the thermal excitation of free charge carriers above 260 K and by the variable range hopping of charged carriers below 260 K. The photocurrent and the absorbance spectra studied in the wavelength region of 214-1550 nm and 300-850 nm, respectively, reveal the existence of six main absorption bands with maximum absorption and maximum

photocurrent located at 320 nm. The maximum peak observed from the two different measuring techniques indicates that the band gap of the poly(DB18C6) film is 3.9 eV.

Poly(DB18C6) film is found to be light sensitive, the photocurrent of which is observed to increase with increasing illumination intensity. It is found from the $I_{ph}-F$ dependence that free carrier life time decreases, remains constant and increases under low, moderate and high applied illumination intensities. The behavior is an indication of the domination of bimolecular and strong recombination at the surface. The I_{ph} -time response is found to be short and repetitive, indicating the ability of using this material in technological applications like optical memory cells and photoconductors.

The synthesis of a new series of bis(2-thienyl) methyl (**I** and **II**) and bis(2-thienyl) ethyl (**III**) units linked by polyether bridges and their respective polymers were studied. The polymers obtained from **I** and **II** exhibit no conductivity due to broken π -conjugation system. On the other hand, polymerization of monomer **III** gave a regular polymer consisting of pseudo-polyether cages. Polymer film can be doped chemically, but in time the resistance increases due to the loss of conductivity. Such decay in conductivity is usually explained most probably due to moisture. In addition, electrochemical and SPEL behaviours of the conducting copolymer of **III** with Th and Py were studied.

REFERENCES

1. T. Ito, H. Shirakawa, S. Ikeda, *J. Polym. Sci. Polym. Chem. Edu*, 12 (1974) 11.
2. H. J. Letheby, *Chem. Soc.*, 15(1862) 161.
3. G. P. Gardini, *Adv. Heterocycl. Chem.*, 15 (1973) 67.
4. M. Armour, A. G. Davies, J. Upadhyay, A. Wasserman, *J. Polym. Sci.*, A1, (1967) 1527
5. M. Jozefowicz, L. T. Yu, G. Belorgey, R. Buvet, *J. Polym. Sci. Part C*, 16 (1969) 2943.
6. A. Dall'Ollio, Y. Dascola, V. Varacca, V. Bocchi, *Comptes Rendus*, C267, (1968) 433.
7. C. K. Chiang, Y. W. Park; A. J. Heeger, H. Shirakawa, E. J. Louis, A. G. MacDiarmid, *Phys. Rev. Lett.* 39 (1977) 1098.
8. H. Shirakawa, E. J. Louis, A. G. Macdiarmid, C. K. Chiang, A. J. Heeger, *J. Chem. Soc.-Chem. Commun.* (1977) 578.
9. A. F. Diaz, K. K. Kanazawa, G. P. Gardini, *J. Chem. Soc., Chem. Commun.* (1979) 635.
10. A. F. Diaz, J. I. Castillo, J. A. Logan, W. Lee, *J. Electroanal. Chem.* 129 (1981) 115.
11. K. Lee, A. J. Heeger, *Synth. Met.* 84 (1997) 715.
12. A. F. Diaz, *Chem. Scr.* 17 (1981) 142.
13. G. Tourillon, F. J. Garnier, *J. Electroanal. Chem.* 135 (1982) 173.
14. Bayer AG Eur. Patent 339,340, (1988).
15. F. Jonas, L. Schrader, *Synth. Met.* 41-43 (1991) 831.
16. G. Heywang, F. Jonas, *Adv. Mater.* 4 (1992) 116.
17. A. Gandini, M. N. Belgancem, *Prog. Polym. Sci.* 22 (1997) 1203.

18. A. Desbene-Monvernay, P.-C. Lacaze, J.-E. Dubois, *J. Electroanal. Chem.* 129 (1981) 229.
19. J. Rault-Berthelot, J. Simonet, *J. Electrochem. Soc.* 182 (1985) 187.
20. A. G. MacDiarmid, A. Epstein, *J. Farad. Discuss. Chem. Soc.* 88 (1989) 317.
21. J. H. Burroughes, D. D. C. Bradley, A. R. Brown, R. N. Marks, K. MacKay, R. H. Friend, P. L. Burn, A. B. Holmes, *Nature* 347 (1990) 539.
22. G. Grem, G. Leditzky, B. Ullrich, G. Leising, *Adv. Mater.* 4 (1992) 36.
23. J. Roncali, *Chem. Rev.* 92 (1992) 711.
24. H. S. O. Chan, S. C. Ng, *Prog. Polym. Sci.* 23 (1998) 1167.
25. J. Roncali, *J. Mater. Chem.* 9 (1999) 1875.
26. J. Roncali, *Chem. Rev.* 97 (1997) 173.
27. J. Heinze, G. Heywang, F. Jonas, *J. Electroanal. Chem.* 369 (1994) 87.
28. B. L. Groenendaal, F. Jonas, D. Freitag, H. Pielartzik, J. R. Reynolds, *Adv. Mater.* 12 (2000) 481.
29. S. Asavapiriyonont, G. K. Chandler, G. A. Gunawardena, D. J. Pletcher, *J. Electroanal. Chem.* 177 (1984) 229.
30. T. Inoue, T. Yamase, *Bull. Chem. Soc. Jpn.* 56 (1983) 985.
31. E. Genies, G. Bidan, A. F. Diaz, *J. Electroanal. Chem.* 149 (1983) 113.
32. A. F. Diaz, J. Bargon, In *Handbook of Conducting Polymers*; Vol. 1; Skotheim, T. A.; Ed.; Marcel Dekker: New York (1986) 82.
33. R. J. Waltman, J. Bargon, *Tetrahedron* 40 (1984) 3963.
34. C. Pinzino, R. Angelone, F. Benvenuti, C. Carlini, A. M. R. Galletti, G. Sbrana, *J. Polym. Chem., Polym. Phys.* 36 (1986) 1901.
35. T. Okada, T. Ogata, M. Ueda, *Macromolecules* 40 (1996) 3963.
36. K. Yoshino, R. Hayashi, R. Sugimoto, *J. Appl. Phys.* 23 (1984) L899.
37. R. Sugimoto, S. Takeda, H. B. Gu, K. Yoshino, *Chem. Express* 1 (1986) 635.
38. M. Pomerantz, J. J. Tseng, H. Zhu, S. J. Sproull, J. R. Reynolds, R. Uitz, H. J. Arnott, *Synth. Met.* 41-43 (1991) 825.
39. N. Toshima, S. Hara, *Prog. Polym. Sci.* 20 (1995) 155.

40. R. H. Baughman, J.-L. Brédas, R. R. Chance, R. L. Elsenbaumer, L. W. Shacklette, *Chem. Rev.* 82 (1982) 209.
41. B. G. Street, T. C. Clarke, M. Krounbi, K. Kanazawa, V. Lee, P. Pfluger, J. C. Scott, G. Weiser, *Mol. Cryst. Liq. Cryst.* 83 (1982) 1285.
42. M. Salmon, K. K. Kanazawa, F. F. Diaz, M. Krounbi, *J. Polym. Sci.* 20 (1982) 187.
43. T. Shimidzu, A. Ohtani, T. Iyoda, K. J. Honda, *J. Chem. Soc., Chem. Commun.* (1982) 361.
44. J. C. W. Chien, *Polyacetylene: Chemistry, Physics, and Material Science*; Academic Press, Inc.: Orlando, (1984).
45. U. Salzner, J. B. Lagowski, P. G. Pickup, R. A. Poirier, *Synth. Met.* 96 (1998) 177.
46. J. L. Bredas, B. Themans, J. G. Fripiat, J. M. Andre, R. R. Chance, R. R. *Phys. Rev. B:Condens. Matter.* 29 (1984) 6761.
47. J. L. Bredas, G. B. Street, *Acc. Chem. Res.* 18 (1985) 309.
48. K. Fesser, A. R. Bishop, D. K. Campbell, *Phys. Rev. B* 27 (1983) 4804.
49. W. R. Salaneck, I. Lundstrom, W. S. Huang, A. G. Macdiarmid, *Synth. Met.* 13 (1986) 291.
50. P. J. Nigrey, A. G. Macdiarmid, A. J. Heeger, *J. Chem. Soc.-Chem. Commun.* (1979) 594.
51. A. N. Aleshin, K. Lee, J. Y. Lee, D. Y. Kim, C. Y. Kim, *Synth. Met.* 99 (1999) 27.
52. N. F. Mott and E. A. Davis, *Electronic Processes in non-Crystalline Materials*, 2nd Ed. Oxford, (1979).
53. A. Dodabalapur, L. Torsi, H. E. Katz, *Science* 268 (1995) 270.
54. A. Kraft, A.C. Grimsdale, A. B. Holmes, *Angew. Chem. Int. Ed.* 37 (1998) 402.
55. J. C. DuBois, O. Sagnes, F. Henry, *Synth. Met.* 28 (1989) C871.
56. P. Novak, K. Muller, K. S. V. Santhanam, O. Haas, *Chem. Rev.* 97 (1997) 207.
57. T. A. Skotheim, R. L. Elsenbaumer, J. R. Reynolds, Eds. *Marcel Dekker: New York* (1998).

58. D. T. McQuade, A. E. Pullen, T. M. Swager, *Chem. Rev.* 100 (2000) 2537.
59. J. –M. Pernaut, J. R. Reynolds, *J. Phys. Chem. B.* 104 (2000) 4080.
60. P. M. S. Monk, R. J. Mortimer, D. R. Rosseinsky, *Electrochromism: Fundamentals and Applications*; VCH: Weinheim, (1995).
61. C. J. Pedersen, *J. Am. Chem. Soc.* 89 (1967) 7017.
62. C. J. Pedersen, *Angew. Chem., Int. Ed. Engl.* 27 (1988) 1021.
63. J. M. Lehn, *Structure and Bonding*, Springer Verlag, Berlin, (1973).
64. J. M. Lehn, *Angew. Chem., Int. Ed. Engl.*, 27 (1988) 89.
65. D.J. Cram, *Angew. Chem., Int. Ed. Engl.*, 27 (1988) 1009.
66. J. J. Christensen, J. O. Hill, R. M. Izatt, *Science* 174 (1971) 459.
67. J. J. Christensen, D. J. Eatough, R. M. Izatt, *Chem. Rev.*, 74 (1974) 351.
68. N. S. Poonia, A. V. Bajaj, *Chem. Rev.*, 79 (1979) 389.
69. I. M. Kolthoff, *Anal. Chem.*, 51 (1979) 1R.
70. M. Takagi, H. Nakamura, *J. Coord. Chem.*, 15 (1986) 53.
71. C. J. Pedersen, H. K. Frensdorff, *Angew. Chem., Int. Ed. Engl.*, 11 (1972) 16.
72. C. J. Pedersen, *J. Am. Chem. Soc.*, 92 (1970) 386.
73. M. Lemaire, R. Garreau, J. Roncali, D. Delabouglise, H. Korri-Youssoufi, F. Garnier, *New J. Chem.*, 13 (1989) 863.
74. J. Roncali, R. Garreau, D. Delabouglise, F. Garnier, M. Lemaire, *J. Chem. Soc., Chem. Commun.*, (1989) 679.
75. J. Roncali, R. Garreau, M. Lemaire, *J. Electroanal. Chem.*, 278 (1990) 373.
76. J. M. Barker, J. D. E. ChaYn, J. Halfpenny, P. R. Huddleston, P.F. Tseki, *J. Chem. Soc., Chem. Commun.*, (1993) 1733.
77. P. Marrec, B. Fabre, J. Simonet, *J. Electroanal. Chem.*, 437 (1997) 245.
78. R. A. Robinson, R. H. Stokes, *Electrolyte Solutions*, Butterworths Scientific Publications, London (1959).
79. P. Marrec, J. Simonet, *J. Electroanal. Chem.*, 459 (1998) 35.
80. Y. Gache, J. Simonet, *J. Chim. Phys.*, 89 (1992) 1027.
81. J. Simonet, *Curr. Top. Electrochem.*, 3 (1994) 227.
82. V. Le Berre, L. Angely, N. Simonet-Gueguen, J. Simonet, *New J. Chem.*, 13 (1989) 131.

83. J. Simonet, J.M. Chapuzet, *J. Electroanal. Chem.*, 322 (1992) 399.
84. C. Destrade, P. Foucher, H. Gasparoux, H.T. Nguyen, A.M. Levelut, J. Malthete, *Mol. Cryst. Liq. Cryst.*, 106 (1984) 121.
85. D. Goldfarb, E. Lifshitz, H. Zimmermann, Z. Luz, *J. Chem. Phys.*, 82 (1985) 5155.
86. V. Le Berre, L. Angely, N. Simonet-Gueguen, J. Simonet, *New J. Chem.* 9 (1985) 419.
87. V. Questaigne, J. Simonet, A. Rousseau, *Bull. Soc. Chim. Fr.*, 129 (1992) 37.
88. V. Le Berre, L. Angely, N. Simonet-Gueguen, J. Simonet, *J. Electroanal. Chem.*, 240 (1988) 117.
89. L. Angely, J. Simonet, J.P. Morel, *New J. Chem.*, 14 (1990) 83.
90. L. Angely, V. Questaigne, J. Rault-Berthelot, J. Simonet, *New J. Chem.*, 14 (1990) 841.
91. V. Le Berre, L. Angely, N. Simonet-Gueguen, J. Simonet, *J. Electroanal. Chem.*, 206 (1986) 115.
92. L. Angely, V. Questaigne, J. Rault-Berthelot, *Synth. Met.*, 52 (1992) 111.
93. L. Angely, J. Rault-Berthelot, G. Peslerbe, *Synth. Met.*, 52 (1992) 273.
94. J. Rault-Berthelot, L. Angely, *Synth. Met.*, 58 (1993) 51.
95. J. Rault-Berthelot, L. Angely, *Synth. Met.*, 65 (1994) 55.
96. A. Morin, F. Beniere, L. Angely, J. Rault-Berthelot, J. Simonet, *J. Chem. Soc. Faraday Trans.*, 87 (1991) 1393.
97. M. Cole, C.R.A. Catlow, F. Beniere, S. Le Mellay, V. Questaigne, J. Simonet, *J. Mater. Chem.*, 3 (1993) 693.
98. F. Beniere, N. Bertru, C.R.A. Catlow, M. Cole, J. Simonet, L. Angely, *J. Phys. Chem. Solids* 53 (1992) 449.
99. M.G. De Backer, F.X. Sauvage, E.B. Mkadmi, J. Simonet, *New J. Chem.*, 17 (1993) 201.
100. S.K. Lunsford, A. Galal, N. Akmal, Y.L. Ma, H. Zimmer, H.B. Mark Jr., *Anal. Lett.*, 27 (1994) 2141.
101. S.K. Lunsford, Y.L. Ma, A. Galal, C. Striley, H. Zimmer, H.B. Mark Jr., *Electroanalysis* 7 (1995) 420.

102. S.K. Lunsford, C.A. Striley, Y.L. Ma, H. Zimmer, G. Kreishman, H.B. Mark Jr., *Anal. Lett.*, 29 (1996) 1309.
103. V. Le Berre, R. Carlier, A. Tallec, J. Simonet, *J. Electroanal. Chem.*, 143 (1982) 425.
104. V. Le Berre, L. Angely, N. Simonet-Gueguen, J. Simonet, *New J. Chem.*, 9 (1985) 41922
105. T. Sone, K. Sato, Y. Ohba, *Bull. Chem. Soc. Jpn.*, 62 (1989) 838.
106. P. Bauerle, St. Scheib, *Acta Polymer.*, 46 (1995)124.
107. M. J. Marsella, P. J. Carroll, T. M. Swager, *J. Am. Chem. Soc.*, 117 (1995) 9832.
108. R. D. McCullough, *Adv. Mater.*, 10 (2) (1998) 93.
109. M. R. Anderson, D. Selse, M. Berggren, H. Jarvinen, T. Hjertberg, O. Inganas, O. Wennerstrom, J.-E. Österholm, *Macromolecules*, 24 (1994) 6503.
110. R. Gonzalez, J. M. Figueroa, H. Gonzalez, *Euro. Poly. J.*, 38 (2002), 287.
111. A. F. Qasrawi, A. Cihaner, A. M. Önal, *Cryst. Res. Technol.*, 39 (1) (2004) 56.
112. B. Demirboga, A.M. Önal, *Synth. Met.*, 99 (1999) 237.
113. M. Tabata, A. Lund, *Z. Naturforsch.*, 38a, (1983) 428.
114. P. Chandrasekhar, "Conducting Polymers, Fundamental and Applications: A Practical Approach", Kluwer Academic Publisher, Boston, (1999).
115. R. M. Hill, *Phil. Mag.*, 24 (1971) 1307.
116. R.H. Bube, *Photoelectronic Properties of Semiconductors*, Cambridge University Press, Cambridge (1992).
117. N. V. Joshi, *Photoconductivity Art, Science, and Technology*, Marcel Dekker INC., (1990).
118. J. Simonet, Y. Gache, N. Simonet-Gueguen, O. Leclerc, *Denki Kagaku*, 62 (1994) 1211.
119. J. Rault-Berthelot, M. Massaoudi, H. Le Deit, J. Simonet, *Synth. Met.*, 75 (1995) 11.
120. K. J. Hoffmann, A. L. Graskopf, E. J. Samuelsen, P. H. J. Carlsen, *Synth. Met.*, 113 (2000) 89.

121. K. J. Hoffmann, E. J. Samuelsen, P. H. J. Carlsen, *Synth. Met.*, 113 (2000) 161.
122. W.-C. Chen, S. A. Jenekhe, *Macromolecules* 28 (1995) 465.
123. B. Abarca, G. Asensio, R. Ballesteros, T. Varea, *J. Org. Chem.*, 56 (1991) 3224.
124. H. Braunling, R. Becker, G. Blochl, *Synth. Met.*, 55-57 (1993) 833.
125. A. Mangini, G. F. Pedulli, M. Tiecco, *Tetrahedron Lett.*, 47 (1968) 4941.
126. J. Roncali, R. Garreau, D. Delabouglise, F. Garnier, M. Lemaire, *Synth. Met.* 28 (1989) C341.

VITA

Atilla Cihaner was born on April 6, 1977 in Ankara. He graduated from Middle East Technical University (METU), Department of Chemistry in 1998. He began his MS studies at Chemistry Department of METU. During this time, he worked on chemical and electrochemical polymerization of halogenated anilines under the supervision of Prof. Dr. Ahmet M. Önal. He began PhD studies in 2000 in the area of synthesis of crowned conducting polymers and matrix isolation. He worked as a visiting graduate student at Enikolopov Institute of Synthetic Polymeric Materials-[Karpov Institute of Physical Chemistry](#) Russian Academia of Sciences, Moscow, Russia in Professor Vladimir Feldman's group and worked on matrix isolation of monomer containing crown ethers. He is a research assistant in Atilim University, Ankara.

He published 7 papers in international journals, and submitted another 2.

- 1) A. Cihaner, A. M. Önal, "Electroinitiated polymerization of 2-allylphenol", *Polym. Bull.*, 45 (2000) 45.
- 2) A. Cihaner, H. N. Testereci, A. M. Önal, "Electrochemical polymerization of 4-allylphenol", *Euro. Polym. J.*, 37 (2001) 1747.
- 3) A. Cihaner, A. M. Önal, "Synthesis and characterization of fluorine-substituted polyanilines", *Euro. Polym. J.*, 37 (2001) 1767.
- 4) A. Cihaner, A. M. Önal, "Electrochemical behaviour and electrochemical polymerization of fluoro-substituted anilines", *Polym. Int.*, 51 (2002) 680.
- 5) A. F. Qasrawi, A. Cihaner, A. M. Önal, "Electrical, optical and photoconductive properties of poly(dibenzo-18-crown-6)", *Cryst. Res. Technical.* 39(1) (2004) 56.

- 6) A. Cihaner, S. Tirkes, A. M. Önal, "Electrochemical polymerization of 9-fluorenone", *J. Electroanal. Chem.*, 568 (2004) 151.
- 7) A. Cihaner, A. M. Önal, "Spectroelectrochemical and thermal properties of poly(dibenzo-18-crown-6) prepared via anodic oxidation", *J. Electroanal. Chem.* (in press 2004).
- 8) S. Tirkes, A. Cihaner, A. M. Önal, "Synthesis and polymerization of 2- and 3-substituted thiophene derivatives linked by polyether bridges", *J. Electroanal. Chem.*, (submitted 2004).
- 9) A. Cihaner, A. M. Önal, "Electrochemical Polymerization of Para-Substituted Haloanilines", *Polymer* (submitted 2004).